Mechanisms of tumor dormancy and awakening in the lymph node

Andrea Lim

A dissertation

submitted in partial fulfillment of the

requirements for the degree of

Doctor of Philosophy

University of Washington

2021

Reading Committee:

Cyrus M. Ghajar, Chair

Peggy Porter

Slobodan Beronja

Program Authorized to Offer Degree:

Molecular and Cellular Biology

University of Washington

Abstract

Mechanisms of tumor dormancy and awakening in the lymph node

Andrea Lim

Chair of the Supervisory Committee:
Cyrus M. Ghajar, Ph.D.
Public Health Sciences Division, Fred Hutchinson Cancer Research Center

Mechanisms of tumor dormancy are being systematically uncovered through the major organs. Yet little is known about lymph nodes (LNs) as harbors of residual disease, despite their well-established prognostic significance for metastasis and direct contribution to metastasis in visceral organs. Further, few mechanisms of awakening from dormancy have been reported. To investigate tumor dormancy in the LN, the niche for dormant disseminated tumor cells (DTCs) was characterized by spatial analysis of LN tissues from a model of spontaneous murine mammary carcinoma dissemination to the lymph node. Ki-67$^-$ DTCs were significantly enriched near blood endothelia but not lymphatic endothelia versus a null distribution control, revealing that the lymph node blood vasculature is the primary niche for quiescent DTCs. An organotypic co-culture model of the LN vascular niche was developed to study the mechanisms underlying

niche regulation of tumor quiescence. Human breast cancer cell line HMT-3522-T4-2 were growth suppressed in the presence of endothelial cells, recapitulating the effect of the vascular niche *in vivo*. RNA sequencing revealed that TGFβ signaling was among the most differentially upregulated pathways in the niches containing blood endothelial cells, which was validated through ELISA. Addition of TGF-β1 to tumor growth-permissive LN stromal cultures suppressed tumor cell growth as seen in vascular niches, providing evidence that TGF-β1 promotes DTC quiescence in the LN vascular niche.

To investigate tumor awakening in the LN, the stable vascular niche was disrupted through sustained inflammation via bacterial lipopolysaccharide (LPS), which resulted in endothelial remodeling and LN expansion. LPS treatment of mice with LN DTCs resulted in over ten-fold increase in LN micrometastases, supporting the emerging theme that tissue dysregulation and loss of homeostasis triggers metastatic outgrowth. The inflamed stroma was transcriptionally profiled using single-cell RNA sequencing, which revealed that expression of the TGFβ pathway decreased upon inflammation. Knocking down requisite TGFβ receptor 2 in tumor cells enhanced micrometastatic outgrowth within the LN, supporting the hypothesis that blood endothelial-derived TGF-β1 is required for DTC quiescence.

These studies reveal that the LN supports DTC dormancy and provide evidence that endothelial TGF-β1 promotes quiescence in the vascular niche. Further, inflammation is sufficient to induce micrometastatic outgrowth in the LN, concomitant with stromal remodeling and loss of endothelial TGFβ expression.

TABLE OF CONTENTS

LIST OF FIGURES

LIST OF TABLES

ACKNOWLEDGEMENTS

In a dissertation about the microenvironment, it would be remiss not to acknowledge the incredible people around me who supported both the work and the researcher.

A huge debt of gratitude to Cyrus, who welcomed me into this exciting field. Your passion for cancer research and enthusiasm helped motivate me over the years, and you always encouraged me to approach problems creatively, think critically, and then go for it. Thank you for teaching me not to let perfect get in the way of the good.

I am also grateful to the members of my thesis committee who were generous with their time, insight, and expertise, and helped improve this project in many ways; to the hard-working staff of Shared Resources; and our generous collaborators.

Many thanks to my labmates for your congenial company, thoughtful insights, volunteer spirit, and patience. David, Erica, Candice, Laura, and Arko, you have been stellar examples scientists and mentors, each in your own way. Sarah, what a pleasure to share the graduate school experience with you. Ryann and Marlowe, thank you for keeping the lab running with wit and good humor. Jing, our unofficial lab mom, thanks for your many contributions to our lab and for your dear friendship. I could not list all the memories that cheered me through the highs and lows of graduate school, but I treasure these experiences and hold you all in high esteem.

For those who supported my personal journey through grad school, your support was invaluable. To the community at Blessed Sacrament, thank you for reminding me what is important in life. To my mother, Joanne Strantz, who cared for my well-being and happiness from 1000 miles away, as only a mother could: you were a port in the storm.

Finally, to those friends near and far, my sincere gratitude for the wealth of support: Albert

and Thomas, for scientific inspiration; Mary, who undid many knots; Joseph and Benedict, for fatherly care; Therese, who taught me to value the little things; Joan, a model of courage in adversity; Faustina, who encouraged me to ask for help; Pier Giorgio, for teaching me how to work and play well; and Fulton, who taught me to speak with conviction.

Thank you, all.

DEDICATION

To my dad,

who would have loved to see

this work completed.

Chapter 1. GENERAL INTRODUCTION

Breast cancer is the most common cancer and source of female cancer mortality in the world, with 2.26 million new cases worldwide in 2020 (Globocan 2020, World Health Organization). Five-year survival rates are twice as high in developed (80%) versus developing (40%) countries due to discrepancies in detection, diagnosis, and treatment [2]. In the United States, approximately 1 in 8 women will be diagnosed with breast cancer in her lifetime [3]. This diagnosis is no longer a death sentence, as advances in care including early detection, neo-adjuvant therapies and targeted therapies, and increased awareness and monitoring of metastasis have contributed to an overall 40% decline in breast cancer-related mortality from 1989-2017 [3, 4].

Yet, despite improvements across stage and subtype, some patient groups are still disproportionately vulnerable. Diagnostic staging stratifies breast cancer patients by disease progression to help manage treatment (American Joint Committee on Cancer, 8th ed.). From 1988-2006, Stage I patients with only localized disease had a 97.8% 5 year-survival rate; this dropped to 92.3% if the patient presented at Stage II (nodal invasion), 75.5% at Stage III (distant and/or increasing nodal involvement), and 24.9 % at Stage IV (advanced metastatic disease) [4]. Survival continued to trend downward in all groups at 10 years post-treatment [4]. Certain subtypes of breast cancer are more aggressive, as triple-negative breast cancer patients have a 5-year survival rate of 91% for localized disease but only 11% with distant metastases (SEER database, 2010-2015, National Cancer Institute). Although early breast cancer patients (Stage I-III) have relatively good prognosis, advanced metastatic patients still bear the most devastating impacts of the disease, with little improvement in recent years [5].

Therefore, although breast cancer is relatively common, it is specifically the metastatic stage of disease that contributes significantly to patient mortality. Indeed, metastasis accounts for at least two-thirds (66.7%) of all solid tumor-related deaths [6]. Although only 6% of breast cancer patients initially present with metastatic disease beyond local lymph nodes (Breast Cancer Facts and Figures 2019-2020), metastases continue to emerge over time, with 11% of patients developing recurrent disease within 5 years of treatment and 20% recurring within 10 years of treatment [7]. Thus, approximately one-quarter of breast cancer patients will develop metastasis over time, even amongst those who complete treatment. This stark reality reshapes our notion of what "curative" therapy looks like and inspires new approaches for interventions.

The danger of metastasis is destruction and failure of vital organs. Unlike local tumors, which can be effectively treated through neo-adjuvant therapy, radiation, surgical debulking, and follow-up adjuvant therapy, metastatic spread can be difficult to detect until advanced symptoms emerge. Effective intervention before critical organ failure is a pressing challenge in the field, given the large proportion of patients whose disease will progress. This outstanding need motivated my work, described in this dissertation.

1.1 BREAST CANCER AT THE PRIMARY SITE

1.1.1 *Etiology of breast cancer*

"Breast cancer" refers to a collection of malignant transformations that occur in the heterogenous cell types within the breast tissue, which includes stratified epithelium (luminal and myoepithelial layers), blood and lymphatic vessels, and stromal cells[8]. The most commonly transformed cells are the epithelia that comprise the milk ducts, leading to *in situ* (localized, 15-20% of breast carcinomas) or invasive ductal carcinoma (75% of breast

carcinomas) [9]. Invasive lobular carcinoma (10-15% of breast carcinomas) originates with the secretory epithelia in the milk glands [10]. Rare forms of breast cancer include Paget's disease of the breast and inflammatory breast cancer, a subtype of invasive ductal carcinoma in which cancer cells block the lymphatic vessels and cause edema of the breast.

Both men and women may develop breast cancer [11], although it is relatively rare in males, accounting for less than 1% of male cancer and less than 1% of breast cancer incidence overall [12]. Therefore, this work focuses on female breast cancer.

Many factors contribute to breast cancer etiology including age, genetic background, race/ethnic group, and reproductive history. Genetic risk factors such as mutations in the BRCA1 and BRCA2, PTEN, TP53, and other genes account for 5-10% of breast cancer cases, and different ethnic/racial groups demonstrate different genetic susceptibilities to breast cancer[13, 14]. Hormones taken therapeutically as in the context of hormone replacement therapy may increase risk [15]. Reproductive history events are also associated with breast cancer incidence, including age of menarche, childbirth, lactation and mammary gland involution cycles, and menopause [16].

1.1.2 *Breast cancer subtyping*

Breast cancer is broadly classified into three major subtypes based on expression of characteristic hormone receptors (HR) including estrogen receptor (ER) and progesterone receptor (PR), and amplification of human epidermal growth factor receptor 2 (HER2)/ERBB2. Breast cancer subtypes include $HR^+/HER2^-$ (expression one or both of the hormone receptors, 70% of breast cancer patients), $HER2^+$ (15-20% of patients), and triple negative breast cancer (TNBC, lacking all both hormone receptors and HER2 amplification, 10-15% of patients) [17, 18].

In addition to these receptor-based subtypes, molecular subgroups were identified based on PAM50 gene expression patterns, identifying the luminal A, luminal B, HER2-enriched, basal-like, and normal-like molecular subtypes [19]. These two classification systems tend to associate in a characteristic manner—for example, HR^+ tumors tend to overlap with luminal A or B class, although luminal A tends to be less aggressive compared to luminal B [20].

Functionally, breast cancer subtypes display different levels of aggression, propensity to metastasize, and preference for metastatic site. Luminal A tumors tend to have the lowest risk of recurrence whereas triple-negative basal-like is consistently more likely to relapse at five and 10-year follow-up than other subtypes, contributing to lower overall survival at these timepoints [21, 22]. Even from an early stage, TNBC tends to be more aggressive, with a stage I disease 5-year survival rate of 85% compared to 94% in HR^+ and 99% in $HER2^+$ subtypes [17, 20]. All subtypes preferentially metastasize to the bone except basal-like, which is more likely to metastasize to the brain, lung, or distant lymph nodes [23]. Luminal/$HER2^+$ and HER2-enriched tumors are more likely to metastasize to the brain, liver, and lung than luminal A/$HER2^-$ tumors [23]. Thus, molecular subtyping predicts risk and site of recurrence.

1.1.3 *Clinical staging of breast cancer*

Breast cancer is currently staged through a system that accounts for Tumor size, spread to lymph Nodes, and Metastasis to distant organs (TNM) (AJCC, 8th ed). The primary tumor is staged on a scale from Tis (carcinoma *in situ*) to T0-T4 depending on size and invasion into the chest wall. Lymph nodes (LN) are assessed for both presence of metastases in the draining (sentinel) LN as well as number of affected nodes in the draining axillary cluster, which have been positively correlated with tumor aggression and metastatic spread. Identification of LN metastases occurs through sampling the biopsied LN either by immunohistochemistry or

molecular techniques like PCR. The N-level corresponds to increasing numbers of involved LNs from N0-3, with additional details about the metastases included after the number. For instance, (i+) refers to "isolated" tumor cells (fewer than 200 cells in an area smaller than 0.2 mm in diameter), and (mi) refers to "micrometastases" (a cluster 0.2-2 mm in diameter). Metastasis is indicated by either M0 (not detected) or M1 (spread to distant organs). Isolated tumor cells no larger than 0.2 mm in diameter may be indicated by M0(i+) as in the LNs.

1.2 BREAST CANCER METASTASIS

1.2.1 *The metastatic cascade*

Metastasis (Gr., *meta*, "next," and *stasis*, "place"), first coined by Jean Claude Recamier in 1829 [24], refers to the migration of individual tumor cells and small clusters to regional or distant tissues through the blood and lymph. Circulating tumor cells (CTCs) are distinguished from cells that have successfully extravasated and entered the tissue (disseminated tumor cells, DTCs). The metastatic process is typically broken down into key steps (**Fig. 1**), although the route and interactions encountered by a given DTC is likely diverse [25]. First, malignant cells acquire genetic mutations that endow them with invasive properties to break cell-cell contacts and detach from the tumor. Undergoing an epithelial-to-mesenchymal transition (EMT) allows tumor cells to resist anoikis associated with loss of contact with the ECM and cell-cell contacts [26]. Tumor cells downregulate attachment molecules, secrete enzymes such as matrix metalloproteinases (MMPs) that degrade the basement membrane and extracellular matrix (ECM), and upregulate proliferation and survival signaling like β-catenin, Wnt, and cell cycle proteins [27]. They subsequently enter local vessels including thin-walled capillaries or lymphatic vessels which pose relatively little barrier for either diapedesis or transcellular

migration [28, 29]. Of the two, lymphatic vessels are thought to be easier to enter due to a lack of tight junctions, reflecting their function to drain excess interstitial fluid [25]. CTCs progress through circulation or lymph by physical forces or chemotaxis following gradients of cytokine signals to certain tissues [30]. The blood is considered a hostile environment, as only a very small fraction (0.1%) of melanoma cells injected intravenously into mice were viable after 24 hours in the bloodstream [31]. Lymph is less harsh, lacking a central pump for pressurized flow, and exposes tumor cells to less oxidative stress and free iron than blood, which has been attributed to increased tumor cell survival and metastasis [32]. In the blood, CTCs may encounter immune cells that promote or antagonize dissemination. For instance, platelets coat CTCs and provide protection from shear forces and immune cells, increase CTC diameter which promotes arrest in small vessels, and increase adhesion along the vessel wall [1]. After arrest, CTCs extravasate into the tissue [33] and may undergo the complementary process of mesenchymal-to-epithelial transition to re-establish connections with the external environment [34]. Different tissues present different barriers to extravasation in the form of tissue-specific endothelia: tissues with fenestrated vessels such as the liver are extremely prone to metastasis, whereas the blood-brain barrier resists invasion through tight junctions and layers of supporting mural cells (see Chapter 2). Colonizing the tissue requires context-dependent adaptions. Until these adaptations for growth are met or barriers to proliferation lowered, DTCs may remain as single cells until the balance shifts through accumulation of mutations or changes to the microenvironment (**Fig. 1**).

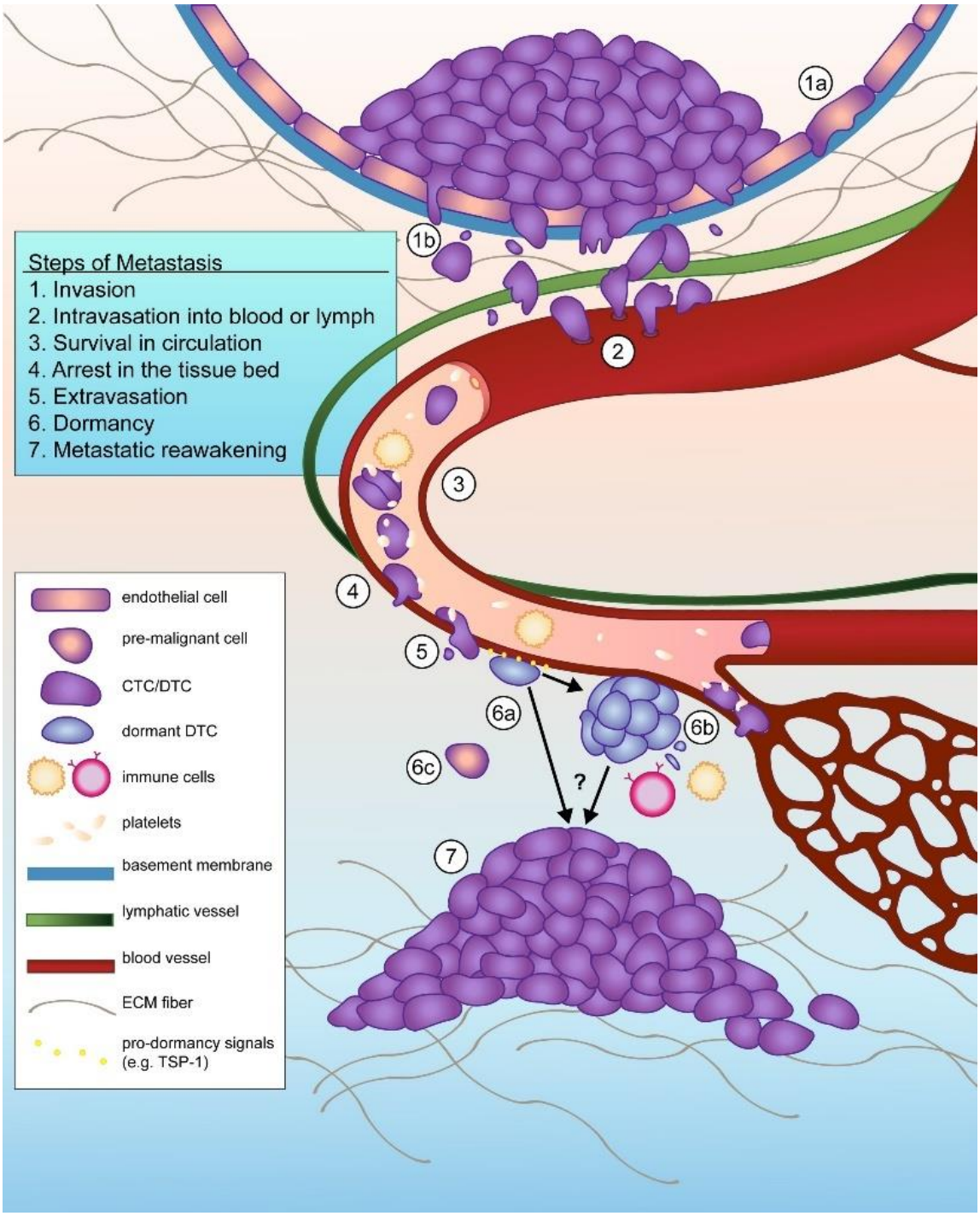

Figure 1. Classical view of the metastatic cascade. 1) Malignant transformation of epithelial cells imbues them with invasive properties (a), enabling local invasion and destruction of the basement membrane (b). 2) Transformed cancer cells intravasate into the blood or lymphatic vessels where they may encounter 3) immune cells and platelets which alter their ability to survive the harsh shear stress of hematogenous dissemination. 4) CTCs arrest on vessel walls through adhesion molecules and/or vessel diameter constraints and extravasate past the endothelia to 5) enter the tissue. 6) Newly disseminated tumor cells (DTCs) first encounter the basal side of the vessel, which may secrete factors that promote DTC quiescence in the basement membrane (a). Through unknown mechanisms, dormant DTCs may activate to grow into clusters that are under a continuous balance of growth and immune surveillance (b). The malignancy of early DTCs is unknown (c). 7) Ultimately, DTCs overcome barriers to growth through unknown mechanisms and produce metastases in the distant tissue [1].

1.2.2 *The metastatic timeline promotes divergent evolution*

Historically, metastasis was thought to occur sequentially after the tumor developed and evolved to a certain size and level of aggression in the so-called linear model of metastasis [35]. This assumption was based on the observation that larger tumor volume positively correlated with risk of metastasis. However, increasing tumor volume also indicates the passage of time, rather than direct contribution to metastatic disease, during which early disseminating cells could gain a foothold in the distant tissue and expand. Experimental models and liquid biopsy studies show that tumor cells are shed much earlier than expected, even without detection of a primary tumor [36-40]. Tumor kinetics and mathematical modeling provided further evidence for the model of parallel progression, which posits that tumor cells disseminate along the course of primary tumor development rather than in sequential steps [35, 41, 42]. Parallel progression implies that DTCs leave the tumor at unsynchronized times and thus metastases sampled at a single timepoint may differ genetically from the primary tumor and each other due to clonal expansion under unique evolutionary pressures at the secondary site [43, 44]. This renders metastases difficult to predict and treat successfully based on profiling the primary tumor. It motivates consideration of metastases at different sites as unique species of cancer, at least until demonstrated otherwise. Conversely, the identification of a common weakness or target across metastases would be a powerful clinical tool for the clinic to overcome inter-patient, inter-lesion heterogeneity [45, 46].

1.2.3 *Challenges in treating metastasis*

Effective treatment of primary breast tumors based on advances in endocrine and targeted agents against subtypes has contributed to the overall decline in breast cancer mortalities in

recent decades [17]. However, there is no standard treatment for metastatic breast cancer [47], which is treated like a primary tumor yet may have evolved under very different circumstances and even switched subtypes [48]. Chemotherapy including anthracyclines (e.g., doxorubicin, epirubicin), taxanes, methotrexate, and 5-fluorouracil targets DNA replication, which is countered by DTCs entering cell cycle arrest or through microenvironment-driven mechanisms of chemoprotection [49]. Hormone and $HER2^+$ targeted therapies are approved for metastatic breast cancer [50], yet outside of the $HER2^+$ subgroup there has been no improvement in disease-free or overall survival over recent decades [5, 51]. Due to these clinical disappointments, the paradigm for treating metastatic breast cancer tends to be palliative rather than curative [17].

New therapeutic modalities offer hope for treating the moving target of metastatic disease. Antibody-drug conjugates, which deliver cytotoxic drugs based on binding to selected targets, elicit a rapid response and may be an effective counter to metastatic evolution [52]. Immunomodulators targeting the PD-1/PD-L1 pathway in combination with chemotherapy [53, 54] were approved for metastatic breast cancer by the FDA in 2019. However, more effective therapy for metastatic breast cancer patients is critically needed, underscoring a need to deepen our understanding of the biology behind metastasis. For example, we are currently unable to predict the timing and location of relapse for an individual patient, leaving it up to "watch and wait" mentality for what we know will happen to 1 in 5 patients in the decades following treatment [7, 55, 56]. Rather than continue to apply the treatment for one disease (localized primary tumor) to another (metastatic cancer), it may be more efficacious to leverage what is known about the natural history and dependencies of metastatic cancer to generate new paradigms of treatment.

Chapter 2. TUMOR DORMANCY

Although dissemination of tumor cells occurs from an early stage in tumor progression, it may be years before metastases are clinically detected—in long-term follow-up of breast cancer patients given endocrine therapy for five years, metastases continued to emerge up to 10 to 15 years post-treatment [7, 55-57]. The biological source of so-called delayed relapse has been postulated to be dormant tumor cells sitting throughout the tissue that are triggered to grow by unknown stimuli. More than 30% of breast cancer patients have bone marrow micrometastases at the time of diagnosis [58], and thus tumor dormancy may affect a significant proportion of the metastatic patients. Deciphering the regulation of dormant tumor cell behavior may generate significant clinical insights to mitigate the risk of future metastases, prior to their awakening [59].

The term "tumor dormancy" is somewhat vague, as it refers to both cell cycle arrest of individual tumor cells (cellular dormancy) and population-level dormancy brought about by a balance of tumor proliferation and death (via insufficient angiogenesis, immune editing, etc.). This works focuses on cellular dormancy, which is defined by long-term survival, reversible quiescence, and resistance to chemotherapy [1, 59]. A fourth hallmark, immune evasion, has been suggested on the basis of rare DTC encounters with immune cells, downregulation of MHC class I, and immune dysfunction in certain tissue niches [60]. The sum of these characteristics is that dormant DTCs essentially go 'off the grid,' in terms of clinical and even immunological detection. Yet, they retain the potential to initiate metastatic growth and thus represent the seeds of future metastases. Although we lack direct evidence that late-arising metastases in patients originate from dormant DTCs, a wealth of clinical evidence, experimental studies, tumor growth modeling, and logical deduction has built the case for the reality of tumor dormancy. Further, the

latency window may be proactively utilized to prevent the outgrowth of DTCs prior to their relapse at an unknown later point [59].

2.1 DEFINING DORMANCY

2.1.1 *A brief history of tumor dormancy*

Rupert Willis formally introduced the concept of "tumor dormancy" in 1934 to account for seemingly inert tumor cells observed in autopsied tissues [61]. He was not the first to document these ectopic cells that seemed to contradict cancer's defining quality of voracious and unbridled growth. The growing consensus among clinicians was that, upon careful examination only possible during autopsies, DTCs could be found throughout most tissues and in far greater numbers than metastases [62]. Ernst Fuchs' idea of tissue predisposition [63] and Stephen Paget's seed and soil hypothesis [62] helped frame in broad terms that certain tissues are more amenable to metastasis than others depending on cancer type; yet, the observation that many tissues contain DTCs argued that colonization, rather than dissemination, is the limiting factor [62]. Twenty years after Willis, the pathologist Geoffrey Hadfield noted in 1954 that, "The anatomical site of these minute quiescent growths must be significant, for in at least 50% of cases of malignant disease recurring after latent periods…was found in the haemopoietic bone marrow" [64]. This is one of the earliest claims that metastases display a tissue preference [65]. Judah Folkman then presented the concept of population-level dormancy due to a dependence on angiogenesis [66]. The concept of the stem cell niche [67] paved the way for analogous conclusions to be drawn for external regulation of tumor dormancy, which was subsequently validated in studies showing that ECM components [68] and niche-specific factors [69] regulated DTC proliferation, survival, and chemoresistance[49].

2.1.2 *Defining terms: What does "dormancy" mean?*

Dormancy refers to both cellular dormancy and population-based dormancy. The latter is more accurately described as a balance of proliferation and death, when growth is antagonized by insufficient nutrients in the environment. It is often related to the inability to induce neo-angiogenesis [70] or recognition and elimination by the immune system upon reaching a certain size [60]. The emerging definition of cellular dormancy is a state of reversible mitotic arrest (quiescence), long-term viability, chemoresistance, and immune-resistance among individual DTCs [59, 60]. Many of these properties are facilitated by signaling from the microenvironment, and it is unknown how much of the dormancy phenotype is pre-determined or acquired prior to extravasation in the tissue, i.e., during the dissemination process.

Quiescence describes a temporary, extended exit from the cell cycle into G0-G1 phase that is distinct from senescence, the permanent loss of proliferative potential [71]. Quiescence has been supported in the tumor dormancy context by experimental and mathematical models [72]. It may arise when growth factors are withdrawn from the environment, leading to downregulation of cell cycle proteins, or through induction of cell cycle inhibitors, conditions which are not mutually exclusive [71]. Examples of non-malignant quiescence in the adult body include hematopoietic stem cells in the bone marrow which are maintained through a plurality of signals derived from the bone microenvironment [73].

Different levels or depths of quiescence have been postulated based on the initiating signal (loss of mitogens versus loss of cell-ECM or cell-cell contacts) [74], although thus far quiescence generally remains a binary distinction in the field. There is no universal definition of quiescence in the tumor dormancy literature, with reports of experimental dormancy ranging from three weeks to eight months of minimal proliferation in the tissue [75-79]. The absence of nuclear protein Ki-67 is a widely-accepted marker of quiescence [75, 76, 80], since it coats

heterochromatin as a chromosomal surfactant and is degraded in G0-G1 phase [81, 82]. Alternatively, some studies use cell cycle inhibitor expression (e.g., p21, p27, p38, p53) [78, 83], fluorescent cell cycle protein systems (e.g., FUCCI) [84], or labelling dye [85, 86] to report on quiescence. It is important to consider that many studies analyze DTCs at a single moment in time (i.e., through fixation and staining), and thus the length of time to establish dormancy is as important as cell cycle marker status, which may be transient. Although dormant DTCs are not actively dividing, they remain dynamic and responsive to stimuli, demonstrated by long-term intravital imaging studies showing non-dividing DTC motility in the brain [87] and the re-engagement of proliferation upon introduction of growth cues into the environment [88]. Thus, dormant DTCs can be considered "poised" in their metastatic potential rather than frozen. It is not currently known what proportion of DTCs in the tissue retain this metastatic potential.

The processes that maintain long-term viability in DTCs are not as well defined. Clinical studies showing that delayed relapse can occur up to 25 years after treatment in breast cancer patients[55, 56] indicate that DTCs may be extremely long-lived. Experimental models showed that *ex vivo* isolation of viable DTCs could be achieved six months after introduction to the mouse [77], which correlates with approximately one-fifth of the mouse lifespan [89]. Mechanistically, autophagy has been shown to directly allow dormant breast cancer DTCs to survive the accumulation of damage from reactive oxygen species (ROS) over time [90].

Chemoresistance refers to the ability to survive cytotoxic therapies that would otherwise kill tumor cells. Evidence for DTC chemoresistance can be found in the steady increase in risk of delayed relapse over time following treatment [7] and in animal studies indicating that some DTCs are not eliminated by chemotherapy [91]. Chemoresistance has been suggested to be a function of reduced proliferation among quiescent cells, since many chemotherapeutics target

DNA replication machinery. Drugs in this class may thus select for non-proliferating DTCs, which displayed little DNA damage after 5-FU treatment [83]. Conversely, chemotherapy may be the actual driver of dormancy by triggering stress pathways which reduce cell proliferation, such as p53 and MET [92]. Chemoresistance can also occur in a cell-cycle independent manner through stromal protection. Carlson, *et al*., showed that the vascular endothelium chemoprotected non-dividing tumor cells through tumor integrin signaling, and that DTCs could be sensitized to treatment by interfering with these integrin pathways [49]. Other studies corroborate these findings by showing that chemotherapy elicits evolution in the DTC niche, altering paracrine signaling that ultimately promotes DTC survival through CXCL1/2 [93]. Thus, whether as a function of their proliferation status or through a protective microenvironment, dormant DTCs selectively survive in the face of chemotherapy

2.2 EVIDENCE FOR TUMOR DORMANCY IN DISEASE

It is a matter of some controversy whether non-proliferative tumor cells initiate late metastasis in patients, since it is not feasible to follow individual tumor cells from dissemination to metastatic colonization over years in a patient. Dissemination has been shown to occur early in tumor progression [40, 94-96], spreading single cells and rare clusters throughout the body, but it has never been observed directly that metastases arise from dormant DTCs in humans.

2.2.1 *Clinical evidence for tumor dormancy*

Several lines of clinical evidence support tumor dormancy, especially in breast cancer. Autopsy studies indicate that asymptomatic DTCs are frequently found throughout the tissue of patients where they reside as single, apparently non-dividing cells [62, 97]. Tissues from donors who previously had malignant disease developed metastases in the recipient without a matched

primary tumor, indicating the apparently "clean" tissue had residual disease [98]. Further, this unexpected outcome suggests that seemingly inactive DTCs were stimulated into metastatic outgrowth upon the trauma of surgery or the new environment. The presence of bone marrow DTCs at the time of diagnosis predicts late relapse [99], and one-fifth of breast cancer patients with no other symptoms relapse 7-25 years after treatment [55, 56]. Adjuvant therapy reduces the rate of early and intermediate relapse but not late relapse (defined as 10 years post-treatment) suggesting that late responders are refractory to therapy[100]. Critically, a clinical trial designed to sample the bone marrow at subsequent intervals after adjuvant therapy found that patients with residual disease were significantly more likely to recur, and sooner, than those without residual disease [101], indicating that persistent bone marrow DTCs are a source for delayed relapse. These studies emphasize that the current limits of clinical detection may not be sufficient to track residual disease, which poses a continuous threat even to the "cured" patient.

2.2.2 *Experimental evidence for tumor dormancy*

Experimental models have helped fill in the gaps in the biological understanding of dormancy. In mouse models of breast cancer, DTCs can survive at least four to eight months as quiescent single cells in organs like the lung or liver[75, 77, 86]. Strong experimental evidence for tumor cell quiescence comes from studies in which tumor cells are inoculated into the animal, then isolated as single cells from tissue and expanded in culture, demonstrating that they retain the capacity for proliferation after quiescence [77, 86, 102]. Parallel studies with *ex vivo* patient bone marrow-derived DTCs confirm that human DTCs share these characteristics[102], validating mouse models of dormancy for the study of a complex human disease. Modern studies have subsequently confirmed clonal expansion from single DTCs to full metastases using

fluorescence [103, 104] or barcode [105-107] based lineage tracing, and models of tumor dormancy across tissues are explored in Chapter 3.

Chapter 3. TISSUE-SPECIFIC DETERMINANTS OF DORMANCY AND AWAKENING

A key observation from the early experimental studies of dormancy was that mammary carcinoma DTCs isolated from the bone marrow, cultured, and re-inoculated in mice were able to form primary tumors in the mammary gland but not the bone marrow [102]. This recurrent pattern of growth-permissive versus growth-suppressive tissues demonstrates that tumor cells capable of growth in "ideal" conditions (*e.g.*, cell culture, the orthotopic site) are constrained at other locations, indicating that extrinsic mechanisms restrain metastatic growth. Autopsy studies confirmed that certain cancer types have a propensity to emerge in certain tissues [62, 108]: for breast cancer, these susceptible tissues include the bones, lungs, liver, brain, and lymph nodes [108]. Stephen Paget's careful examination of 735 women who died of breast cancer inspired his famous seed and soil hypothesis, which postulates that certain tissues are more fertile sites for metastasis than others[62]. Since DTCs spread throughout the body but do not all yield metastases [97], successful metastatic growth is the exception rather than the rule.

What makes a tissue "fertile" or "infertile" (that is, permissive or refractory to metastasis) is an area of great interest to the field and the clinic, since it could inform a patient's risk for late recurrence. Further, a better understanding of external mechanisms of regulation may lead to new therapeutic approaches to control DTC behavior in patients.

The use of animal models has allowed mechanisms of dormancy to be deciphered on a tissue-by-tissue basis, and much work has unveiled tissue-specific signals that contribute to quiescence, survival, and chemoresistance[1] (**Table 1**). The diversity of mechanisms employed by both the stroma and DTCs to regulate dormancy is reminiscent of a host-pathogen arms race in which DTCs are constantly forced to adapt to new, potentially hostile environments to survive. For example, dissemination to the liver triggers endoplasmic reticulum stress in pancreatic

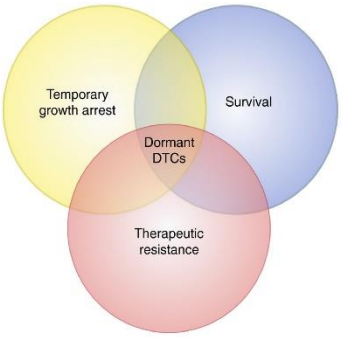

Organ	Molecule	Ref.
Lung	BMP4	(Gao, Chakraborty et al. 2012)(Lee, Bhang et al. 2014)
	TSP1	(Lee, Bhang et al. 2014)(Ghajar, Peinado et al. 2013)
	CXCL12	(Phillips, Burdick et al. 2003)
	TNF	(Acharyya, Oskarsson et al. 2012)
Bone	ANG1	(Arai, Hirao et al. 2004)
	BMP7	(Kobayashi, Okuda et al. 2011)
	CXCL4	(Bruns, Lucas et al. 2014)
	CXCL12	(Price, Burness et al. 2016)
	E-selectin	(Price, Burness et al. 2016)
	GAS6	(Shiozawa, Pedersen et al. 2010)
	LIF	(Johnson, Finger et al. 2016)
	SCF	(Ding, Saunders et al. 2012, Ding and Morrison 2013)
	TGF-β2	(Bragado, Estrada et al. 2013)
	TSP1	(Ghajar, Peinado et al. 2013)
	CXCL12	(Shiozawa, Pedersen et al. 2010)
	CXCL12	(Becker 2012)
	Osteopontin	(Boyerinas, Zafrir et al. 2013)
Brain	Ephrin B2	(Ottone, Krusche et al. 2014)
	CXCL12	(Gatti, Pattarozzi et al. 2013)
	Laminins	(Lathia, Gallagher et al. 2010)(Lathia, Li et al. 2012)
	Notch ligands	(Zhu, Costello et al. 2011)
	Osteopontin	(Pietras, Katz et al. 2014)
	Nitric oxide	(Charles, Ozawa et al. 2010)
	Osteopontin	(Pietras, Katz et al. 2014)
Liver	sJAG1	(Lu, Ye et al. 2013)(Cao, Ding et al. 2014)
Thymus	IL-6	(Gilbert and Hemann 2010)
Lymph node	Unknown	

Table 1. Tissue-specific molecules that contribute to dormancy. Molecules are categorized by their contribution to quiescence (yellow), survival (blue), or chemoresistance (red). Currently, there are no known molecules that contribute to tumor dormancy in the lymph node [1].

DTCs that push them into latency, yet coincides with MHCI downregulation, allowing them to evade immunity [76]. Conversely, other tissues contain pre-existing biological infrastructure seemingly tailored to foster dormant DTCs: for example, HSC niches in the bone marrow are occupied and even outcompeted for by DTCs, which then benefit from the microenvironment signals intended to preserve HSC stemness[109].

A longitudinal perspective of tumor dormancy across tissues reveals common themes that are critical for tumor dormancy: (1) the prominent role of the perivascular niche, (2) co-option of

pre-existing quiescent niches, (3) the requirement for site-specific adaption, especially metabolic adaption, (4) immune evasion or suppression, and (5) tissue dysregulation as a trigger for metastatic outgrowth. These themes help identify which mechanisms may be crucial to control the trajectory of tumor dormancy in the clinical setting. Further, they inform future studies of less well-studied tissues and even organs that rarely foster metastases [110], which may provide useful clues to prevent dormancy systemically. To build a foundation to approach these questions, tissue-specific mechanisms of dormancy and awakening will be discussed in detail.

3.1 BONE

The bones are the third most common major organ site of all solid tumor metastasis after liver and lung [108], reflected in the high rate of incidence of bone metastasis at diagnosis [111] and 10-year follow up [112]. A meta-analysis of SEER bone metastasis data found that 88.4% of metastatic prostate cancer patients have detectable bone metastases at diagnosis, followed by breast (53.71%), renal (38.65%), and lung adenocarcinoma (36.86%) [111]. Bone metastasis results in the painful destruction of hard bone and nerves, soft tissue inflammation, risk of fracture, and debilitation of the hematopoietic stem cell pool.

Tumor cell dissemination to the bone occurs frequently, as marrow aspirates reveal that 15.0-30.6% of breast cancer patients [58, 113-115], and 57% of prostate cancer patients [116] who show no other evidence of disease harbor bone DTCs or micrometastases, and these correlate with worsened outcomes. The prevalence of DTCs in the bone has been attributed to two factors: 1) the low blood pressure system of the sinusoidal beds, which aids in DTC extravasation [117]; and 2) DTC homing to the bone marrow via chemoattractant gradients including CXCL12 (SDF-1) via CXCR4 [118, 119]. The presence of DTCs in the bone predicts late relapse at that site and elsewhere [58, 99, 113, 114, 120, 121]; however, the discrepancy

between high incidence of bone DTCs and relatively few detectable metastases in clinical observation and pre-clinical models [122] suggests growth-restrictive mechanisms in this niche.

3.1.1 *The bone microenvironment*

The bone is composed of hard, cancellous bone matrix surrounding an inner medullary cavity filled with vascularized fatty marrow. The inner surface of the hard bone, the endosteum, is a dynamic surface for cell interactions. It undergoes cycles of bone absorption and remodeling mediated by osteoclasts and osteoblasts, respectively, at punctuated sites across an otherwise homeostatic landscape[123, 124]. Arteries pass through the trabecular bone to the central cavity, emerging from the endosteum as arterioles. The endosteum therefore interfaces closely with arterioles, and associated cells including nestin promoter $(Nes)^+$ neural/glia antigen 2$(NG2)^+$ αSMA^+ mesenchymal stem cells (MSCs)[125], sympathetic neurons and associated non-myelinating Schwann cells [126], adipocytes, and bone-specific immune cells [127-129]. Arterioles extend into the central cavity where they transition into venous sinusoids which serve as the route of egress for mobilized bone marrow cells (**Fig. 2**). Sinusoidal vessels form a distinct vascular niche that includes immune cells and several lineages of mesenchymal-derived cells bearing overlapping markers: CXCL12-abundant reticular (CAR) cells [130, 131], leptin receptor $(LepR)^+$ cells, Nes^+ cells, and $NG2^+$ cells, collectively referred to here as MSCs (reviewed extensively in [132]) (**Fig. 2**). Another critical resident of the bone marrow is the hematopoietic stem cell (HSC), long-lived and reversibly quiescent stem cells that populate the blood lineages. The HSC niche is powerfully quiescent, and HSCs can be found in endosteal [133-137], arteriolar [138], and sinusoidal [137, 139, 140] compartments under the influence of

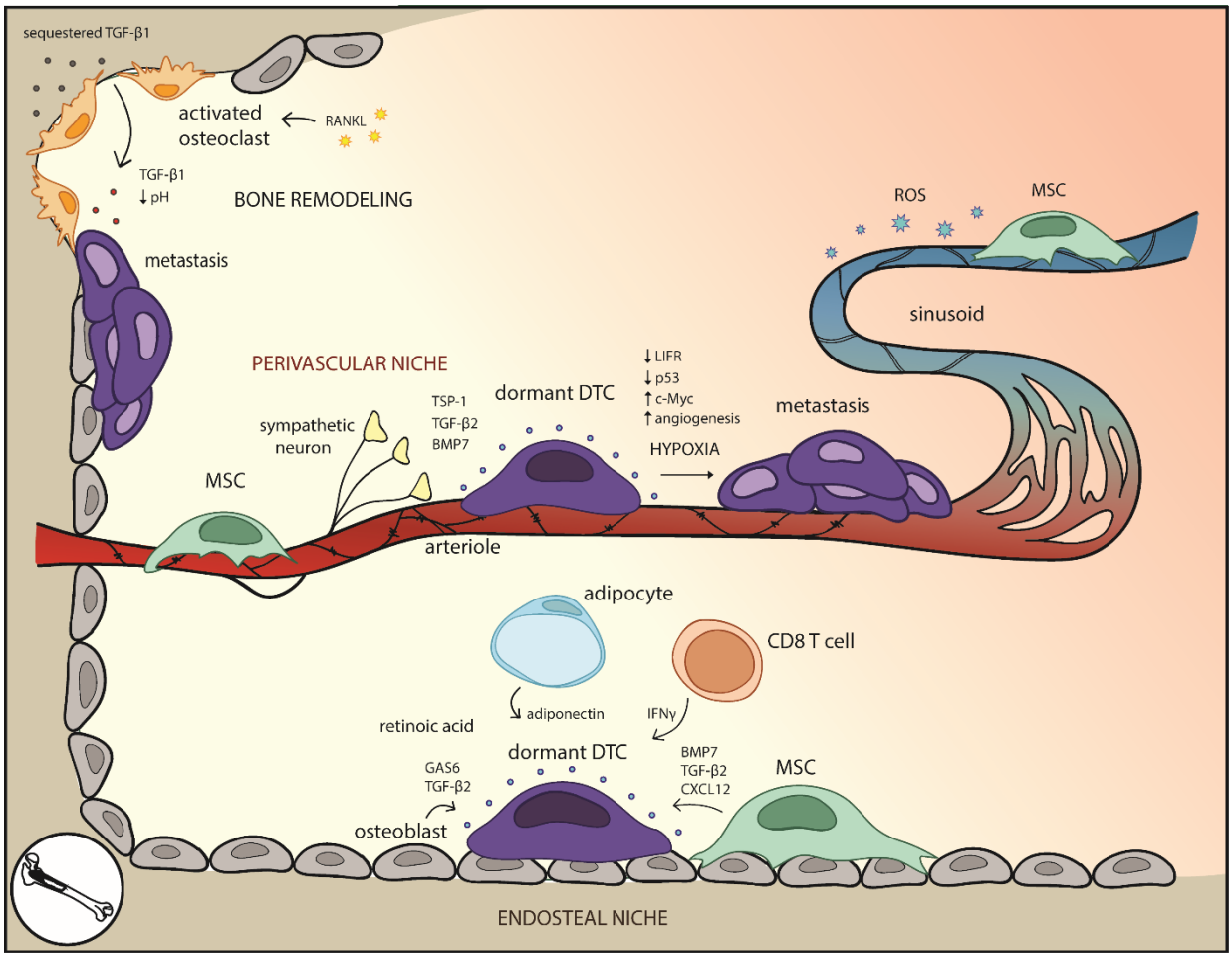

Fig. 2. The bone marrow microenvironment for dormant DTCs. DTCs co-opt quiescent niches that maintain HSC stemness and quiescence, including the endosteal and perivascular niches. Angiocrine, neural, and other stromal factors maintain quiescence in the perivascular niche, which is formed by both the arteriolar and sinusoidal vessels. Hypoxia can induce angiogenesis, resulting in loss of quiescence factors and metastatic outgrowth. At the endosteal surface, osteoblasts and stromal cells maintain DTC dormancy, but bone remodeling by osteoclasts can release TGF-β1 from cancellous bone, resulting in local acidification and metastasis as part of the "vicious cycle."

osteoblastic cells, MSCs, neurons, and endothelia. The HSC capacity for reversible quiescence while maintaining stemness is remarkably similar to properties of dormant DTCs, and therefore many studies have investigated parallel mechanisms of regulation (reviewed in [141]).

Animal models show that the endosteal niche [118, 122] and the perivascular niche [69, 139, 142, 143] harbor DTCs, and identifying the specific interactions that enable and regulate tumor dormancy is the next critical step. There is substantial overlap between the endosteal niche and endothelial niche considering that the endosteum interfaces with arterioles (reportedly, 90%

of osteoblasts are within 20 μm of a blood vessel [144]), but unique features of each niche drive distinct quiescence programs.

3.1.2 *The endosteal niche*

The endosteum is a primary niche for HSCs and can be co-opted by DTCs. Osteoblasts secrete pro-quiescence factors like osteopontin [145, 146] and growth arrest specific-6 (GAS6), which regulates cell division through binding specific TAM (Tyro3/Sky, Axl, Mer)-family receptor kinases: Tyro3 induces cell division while Axl promotes quiescence via ERK1/2 signaling, survival, and chemoresistance [109, 147]. Notably, slow-cycling prostate cancer cells [147] and quiescent multiple myeloma cells [122] in the bone express high levels of Axl. DTC binding to osteoblasts [148] or osteoclasts [109] upregulates Axl, which is stabilized by the hypoxic environment of the endosteal niche [149]. Despite its anti-proliferative effects, Axl cannot maintain long-term dormancy on its own, indicating that it collaborates with other quiescence drivers [150].

Osteoblasts also secrete transforming growth factor beta (TGF-β) family members, which suppress tumor progression at early stages through activation of cyclin-dependent kinase (CDK) inhibitors [151-153] (reviewed in the tumor dormancy context in [154]). TGF-β1 is a key component of the vicious cycle of bone metastasis [155]; conversely, TGF-β2 limits DTC growth. Osteoblast-derived TGF-β2 induced quiescence in prostate cancer DTCs through TGF-β receptor RI (TβRI) and TβRIII [156], similar to its effect on head and neck squamous cell carcinoma DTCs through p38α/β, p27, and DEC2 upregulation and CDK4 downregulation [78]. DTCs themselves express elevated levels of TGF-β2 mRNA [157], which can be induced by Axl-GAS6 binding [148]. Endosteal $NG2^{+}$/$Nestin^{+}$ MSCs produce TGF-β2 and BMP7, which promote breast and HNSCC DTC dormancy in bone [158]. Estrogen-receptor positive breast

cancer patients with high levels of TGF-β2 and BMP7 in the bone marrow experience decreased risk of systemic recurrence and prolonged metastasis-free survival [158]. These studies collectively support the quiescence-promoting role of bone marrow TGF-β2 signaling and suggest therapeutic avenues to restrict metastatic growth.

In addition to TGF-β2, MSC-derived BMP7 promotes a quiescent epithelial phenotype for prostate cancer DTCs [159] through a Smad-independent pathway involving p38, p21, p27, and NDRG1 [160]. Intriguingly, MSC BMP7 can be induced by SPARC secreted by indolent prostate cancer DTCs, revealing that DTCs actively elicit support from their microenvironment [161]. MSCs also secrete CXCL12, which promotes quiescence of chronic myeloid leukemia stem cells [162], on top of its well-studied roles in bone marrow trafficking and HSC maintenance [163]. MSC-derived exosomes containing microRNAs like miRNA-23b [164] and miRNA-222/223 [165] induced quiescence and chemoresistance in breast cancer cells in culture and *in vivo*. The breadth of mechanisms through which MSCs interact with DTCs underscores their diverse functions as master regulators and maintainers of homeostasis within the bone microenvironment (**Fig. 2**).

Bidirectional interactions between DTCs and their niche have been identified in myeloma [122], breast [166], and prostate cancer [148, 161]. Breast cancer DTCs bias osteoblasts through direct contact to decrease secretions of IL-6, MMP3, and type I collagen [166], molecules shown to elicit proliferation [167, 168]. Direct co-culture of tumor-experienced osteoblasts and breast cancer cells results in increased p21 in the cancer cells, indicating that DTC-associated osteoblasts induce DTC cell cycle arrest through direct signaling and altered ECM deposition [166].

Acellular factors like oxygen tension also affect DTC behavior. Despite high

vascularization throughout the bone marrow, hypoxic regions along the endosteum support HSC stemness by minimizing DNA damage from free radicals [169-171]. However, hypoxia may also promote escape from dormancy by inducing angiogenesis [69] and repressing leukemia inhibitory factor receptor (LIFR) in a hypoxia-induced factor (HIF)-independent manner [169]. LIF ligand is an IL-6-family cytokine that promotes proliferation in primary tumors [172] but inhibits DTC proliferation in the bone [169]. LIFR knockdown in different breast cancer cell lines correlated with decreased expression of quiescence and stemness genes including thrombospondin-1 (Tsp-1), TGF-β2, and p53, as well as increased expression of proliferative genes c-Myc and pSrc, suggesting that LIFR is an environmentally-tuned gatekeeper for dormancy [169]. The seemingly contradictory role of hypoxia in the stem cell versus DTC niches reflects a nuanced balance between protection from free radical damage versus hypoxic stress.

3.1.3 *The perivascular niche*

In bone marrow, the perivascular niche refers to the microenvironment in and around arterioles concentrated at the endosteum and the sinusoids located in the central bone marrow cavity [173]. Arterioles are tight, VE-cadherin^{hi} vessels supported by NG2^{+} MSCs, sympathetic nerves, and associated non-myelinating Schwann cells, whereas sinusoids are fenestrated, leaky vessels supported by CAR^{+} LepR^{+} MSCs. There is evidence that both niches support HSCs: quiescent HSCs depart from arterioles when activated by radiation injury [174] and in a mouse model of overactive HSCs[138]; in contrast, up to 85% of HSCs may be perisinusoidal [137, 139]. Differences in vessel permeability regulate HSC differentiation via ROS, with ROS^{low} arterioles maintaining HSC stemness and ROS^{high} sinusoids promoting HSC activation [175]. In the tumor context, spontaneously dormant DTCs preferentially reside in the perisinusoidal niche in the calvarium, whereas micrometastases are only detected in non-sinusoidal, non-perivascular

regions [143]. Although these studies do not resolve the discrepancy between the arteriolar and sinusoidal niches, they provide strong evidence that the perivascular niche is critical for maintaining DTC dormancy.

Endothelia comprising blood vessels are the first residents of a tissue to interact with extravasating DTCs. Mouse models show that quiescent DTCs preferentially reside on the basal side of vessels in bone marrow [69] where they are exposed to quiescence factors including TSP-1, TGF-β2, and BMP7 [158, 160, 176]. The perivascular niche chemoprotects DTCs through integrin signaling, in a manner distinct from quiescence regulation[49]. Doxorubicin treatment selected for perivascular DTC survival, and knocking down integrins β1 or αvβ3 in tumor cells or their ligands (VCAM-1 or von Willebrand Factor, respectively) in an organotypic co-culture model of the bone marrow ablated the chemoprotective effect without altering proliferation. Inhibiting these integrins resulted in substantially fewer bone metastases (but was not totally preventative), providing a strategy to disrupt this protection [49].

3.1.4 *Other bone marrow niche components that regulate tumor dormancy*

Sympathetic nerve fibers and nonmyelinating Schwann cells regulate HSC quiescence through β-adrenergic signaling [138, 177] and TGF-β1 [126]. Given the parallel nature of the HSC and DTC niches, neural components regulate DTC quiescence through proliferative norepinephrine and through downregulation of osteoblastic GAS6 [178]. Chronic stress activated the sympathetic nervous system to induce RANKL signaling in osteoblasts, promoting breast cancer migration to the bone [179]. These studies highlight the neural response to stress that can, in turn, affect metastasis.

Adipocytes fill the spongy marrow of the central cavity, stratified into adipocyte-rich yellow marrow and adipocyte-poor red marrow. Red marrow is enriched in HSC activity,

whereas yellow marrow suppresses hematopoiesis through pro-quiescent cytokines like adiponectin [180, 181], leading to the question of how adipocytes influence DTCs. Adipocyte-rich environments inhibited T-cell acute lymphoblastic leukemia (T-ALL) proliferation, resulting in slow-cycling, metabolically-altered, chemoresistant DTCs [182], and chemoprotected multiple myeloma cells through inducing anti-apoptotic autophagy [183]. Future studies should assess the effect of adipocytes on solid tumor DTCs.

Acellular environmental factors also play prominent roles in the dormancy niche. Fibrillar fibronectin associated with urokinase plasminogen activator receptor suppresses p38 and de-represses ERK1/2 in tumor cells [68]. The result is akin to simultaneously accelerating and lifting the breaks off dormant DTC growth. Environmental retinoic acid (RA) maintains HSC stemness [184], so it is no surprise that RA promotes DTC survival and cell cycle arrest through the orphan receptor NR2F1 and transcription factor NANOG [80]. This mechanism is bone marrow-specific, as RA promotes quiescence in other tissues like the lung [80].

3.1.5 *Immune regulation of bone dormancy*

As the site of B cell production, the bone marrow is a critical immune organ[185]. Immune profiling DTC^+ patient bone marrow revealed an overall depletion of $CD3^+$ T cells but enrichment for tumor antigen-specific T cells, suggesting active immunity that DTCs manage to evade[186]. DTCs may escape immune recognition through downregulating MHCI[187], so enhancing antigen presentation (e.g., via interferon gamma (IFNγ) treatment) may enhance endogenous immunity. IFNγ induced DTC dormancy through antiproliferative STAT1 signaling [188] and cyclin suppression[189], mirroring $CD8^+$ T cell IFNγ induction of B cell leukemia cell cycle arrest [190]. IFN response genes were lost in proliferating bone-derived prostate cancer DTCs compared to those derived from the lung, and suppressing Type I IFN signals activated

dormant prostate cancer DTCs to generate metastases in the bone [191]. Collectively, these data point to IFN signaling as an immune-derived mediator of dormancy in bone marrow. Perivascular cells such as MSCs may also alter the immune landscape for DTCs by inhibiting $CD4^+$ and $CD8^+$ T cell proliferation [192] and enhancing Treg and Th2 $CD4^+$ T cell proliferation [193], creating a more immunosuppressive environment.

3.1.6 *Activation of quiescent DTCs in the bone*

Activation of quiescent DTCs can be attributed to loss of the quiescent niche. Physiologic bone remodeling provides an illustrative example. The endosteum experiences local upheaval where bone is resorbed and remodeled. Osteoclast-driven resorption sites are rare, representing 1% of the endosteum, while osteoblast-driven remodeling of the bone occurs more frequently, across approximately 20% of the endosteum at a given time [123, 124, 194]. During remodeling, RANKL-activated osteoclasts secrete proteolytic enzymes that dissolve the bone matrix, releasing sequestered growth factors such as TGF-β1 (**Fig. 2**). These enzymes also cleave endosteal factors that maintain HSC and/or DTC quiescence including SCF, CXCL12, and osteopontin [195]. Decreasing oxygen levels and proton release result in an acidified, hypoxic environment [196] that can induce DTC proliferation directly or through angiogenesis [69, 169]. The capillary network directly above remodeling sites increases in density, enhancing trafficking of stromal cells and potentially DTCs as well as undergoing angiogenesis [194]. Endothelial sprouting induces proliferation of dormant breast cancer DTCs through loss of TSP-1 and increased TGF-β1 and periostin (POSTN) in the niche [69]. This is supported by the observation that perivascular cells around remodeling endosteal capillaries increase proliferation [194], alluding to consequences for dormant perivascular DTCs.

The dynamic resorption environment directly activates quiescent DTCs [122], although

the relatively low incidence of remodeling sites may explain the disparity between the frequency of bone DTCs and actual colonization and lesion formation. Activating osteoclasts led to fewer DTC niches and non-dividing myeloma DTCs, but curiously did not correlate with increased overall tumor burden [122]. A two-hit strategy of disturbing the quiescent niche and blocking the immune response would help parse out the source of DTC elimination. Increasing osteoclast activity and recruitment through enhanced VCAM-1 expression was also sufficient to induce dormant mammary DTC activation [197], supporting the role of osteoclasts in dormancy reversal.

The bone marrow is susceptible to changes due to fluctuating hormones during menopause, which is especially relevant for ER^+ breast cancer DTCs. In a modified bone marrow microvascular niche model, loss of estrogen induced angiopoietin-2 expression antagonized endothelial receptor Tie2 and TSP-1, leading to ER^+ breast cancer cell growth on previously suppressive endothelial niches [198]. Menopause may be a key point to anticipate relapse of residual bone marrow disease.

3.1.7 *Therapeutic outlook*

Adjuvant therapies against bone metastases have been successful particularly in breast (50% response) and prostate (70-80% response) cancer [199], but the treatment of dormant DTCs in bone is largely unaddressed. G-CSF mobilizes DTCs from supportive niches [200] and may chemosensitize DTCs when used prior to treatment; conversely, quiescence could be enforced by antagonizing bone resorption. Treatments such as the bisphosphonate zoledronic acid and anti-sclerostin antibodies counter bone resorption by killing osteoclasts [201, 202]; such an approach would preserve quiescent niches to maintain DTC dormancy. However, pharmacological inhibition of niche remodeling was behind the development of anti-RANKL

therapies, targeting a pivotal signaling node associated with osteolytic bone degradation and metastasis [203]. Although anti-RANKL treatment benefitted lung cancer patients [204] and resulted in fewer fractures for postmenopausal breast cancer patients [205], it ultimately did not extend disease-free or bone metastasis-free survival in a large five-year breast cancer clinical trial [2]. Therefore, more approaches to target the bone marrow niche for DTCs are needed.

3.2 LUNG

Breast and colorectal cancer have the highest incidence of metastasis to the lung. In a SEER meta-analysis, 36.4% of metastatic breast cancer patients [206] and 32.9% of metastatic colorectal patients [207] develop lung metastasis, which autopsies indicate could be as high as 71% of metastatic breast cancer patients [208]. Although only 3.6% of metastatic prostate cancer have pulmonary metastasis [209], hormone therapies may enhance this rate through transdifferentiation of the tumor into the androgen therapy resistant neuroendocrine subtype [210, 211], which is more likely to generate visceral metastases [212, 213].

Despite the frequency of lung metastasis, isolated lung metastases without a secondary metastatic site are rare across cancers [214, 215], suggesting that lung metastasis is driven by accessibility and permissiveness rather than site specificity. Nevertheless, the lungs are frequently studied in tumor dormancy, with ECM organization and immune influx as major contributors to dormancy regulation.

3.2.1 *The lung microenvironment*

Human lungs are comprised of five lobes, three on the right and two on the left side of the thoracic cavity. Each lobe contains branching units of alveoli that facilitate gas exchange with the adjacent capillary network. The small capillary diameter may slow circulating tumor

cells to aid extravasation. The alveoli are lined by epithelial sheets line and surrounded by stroma including pericytes, fibroblasts, and mesenchymal stem cells (**Fig. 3**). These cells contribute to the epithelial and endothelial basement membrane of the lungs, provide contractile support, maintain the vasculature, and attract migrating immune cells [216]. The ECM of the lung is primarily composed of collagens, laminin, elastin, and glycosaminoglycans, which contribute to alveolar elasticity [217, 218]. Lung metastases tend to be concentrated in the basal and peripheral regions of the lobes due to their increased vascular density, and, potentially, frequency of DTC extravasation [219].

3.2.2 *Mechanisms of DTC dormancy in the lung*

The lungs are especially prone to metastasis, so it is of great interest to understand tumor progression at this site (**Fig. 3**). Serial passaging breast cancer cells through the lungs generated a lung metastasis signature of 54 genes associated with relapse including chemokines, ECM remodeling proteins, cell adhesion, and transcriptions factors [220]. VCAM-1 was identified as enriched on lung DTCs in a mammary tumor mouse model, enabling newly extravasated DTCs to survive by binding macrophage integrin α4 and activating the PI3K/Akt survival pathway [221]. VCAM-1 expression may be a selection force for pulmonary DTCs since the lungs are leukocyte-rich.

BMP signaling, implicated in bone dormancy [160], is even more active in the lung [222]. BMP4 produced by lung stroma suppresses DTC proliferation through inhibition of stem cell genes Nanog, Sox2, and Oct4 and induction of metastasis suppressors KIAA1199 and NDRG1 [222]. BMP4 is antagonized by the secreted protein Coco. Knocking down Coco imposed dormancy on highly metastatic 4T1 mammary tumor cells in the lung, but did not prevent metastases to brain, bone, or thyroid. Thus, BMP4 regulates lung-specific dormancy in

opposition to Coco [222].

In lung, the perivascular niche is again implicated in promoting DTC dormancy through endothelial TSP-1, which is involved in vessel stability [223] and differentiation of alveolar epithelial cells [224]. Upon disruption of the vasculature due to angiogenesis, TSP-1 is lost around sprouting tip cells, which promotes dormant DTC outgrowth [69].

The lung epithelia constitute a newly described DTC niche and stimulate D2.0R mammary carcinoma expression of SFRP2, which mediates integrin and survival pathways in a Src-dependent manner [79] (**Fig. 3**). SFRP2$^+$ DTCs deposit fibrillar fibronectin and form cell protrusions to engage with the matrix, coinciding with increased lung metastasis. Although the epithelial signal that induced tumor cell SFRP2 was not identified, these results highlight integrin-ECM interactions as key mediators of lung DTC survival. Fibrillar fibronectin and Rho kinase have also been tied to quiescence in a cell culture model of breast cancer, strengthening the association between matrix organization and dormancy [225].

3.2.3 *Immune regulation of lung dormancy*

Several studies suggest that lung DTCs are constrained by the adaptive immune system [60, 226], and slow-cycling breast and lung carcinoma cells downregulate ligands for natural killer group 2 member D (NKG2D) receptors to evade NK cell detection [227]. CD8$^+$ T cell depletion or autologous tumor antigens allowed emergence of previously undetectable DTCs in the lungs from fibrosarcoma [228], melanoma [226], and mammary carcinoma [229, 230], while CD4$^+$ T cell depletion only partially suppressed fibrosarcoma metastasis [228]. Intriguingly, suppression of melanoma and mammary carcinoma metastasis was tied to a cytostatic effect of CD8$^+$ T cells [226, 229]. Metastatic outgrowth could be phenocopied by adoptive transfer of pro-tumorigenic MDSCs, which suppress CD8$^+$ T cell activity [230]. While it is unclear whether

CD8^{+} T cells directly suppressed cell cycle engagement or selected for non-proliferating cells through immune editing, adaptive immunity actively suppresses tumor awakening in the lung.

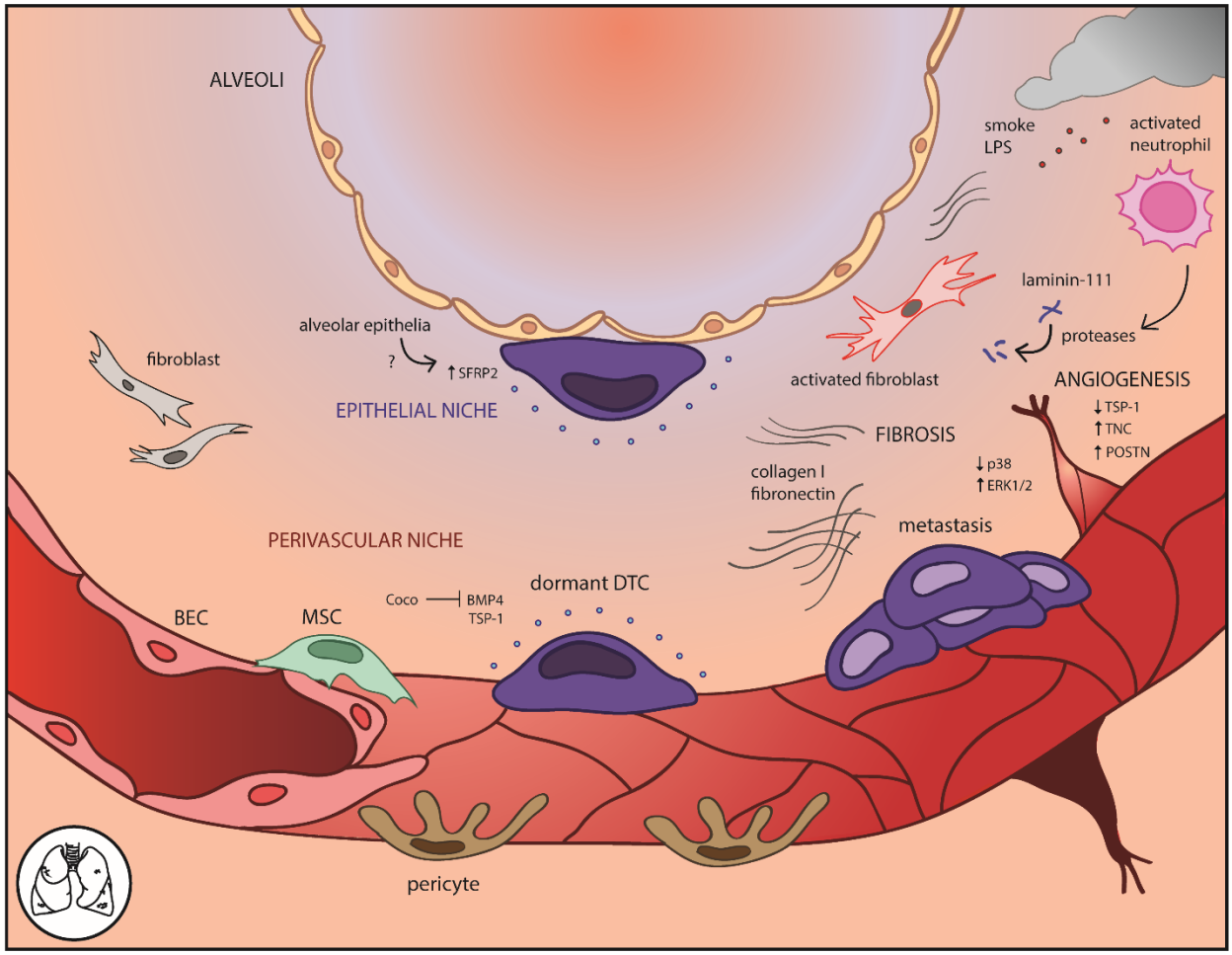

Fig. 3. The lung microenvironment for dormant DTCs. The perivascular niche is the primary source of dormancy factors including angiocrine TSP-1. BMPs are also active in the lung but inhibited by Coco. The newly described epithelial niche induces SFRP2 in DTCs which promotes quiescence through an unknown epithelial factor. Tumor awakening occurs with environmental damage and subsequent inflammation in the lungs, which can induce fibrosis or alter the ECM through activated neutrophils.

3.2.4 *Activation of quiescent DTCs in the lung*

As an air-tissue interface, the lungs are on the frontlines of environmental and pathological insult. Inflammation awakens dormant lung DTCs through influencing DTCs as well as the stroma and immune milieu, indicating that therapeutic strategies targeting

inflammation may be particularly effective in this tissue [231].

The lung ECM is dominated by type I and II collagens, with additional type III collagen and elastin in the alveolar interstitium [217, 218]. The ECM organization becomes altered through environmental insult. Lung fibrosis dominated by collagen I (col-1) enabled integrin β1-mediated outgrowth of dormant mammary D2.0R tumor cells through phosphorylation of Src, FAK, myosin light chain kinase, and actin stress fiber formation[167, 232]. Fibrillar col-1 also promoted metastatic colonization through binding discoidin domain receptor 1 (DDR1) on the tumor cell membrane, subsequently activating PKC/JAK2/STAT3 signaling via syntenin 2 and tetraspanin TM4SF1 [168]. Fibrillar fibronectin led to dormancy awakening through independent but synergistic inhibition of cell cycle repressor p38 and de-repression of ERK1/2 [68]. While lung HNSCC DTCs were not as dormant as those in the bone marrow, p38 was required for short-term HNSCC dormancy [68] and colon cancer dormancy in the lung [233]. Concordantly, MMP-2 degradation of a fibrillar fibronectin matrix led to tumor cell outgrowth in culture [225], further pointing to the importance of ECM architecture to suppress DTC outgrowth.

As the mechanisms underlying the fibrotic awakening response are better understood, it is critical to identify what triggers fibrosis in the first place. Chronic inflammation is a well-known inducer of systemic stress, which can lead to fibrosis. But recently, it was shown that even short, sustained inflammation from either bacterial lipopolysaccharide (LPS) or cigarette smoke can modulate a suppressive niche into a growth permissive one via the immune system. Brief LPS exposure or cigarette smoke activated release of neutrophil extracellular traps (NETs) and proteolytic enzymes that cleaved laminin-111 to liberate a peptide that activates dormant D2.0R DTCs, and cleaved quiescence factor TSP-1, permitting DTC outgrowth [75, 234] (**Fig. 3**). Fibrosis may also be induced by surgery through lysyl oxidase-mediated collagen

crosslinking, which allows metastatic outgrowth of undetectable DTCs in lung [235]. Surgery plays a secondary role in activating T cell-dependent lung metastasis [231]. The effect could be abrogated with anti-inflammatory treatment, linking inflammation to adaptive immunity and tumor progression. This phenomenon appears to hold up in patients [236], offering an inexpensive intervention to counter inflammation and prevent DTC emergence.

Inflammation directly induces EMT of dormant DTCs, the transition from quiescent, differentiated epithelia to an invasive, dedifferentiated mesenchymal phenotype. Different environmental stressors converge on an EMT response, imbuing dormant DTCs with metastatic capability. LPS induced EMT in a latent D2A1 subline through Zeb1, greatly enhancing metastasis in the lung [237]. Hypoxia also induced EMT of DTCs through upregulation of LOXL2 [238]. Canonically a crosslinking enzyme [239], LOXL2 initiated EMT and a stem cell-like phenotype in dormant mammary DTCs, resulting in lung metastasis [238].

Finally, inflammation has been linked to dormancy awakening through angiogenesis and concomitant loss of perivascular quiescence factors and gain of pro-metastatic factors like tenascin-C (TNC) and POSTN [69, 240]. Adult angiogenesis occurs during wound healing, hypoxia, or under oxidative stress, which is especially relevant to the lungs. Notably, TNC can be secreted by lung DTCs themselves to promote survival and invasiveness through Notch/Wnt signaling [241]. DTCs within the lung also instruct the stroma to produce POSTN, which further promotes metastasis [242]. Thus, under inflammatory conditions, dormant DTCs in the lung receive autocrine or paracrine growth cues, ultimately leading to metastatic awakening.

3.3 BRAIN

Brain metastases are detected in 8.5-20% of metastatic patients, most commonly in lung, renal, breast, melanoma, and colorectal cancer [243-246]. Autopsy studies indicate the incidence may be much higher, with up to 30% of breast cancer patients exhibiting metastatic lesions [246, 247]. The incidence of brain metastasis seems to be increasing due to more accurate imaging technologies and systemic therapies that extend patient survival, such as trastuzumab for HER-2^+ breast cancer or taxanes for ovarian cancer [245, 248, 249] (although not all studies agree [243]). The increasing incidence of brain metastasis highlights a critical need to understand the niche(s) that enable DTC survival better so we can identify vulnerabilities and prevent metastasis.

Brain metastases tend to emerge at watershed areas between vascular beds [250]. These regions are supplied by the smallest arteriolar branches, suggesting that vessel diameter aids DTC extravasation. The cerebellum is an overrepresented target for breast and gastrointestinal metastases and the frontal lobe for melanoma metastases when normalized for lobe volume [251], suggesting microenvironmental differences between the different lobes. The distribution of DTCs in different mouse models varies (e.g., brain-tropic MDA-MB-231 breast cancer cells were enriched in the frontal and parietal cortex following intracardiac injection) [252], suggesting species-specific differences that may necessitate new models to understand the differences observed in humans.

3.3.1 *The brain microenvironment*

The brain is a dense network of neurons, glia, and other stromal cells. The immune compartment consists of resident macrophages (microglia) as well as adaptive immune cells and natural killer cells at homeostasis and in disease states such as acute viral infection [253-260].

Fibrous ECM components like fibronectin and collagen are nearly absent from the adult brain, whereas proteoglycans fill the intercellular space and support synaptic contacts [261-263]. Endothelia bearing tight junctions, smooth muscle cells, pericytes, astrocyte endfeet, and neural synapses form a physical and molecular seal between solutes and the central nervous space called the blood-brain barrier (BBB) (**Fig. 4**). The basement membrane (BM) subtly changes between the vasculature and the outer side of the parenchyma (e.g., in laminin composition) [264-266]. Lymphatic vessels, only recently observed in the superficial dura mater, drain excess interstitial fluids but do not penetrate into the gray matter [267, 268].

3.3.2 *Mechanisms of DTC dormancy and activation in the brain*

Cellular dormancy of brain DTCs is not as well-established as in other organs, with notable exceptions [269, 270]. Our understanding of the brain dormancy niche is thus informed by clinical data [243], primary glioma research [271-273], and intravital imaging aided by a literal window to the brain [87, 274] (**Fig. 4**).

Tumor cell dissemination to the brain is not uncommon [97] but nevertheless is extremely strenuous[87, 274, 275]. Certain molecules are required to cross the BBB including the adhesion protein ST6GALNAC5 [276], proteolytic enzyme cathepsin-S [277], chemokine receptor CCR4 [278], and MMP9 for stromal remodeling [274]. Tumor-secreted exosomes containing cell migration-inducing and hyaluranon-binding protein (CEMIP) enhanced brain invasion and vascular interactions [279]. Fittingly, DTC extravasation to the brain takes longer than other tissues [280]. Once in the brain, the next major bottleneck for DTCs is overcoming microenvironmental barriers to growth. The emergence of brain metastasis only after chemotherapy and frequency of delayed relapse of a year or more after initial diagnosis (~28%, 66/232 cancer patients with brain metastasis) [243] suggests two interesting points: 1) that brain

DTCs need time to overcome these barriers to growth, and 2) that DTCs are protected from chemotherapy.

Intravital imaging highlights the critical role of blood vessels in DTC survival. The endothelia are the first cell type that an extravasating DTC encounters, and failure to generate appropriate contacts with vessels leads to cell death [87, 269, 281]. Within this niche, some tumor cells (e.g., melanoma) are highly motile whereas others (lung carcinoma) remain static [87]. DTCs specifically engage in distinct 'spreading' over the vessels via the cell adhesion molecule L1 (L1CAM) (**Fig 4**.), which displaces vessel pericytes and promotes colonization

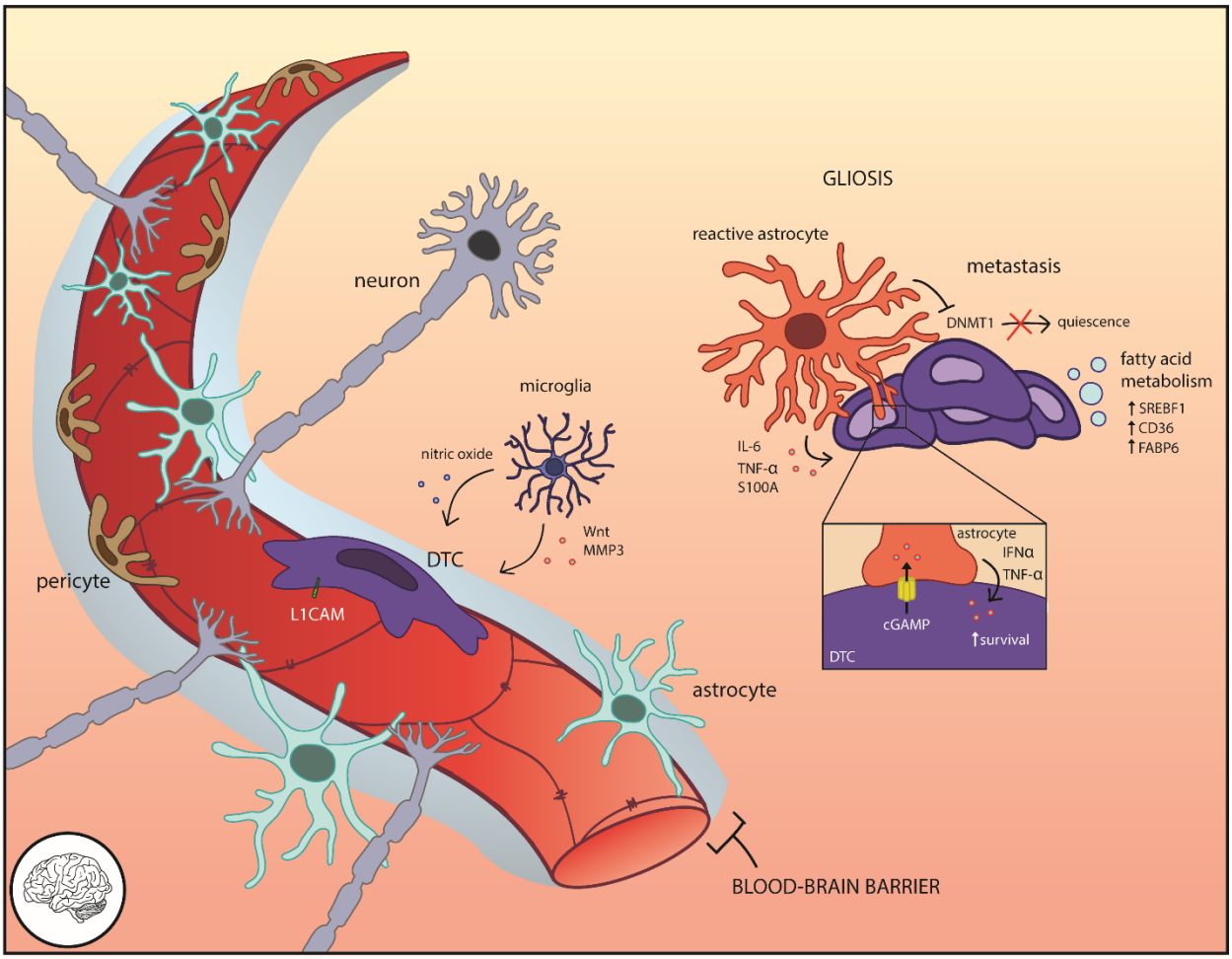

Fig. 4. The brain microenvironment for dormant DTCs. The brain niche for dormant DTCs is not well defined, but intimate association with the brain vasculature is essential for DTC survival. The brain's unique lipid make-up requires that DTC adapt their metabolism to grow. During gliosis, stromal astrocytes activate and secrete inflammatory cytokines that can trigger metastasis. They also engage in direct exchange of molecules with DTCs that promote survival.

through the mechanically-activated Yes-associated protein (YAP) and myocardin-related transcription factor (MTRF) [282]. VEGF-A blockade prevented lung carcinoma DTCs from progressing (ostensibly by stabilizing the vessels [69]) and pushed DTCs to adapt to different vessel interactions[87], highlighting a functional dependency on the vasculature. Brain endothelia provide chemoprotection to murine mammary tumor cells in culture through gap junction communication and secreted endothelin, resulting in 50% reduction of tumor cell death with taxol treatment [283]. When inflamed by tumor-secreted $CEMIP^{+}$ exosomes, the endothelia commence vascular remodeling that promotes metastasis [279].

After emerging on the abluminal side of the vasculature, brain DTCs encounter glial and mural cells that support the vessels. Astrocytes are a significant cellular component of the brain parenchyme. At homeostasis, astrocytes support the integrity of the BBB through endfoot contact with the vessels and expression of Fas ligand, which repels infiltrating lymphocytes [284]. But in response to inflammation, metastasis, or glioma-secreted exosomes, astrocytes undergo reactive gliosis and become pro-metastatic [252, 274, 285-287]. Tumor cells directly transfer cGAMP to astrocytes through gap junctions which activates astrocytes to secrete paracrine IFNα and TNF back to the tumor cells, promoting survival and chemoprotection through STAT1 and NF-κB pathways [288, 289]. Reactive astrocyte gap junctions also chemoprotect DTCs through endothelin-IL-6/IL-8 signaling in breast and lung cancer cells[283], and sequester intracellular calcium from melanoma cells [290]. Reactive astrocytes suppressed DNA methyltransferase 1 (DNMT1) in human melanoma, breast, and lung DTCs through an unknown secreted factor, which activated pro-survival L1CAM and the anti-apoptotic molecular chaperone αB-crystallin (CRYAB) [270]. Astrocytes promote metastatic growth through secreted IL-6 and TNF-α [291] and S100A under systemic estrogen [292]. Strikingly, breast DTCs encouraged neural progenitor

cell differentiation into astrocytes via BMP2, fine-tuning their niche into a permissive environment [293].

However, reactive astrocytes can also prevent metastasis through cytostatic functions. They produce plasminogen activator (PA), which liberates paracrine FasL to kill invading DTCs, and inhibit L1CAM to prevent spreading and vascular co-option[281]. Brain-metastatic DTCs neutralize PA through serpin expression, which is canonically utilized by neurons [281].

The chemical composition of the brain may present an additional barrier to DTC growth. The brain relies on specialized lipids instead of triacylglycerols to support neural activity [294], generating a unique lipid microenvironment to which brain DTCs must metabolically adapt. Two metabolic adaptations have been reported: upregulation of SREBF1, a transcription factor that alters DTC fatty acid metabolism and enables proliferation of micrometastases, and engaging the fatty acid transporter CD36 and fatty acid-binding protein FABP6 to acquire lipids [295].

3.3.3 *Immune regulation of brain dormancy*

Brain DTC-immune cell interactions are similarly context-dependent. Microglia accumulate in or near metastases [138, 274, 296, 297]. They are canonically cytotoxic through secretion of nitric oxide [298] but assist DTC invasion through Wnt signaling [299] and MMP3 activation [300]. Contrary to most organs, inflammation reduced the pro-invasive effect of microglia, underscoring brain-specific protection from excessive inflammation [299]. Microglia-conditioned media upregulated quiescence and survival factors including TSP-1, BCL6, SMAD3, LIF, L1CAM [271] and GAS1 [272] in glioma organoid spheres, and it would be interesting to assess their effect on metastasizing cell types. NK cells actively survey for DTCs, which shed NKG2D ligands upon quiescence [301] and express them with re-entry into the cell cycle, resulting in elimination by NK cells [282].

As more barriers to growth in the brain are elucidated, we will gain a better understanding of the dormancy niche, and the diverse ways DTCs must adapt to co-opt the niche to survive (**Fig. 4**). Future studies should consider the role of adaptive immunity [254, 302], which will be aided by advancing technologies and pre-clinical models of metastasis, *en route* to therapeutic approaches for this devastating aspect of metastasis.

3.4 LIVER

The liver is an enzyme-rich organ that processes metabolites, synthesizes bile, and maintains blood glucose levels. It is the most common major organ site of distant metastases (excluding lymph nodes) [303, 304]: across metastatic patients, liver metastases are most frequently found in colorectal (78%), pancreatic (85%), and esophageal cancers (52%), as well as metastatic breast (30%) and lung (16%) cancer patients [305]. Treatment options for liver metastasis are limited and surgical resection remains the standard of care [306]. Although pre-surgical chemotherapy improves response to resection, it does not significantly benefit survival [307, 308], and relapse within two years following surgery is common [306, 309, 310]. Breast cancer patients experience a 5-year survival rate of 22-41% following liver resection [311, 312]. Thus, better treatment options are crucially needed to manage metastatic liver disease, ideally before surgical intervention.

Tumor dormancy in the liver is well-supported by autopsy and clinical samples [97, 313, 314] as well as experimental models [86, 314-317]. Mammary carcinoma DTCs persist as single cells in the liver for 11 weeks post-injection and reinitiate growth upon *ex vivo* isolation [86]. DTCs access the liver with relative ease through low-pressure, fenestrated sinusoids [318] and intravital imaging confirms that the liver is more prone to DTC extravasation than the lungs [319]. The liver also exhibits high retention rate of tumor cells: meta-analyses determined that

the liver is the most frequent secondary site for metastases, and, conversely, primary liver cancer metastasizes the least compared to other primary tumor types [303, 304]. This paints a picture of the liver as a "sink" from which primary tumors or secondary metastases are less likely to spread. Although the steps of metastatic liver colonization have been described [320], describing interactions between DTCs and the liver niche particularly during dormancy would illuminate the liver niche capacity for supporting dormancy.

3.4.1 *The liver microenvironment*

Macro- and micro-levels of organization foster liver cell specialization and function [321, 322]. Epithelial sheets of hepatocytes, the parenchymal cell that comprises the bulk of the liver mass and functions in metabolism, storage, and bile secretion, converge on central portal tracts made up of a triad of vessels: a portal vein, artery, and bile duct (**Fig. 5**). The portal triad is orthogonally connected to an efferent central vein via fenestrated sinusoids that run between the hepatocyte sheets. The sinusoids are comprised of liver sinusoidal endothelial cells (LSECs) and lack a typical organized basement membrane [323]. 70-80% of the liver's blood supply passes through the low pressure portal vein and the remaining 20-30% comes from the portal artery [318, 324]. These blood supplies intermix as they flow across the sinusoids, another low-pressure system where Kupffer cells, the resident macrophage, reside. The subendothelial Space of Disse drains lymph and contains hepatic stellate cells (HSteCs) that store fat-soluble metabolites like retinoids and produce the majority of ECM fibers in a loose subendothelial basement membrane [325]. HSteCs also have contractile function and regulate sinusoidal blood flow through LSEC-generated nitric oxide and endothelin signaling [326].

Single-cell analysis of the liver revealed stromal subpopulations and specializations across the hepatic zones [321], which radiate outward from the portal triad to the central vein

following an oxygen and nutrient gradient [327]. Zone 1, closest to the portal triad, experiences approximately twice the oxygen tension and higher levels of ROS versus Zone 3, closest to the central vein [328]. Gluconeogenesis and ureagenesis occur in Zone 1, whereas Zone 3 is glycolytic and the site for glutamine synthesis [327]. ECM composition also changes between zones, with Zone 1 rich in type I and III collagens and Zone 3 in collagens IV and VI [329]. LSECs in Zone 3 undergo a greater fibrotic response to cirrhotic injury compared to Zone 1 LSECs, revealing differential vulnerability or activation thresholds across the zones [330]. How zonation impacts tumor dormancy is unknown.

3.4.2 *Mechanisms of DTC dormancy in the liver*

The liver imposes a strong quiescent phenotype on DTCs, as liver-derived mammary DTCs required two to three times as long to resume proliferation *ex vivo* compared to DTCs derived from the lung [315]. Patient autopsies revealed single tumor cells scattered throughout the liver that had not progressed to metastasis [97]. Additionally, primary hepatocellular carcinoma undergoes reversible quiescence and differentiation into normal stroma upon MYC inactivation [331]. Together, these studies indicate the liver microenvironment resists metastatic growth, but few studies have directly addressed the liver dormancy niche. Here, we examine known mechanisms of quiescence and potential dormancy niches to aid in this challenge (**Fig. 5**).

Metabolism is a primary function of the liver, and DTCs need to adapt accordingly in order to survive and grow. Inability to resolve ER stress in pancreatic ductal adenocarcinoma DTCs led to quiescence and, critically, MHCI downregulation, which could be restored through pharmacological relief of ER stress or rescuing unfolded protein response machinery [314]. The immune system plays a key role in selecting for quiescent $MHCI^-$ DTCs: in T cell-depleted mice, quiescent DTCs reverted to an $MHCI^+$ proliferative phenotype, whereas few

DTCs or metastases could be detected in an immune-competent setting [314]. DTCs did not express NKG2D ligands required for NK recognition, so T cells are likely the dominant immune cell. Indeed, a 'wave of apoptosis' has been described in mouse models of hepatic mammary carcinoma metastasis as the immune system eliminates lesions [86]. Although immune recognition can be enhanced through relieving ER stress, this carries the risk of awakening quiescent DTCs. Alternatively, treatment with an ER stressor (tunicamycin) drove DTCs into quiescence, suggesting a strategy for maintaining dormancy if toxicities can be minimized [314]. Thus, adapting to the liver requires a trade-off between metabolic adaptation and immune evasion.

Although the preferential dormancy niche(s) for liver DTCs is unknown, the perisinusoidal space which DTCs are likely to enter upon extravasation is rich in fibrillar collagens type I, III, and V, non-fibrillar collagens type IV and XVIII, as well as basement membrane components including fibronectin, perlecan, and laminins [329, 332, 333]. Type IV collagen promotes both survival and metastasis for liver DTCs [334, 335], and laminins and perlecan are noted quiescence promoters in other tissue sites [336, 337]. *Ex vivo* imaging confirms that vessel association is critical for extravasated DTC survival [319], but must be examined thoroughly in preclinical models.

Hepatocytes induced MET and quiescence in prostate cancer cells via p38 and ERK1/2 within a co-culture model [338]. Prostate and breast cancer models confirm that hepatocytes are critical for DTC quiescence and proliferation-independent chemoresistance [339-341]. Further, breast cancer DTCs adopt an intriguing hepatocyte-like 'replacement' organization in human patients [342], suggesting that communication with the parenchyma is beneficial for DTCs. Co-culture studies indicated that hepatocytes are the primary effectors of tumor quiescence

compared to NPCs [343]; however, growth of HSteCs on plastic activates them and is a surrogate for inflammation [344], which could confoundingly enhance tumor outgrowth. Thus, it is likely that both hepatocytes and NPCs contribute to the dormant DTC phenotype in healthy, homeostatic tissue, which is lost upon stromal activation in response to injury.

Non-parenchymal cells (NPCs) including LSECs, Kupffer cells, and HSteCs support trafficking and quiescence of resident liver cells, and it is conceivable that these mechanisms apply also to DTCs. For example, LSECs attract $CXCR4^{+}$ DTCs via CXCL12 secretion [345] and neutrophil-derived NETs contribute to hepatic arrest [346]. NPCs also engage in reciprocal

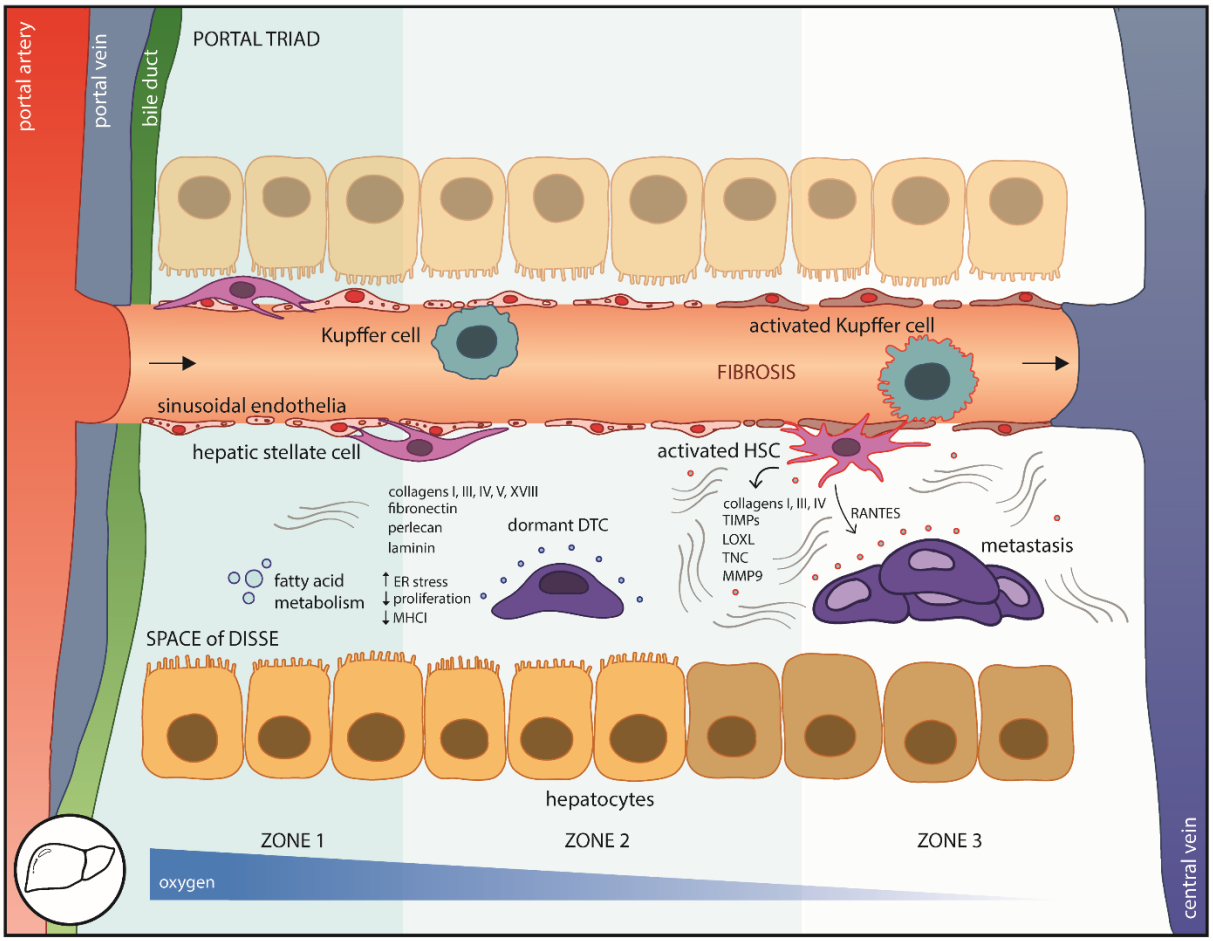

Fig. 5. The liver microenvironment for dormant DTCs. The liver is relatively easily accessible by DTCs due to low pressure, fenestrated blood vessels. The liver ECM is carefully regulated by stromal hepatic stellate cells. Upon chronic inflammation, stellate cells become activated and deposit vast quantities of ECM fibers, which can destroy the liver lobule architecture and promote DTC outgrowth through pro-metastatic fibers including collagens, LOXL, TNC, and more.

regulation of activation state through paracrine signaling, such as the feedback loop between LSECs and HSteCs. LSECs secrete nitric oxide, which promotes HSteC quiescence and contractility, whereas HSteCs secrete VEGF and nitric oxide to promote vessel integrity [347, 348]. When these NPC interactions are functioning in a healthy tissue setting, they resist metastasis [349]—for instance, breast cancer cells treated with conditioned media from quiescent HSteCs exhibited decreased proliferation when compared to conditioned media from activated HSteCs [350]—but become permissive to metastasis upon inflammation.

3.4.3 *Activation of quiescent DTCs in the liver*

While conditions promoting hepatic metastasis are well-studied, dormancy awakening in the liver niche has not been thoroughly investigated. Two major sources of physiological change within the liver, fibrosis and regeneration after injury, are associated with metastasis [351-354] and may be key turning points in the dormancy timeline that promote awakening.

Liver fibrosis is the result of stromal cell activation following injury. It has numerous etiologies such as alcohol abuse, hepatitis, fatty liver disease, or surgery which converge on a state of inflammation [352, 355]. HSteCs are the primary effector of fibrosis, and activate from quiescent to proliferative hepatic myofibroblasts (HMFs), upregulate αSMA, lose their retinoid stores, and increase deposition of ECM fibers, especially collagens [356]. TGF-β1 [357, 358], PDGF [359], FGF [360], and a stiff ECM [361] contribute to the HSteC activation process, creating a pro-fibrotic feedback loop. The ECM becomes stiff as HSteCs deposit excessive collagen (predominantly collagens I, III, and IV [325, 362]), tissue inhibitor matrix metalloproteinase (TIMP) enzymes which antagonize MMPs to prevent matrix degradation, and LOX, which crosslinks collagen further [363, 364]. The liver sinusoids undergo capillarization [365] and hepatocytes lose their microvilli [366]. Proteins that are not normally a component of

the healthy liver ECM, such as pro-metastatic TNC and MMP9, appear [367, 368]. Increased matrix stiffness [316, 369] and HMFs [349, 350] are associated with metastatic outgrowth and potentially produce awakening signals for dormant DTCs. HMFs secrete proliferative cytokines including RANTES [370] which may act on DTCs and inhibit T cell activity through B7-H1/PD-L1 ligation [371, 372]. Thus, activated HSteCs promote DTC outgrowth and metastasis by altering ECM, direct proliferative signaling, and immune suppression. Targeting the underlying causes of fibrosis [373-375] may be a viable strategy for maintain tumor dormancy [376]. A key aspect is restoring HSteC quiescence, which has been achieved through all-trans retinoic acid [349], vitamin D [377], and exposure to homeostatic LSECs producing nitric oxide [347], indicating that restoring one cellular target may have a calming effect on the whole niche.

Liver regeneration is the controlled healing response to tissue injury such as surgical resection. Surgery is associated with relapse as a result of inflammation [231, 378, 379], but liver regeneration is unique from the trauma of surgery. During regeneration, the liver stroma undergo rapid yet controlled hyperplasia without incurring inflammation and actually suppress fibrosis [380, 381]. The endothelium may be at the heart of the balance between fibrosis and regeneration, as the angiocrine response to injury hinges on the dominance of CXCR7 versus CXCR4 signaling and the sphingosine-1-phosphate receptor [381, 382]. Depending on the balance of signals, activation is transduced from LSECs to HSteCs, cascading into either the fibrotic or regenerative response. When regeneration commences, hepatocytes and NPCs exit G0 phase and undergo mitosis under a plethora of controlled cytokines including TNF-α, NF-κB [383], IL-6 [384], and growth factors [385, 386], while TGF-β and activin terminate stromal proliferation [387]. In this context, a bystander dormant DTC may be exposed to the rich proliferative signals in the regenerative microenvironment and enter the cell cycle. The role of

liver regeneration in metastasis is well-studied [309, 354, 388], but the relationship between regeneration and awakening from dormancy has not been elucidated [317]. Since surgical resection is a standard treatment for liver metastasis, it is critical to understand how fibrosis and regeneration impact dormant DTCs to avoid incidental DTC awakening.

In summary, the liver provides a dormancy niche for DTCs, which can be perturbed through fibrosis and injury. More research is needed to investigate hepatic regulators of quiescence and the interactions between DTCs and the stroma. While fibrosis activates the quiescent tissue, preventing inflammation or reversing it may help sustain DTC dormancy [376].

3.5 LYMPH NODE

The LN is the most frequent site of metastases across tumor and tissue types [304]. Although LNs themselves are not vital organs, LN metastasis strongly associates with distant metastases and is a key prognostic factor in staging protocols [389-394]. However, there is some controversy over their significance [395]: Do LN DTCs contribute to distant metastases, or is dissemination to the LN a dead-end and merely indicative of systemic spread? Does the ability to disseminate to LNs indicate tumor aggression, or is the LN simply an easily accessible, non-selective tissue? How do the inevitable tumor-immune interactions within the LN influence tumor development at local and distant sites?

3.5.1 *Contribution of the lymph node to metastasis*

While we cannot track the cell of origin for a metastatic lesion within a human patient, mounting experimental evidence has convincingly shown that LN DTCs can migrate to subsequent LNs [396] and seed metastases in distant tissues [107, 394, 397-399], through blood or lymph [399-401]. Clinical evidence supports the notion that LN DTCs contribute to disease,

especially over a longer duration of follow-up. The strongest example of this has been in breast cancer, where the MIRROR (Micrometastases and Isolated Tumor Cells: Relevant and Robust or Rubbish?) study, NSABP B-32 clinical trial, and meta-analyses have shown that isolated tumor cells in patient LNs independently predict worsened overall and disease-free survival over five to ten years post-diagnosis versus node-negative patients [402-407]. This may be a conservative measurement given that 13-25% of histologically "node-negative" patients have occult metastases upon closer examination [404, 406, 408, 409]. Cumulative incidence curves comparing breast cancer patients stratified by nodal status reveal a latent phase in the isolated tumor cell ($pN0_{(i+)}$) group that lasts approximately 36 months before the rate of adverse events rapidly increases [406, 410, 411]. While it is not possible to assign a cause for this rapid switch based on these data, it aligns with the paradigm of tumor dormancy in which single or small clusters of tumor cells reside in a quiescent niche within a tissue in a state of cell cycle arrest until stimulated to divide [59]. Late recurrence in LNs more than 10 years after diagnosis has also been documented for melanoma [412, 413] and gastric cancer [414], supporting the notion that LNs may harbor dormant DTCs for long periods of time.

Advancing markers and imaging technologies have aided experimental approaches to track DTCs through the metastatic process, and several studies have shown that LN metastases contribute to downstream metastases. Brown, *et al.*, and Pereira, *et al*., tracked LN-disseminating tumor cells through lymphatic microinfusion or photoconversion to determine that LN DTCs establish metastases in the lungs [397, 398]. Kodama, *et al*., showed that this was possible through hematogenous dissemination from the LN [399], opening up the routes of egress to the blood circulation. Phylogenetic studies show that 35% of visceral colorectal cancer metastases are more closely related to matched LN metastases than the primary tumor, indicating a discreet

route of dissemination and selection pressures that give rise to distinct genetic backgrounds [107]. Recent lineage tracing studies have quantitatively described the LN as transit hub that allows DTCs to pass through and colonize downstream tissues [106, 415]. Together, these studies provide direct experimental support of the long-held notion in the clinic that the LN is not a blind-ended DTC sink, but rather a transit point for a significant proportion of DTCs [396], lending urgency to understanding DTC behavior at this site.

3.5.2 *Organization of the lymph node*

The lymphatic system is a network of one-way, leaky, fenestrated vessels that collect the interstitial fluid lost in peripheral capillary beds and return it to circulation through the thoracic duct to maintain blood pressure. This fluid, called lymph, carries proteins, cell debris, and immune cells, as well as pathogens and disseminating tumor cells. Intermittent nodules along the lymphatics serve as 'field headquarters' for peripheral immunity, allowing lymph to be surveyed by resident antigen-presenting cells and adaptive immune cells in a centralized hub. To facilitate antigen sampling and presentation, LNs are highly compartmentalized, including four major subsets of stromal cells: lymphatic endothelial cells (LEC), blood endothelial cells (BEC), fibroblastic reticular cells (FRC), and a group of $CD31^{-}PDPN^{-}$ 'double negative' (DN) cells recently described as contractile pericytes [416, 417].

FRCs are the main parenchymal cells that provide structural and functional support to the LN resident cells. They produce and ensheath the conduit network, a series of ECM tubules that facilitates antigen sampling and serves as a scaffold for migrating leukocytes. The tubule core contains collagen I, IV, and XIV and proteoglycans (*e.g.*, decorin, biglycan, and fibromodulin), surrounded by an outer layer of fibrillin, collagen VI, TNC and laminin-332 [417-419]. FRCs also control T cell migration [420] and egress [421], and regulate LN expansion through

interactions with active dendritic cells [422].

LN LEC form the outer capsule and internal sinuses. When lymph enters via the afferent vessel, it flows into the subcapsular space (SCS) which is separated from the parenchyma by a layer of LEC. Lymph-borne particles are separated by size: small molecules less than 70 kDa can enter the conduit network and flow into the parenchyma, whereas larger particles are confined to the SCS to prevent possible pathogens from accessing the blood [423]. Dendritic cells sample small molecules within the conduit system [418, 424] and specialized subcapsular macrophages [425] and DCs [426] sample larger molecules in the SCS [423].

The outer cortex contains multiple lymphoid lobules consisting of B cells, follicular dendritic cells, and supporting stroma. Lymphatic sinuses interdigitate between the lobules, reaching down to the medulla near the base of the node, which collects lymph from the sinuses into the efferent vessel. T cells reside and activate in the inner paracortex region. Throughout the parenchyma, LN BEC form two distinct vessels: arteries that enter at the hilar base and branch into smaller capillaries, and high endothelial venules (HEVs) that promote and regulate enable lymphocyte trafficking through adhesion molecules and the absence of tight junctions [427].

The LN is a site of carefully coordinated chemokines to set up the appropriate cues and compartments for immune function. Tumor cells co-opt these signals to enhance LN invasion. Initially, DTCs access the LN through intra- or peritumoral lymphatic vessels [428], as well as the blood circulation [397-399]. Migrating cells entering via the afferent lymphatics express CCR8 which binds to LEC CCL1 to increase motility and facilitate entry into the LN [429]. Inhibiting CCR8 caused melanoma DTCs to accumulate at the junction of the afferent vessel and LN capsule, conferring a gatekeeping function on CCL1-CCR8 signaling. Migrating DCs and T cells rely on gradients of CCL19, CCL21, and CXCL12 from FRCs and HEVs to transverse the

LEC subcapsular floor and migrate into the parenchyma [430-433]. Human breast cancer cells have demonstrated an ability to perforate LEC monolayers through the metabolite 12S-HETE [29]. Breast, melanoma, and prostate cancer DTCs also express the cognate receptors CCR7 and CXCR4 [434-436], and inhibition of CXCR4 prevented breast cancer metastasis to the LN [434], suggesting DTCs follow the same cytokines gradients. Together, the immune and stromal subcompartments form very distinct niches for LN DTCs. Currently, it is a mystery how they may affect DTC phenotype (**Fig 6.**).

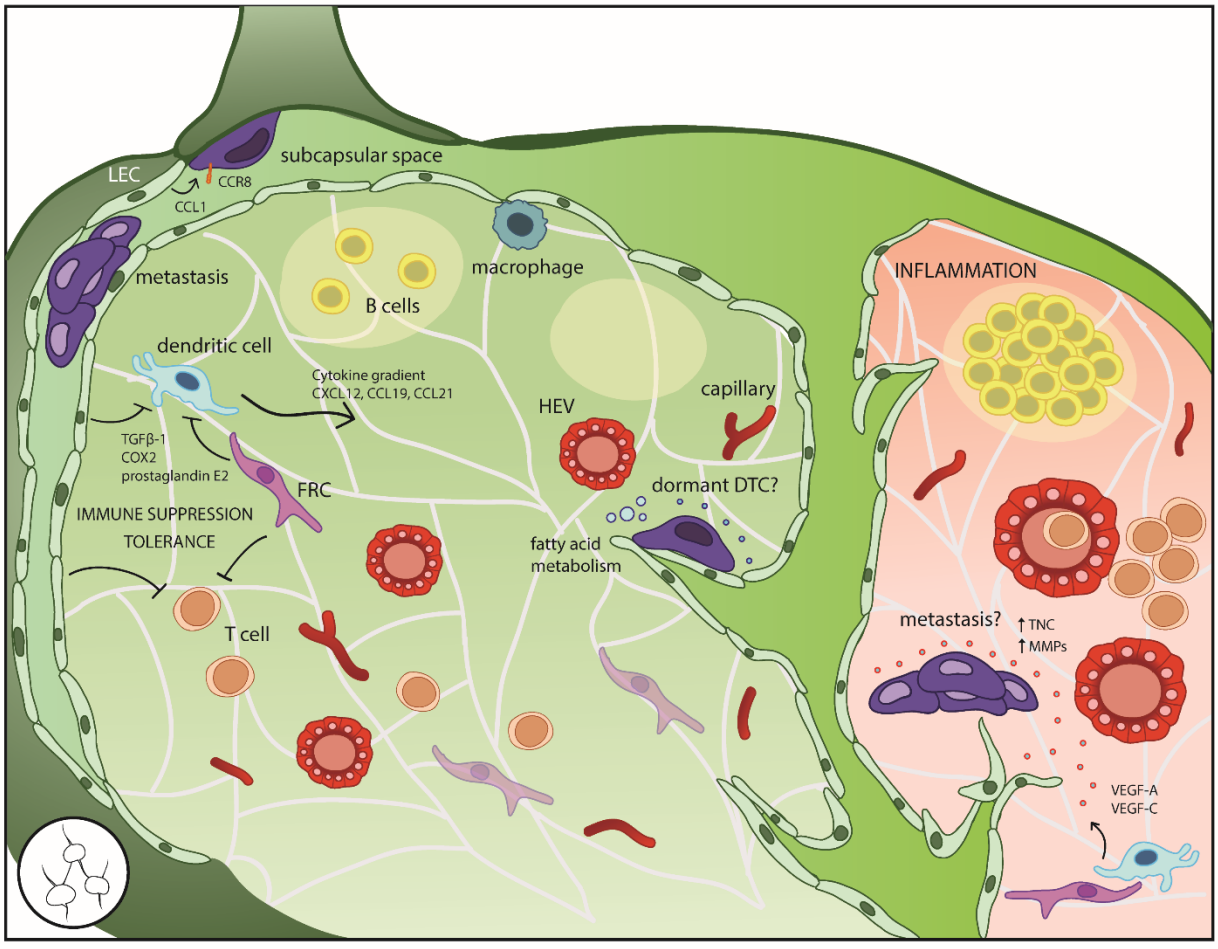

Fig. 6. The lymph node microenvironment for dormant DTCs. The lymph node (LN) is relatively understudied as a dormancy niche. The stroma regulate entry of both immune cells and DTCs into the node. DTCs entering via the afferent lymphatics must express certain markers (e.g., CCR8) in order to enter the subcapsular space. They must cross the subcapsular floor to enter the parenchyma, following the same chemokine gradients as professional antigen presenting cells. Within the LN, blood and lymphatic endothelia form a prominent niche, although it is unknown whether they affect DTC dormancy. Upon inflammation, the LN stroma undergoes massive remodeling and inflammation, and may contribute to metastatic outgrowth although this has not been tested directly.

Chapter 4. THE LYMPH NODE NICHE FOR DORMANT DISSEMINATED TUMOR CELLS

4.1 INTRODUCTION

Despite the well-established prevalence of LN metastases [108], relatively little is known about the LN as a dormancy niche, especially compared to the major metastatic organs (**Table 1, Fig. 6**) [1, 389-394]. One reason for this may be the historical uncertainty of whether LN metastases contribute to overall disease or simply serve as a bellwether for metastatic competence. This question has been addressed directly through clinical studies showing that isolated tumor cells in the LNs are sufficient to stratify patients by poorer overall and disease-free survival [402], as well as experimental studies showing that LN metastases evolve independently [106, 107] and contribute directly to visceral metastases [107, 397-399]. The shift in thinking about LN DTCs as potential metastatic seeds rather than byproducts of primary tumor progression highlights a population of tumor cells that may be targeted upstream of vital organ metastasis.

Tumor suppression within the LN has been considered previously from immunological [437-439] and metabolic standpoints [440], but stromal constituents to the cellular dormancy niche have yet to be defined. Since the perivascular niche has proven crucial for regulating tumor dormancy in the lungs and bone marrow [69, 158], we speculated that LN endothelia might contribute to the dormancy niche. While they come from a common endothelial progenitor [441], LN BEC and LEC are distinct in function and interactions with tumor cells. In one of the few studies addressing LN ECs and DTCs directly, human BEC did not affect breast cancer tumor growth when co-injected into mice, whereas LEC promoted tumor growth due to secreted EGF and PDGF-BB [442]. Further study would shed light into the functional distinction between

these endothelial compartments.

Given the critical yet obscure nature of the LN niche in DTC dormancy and awakening, we investigated the LN dormancy niche and its mechanisms regulating tumor dormancy. We utilized two orthotopic mouse models to demonstrate that the vascular niche is a central regulator of DTC quiescence, in contrast to the lymphatic endothelia.

4.2 RESULTS

4.2.1 *Quiescent disseminated tumor cells are enriched within the lymph node vascular niche.*

To establish whether the LN harbors dormant DTCs, we investigated tumor dormancy in immunocompetent models of spontaneous mammary cancer metastasis. Syngeneic 4T07 mammary carcinoma cells stably expressing enhanced green fluorescent protein (eGFP) were injected into the fourth mammary fat pad of female BALB/c mice, where they generated a primary tumor (**Fig. 7a**). 4T07 are weakly metastatic compared to the more aggressive sister line 4T1 [443]. To mimic the disease trajectory of a human patient, primary tumors were resected at volume of approximately 250 mm^3. Although there is no universally accepted timeline to establish dormancy, which is likely cancer- and tissue-dependent, many studies allow for three weeks or more of minimal DTC proliferation *in vivo* and use absence of a cell cycle marker such as Ki-67 [81, 82] to confirm quiescence [75, 76, 78, 79]. We harvested LNs six weeks after primary tumor resection and analyzed them for DTC outgrowth. No visible metastases were detected on the metastases, indicating that 4T07 maintain dormancy in the LN for at least six weeks post-resection. LNs are highly compartmentalized organs subdivided into distinct zones for efficient cell trafficking and immune surveillance [444] (**Fig. 8**). We observed that DTCs were predominantly located within the medullary network of lymphatic sinuses and vasculature

(**Fig. 7b, c**), in contrast to reports that DTCs traffic primarily through the afferent lymphatics to the subcapsular sinus [397, 445-448]. While it is possible that the DTCs in our models enter the LN through the afferent lymphatics and migrate to the medulla, our observations suggest that DTCs may also enter the LN hematogenously through high endothelial venules or capillaries in the medulla.

Given the prominent overlap of DTCs in lymphovascular regions of the LN and the established role of endothelia in the dormancy niche of bone marrow and lungs [69], we investigated whether LN DTCs preferentially occupy a perivascular niche. The Euclidean distance from each DTC to the nearest $CD31^+$ blood and LYVE-1^+ lymphatic endothelial cell (D_{BEC} and D_{LEC}, respectively) was measured at three levels of depth through each LN, with respect to Ki-67 status (n=4 mice, mean ± S.D., 207 ± 63.6 DTCs analyzed, **Figs. 9a, b**). The majority of LN DTCs were Ki-67^- (mean ± S.D, 90.6% ± 3.24% Ki-67^-, **Fig. 9c**), demonstrating that the LN microenvironment sustains if not promotes quiescence. The endothelial 'niche' was defined as the space within 10 μm of BEC and/or LEC, a range previously established by spatial localization studies [128, 137, 449, 450]. As a null control distribution, randomly generated dots representing DTCs were applied to the same LN tilescan images and the distances between random 'DTCs' to BEC and LEC were measured (**Fig. 10**). Compared to the random dot ('Ran') distribution, observed DTCs ('Obs') were significantly enriched in the BEC niche (P=0.009) and non-significantly enriched in the LEC niche (P=0.0615) (paired Student's t test for difference of proportions, **Fig. 9d**). Complementing this preference for the blood vasculature, DTCs skewed towards BEC compared to LEC in aggregate (median D_{BEC} = 4.72 μm; median D_{LEC} = 9.51 μm) (**Fig. 9e**). To determine whether there was an association between occupying a particular niche and proliferation status, DTC localization to endothelia was assessed relative to Ki-67 signal.

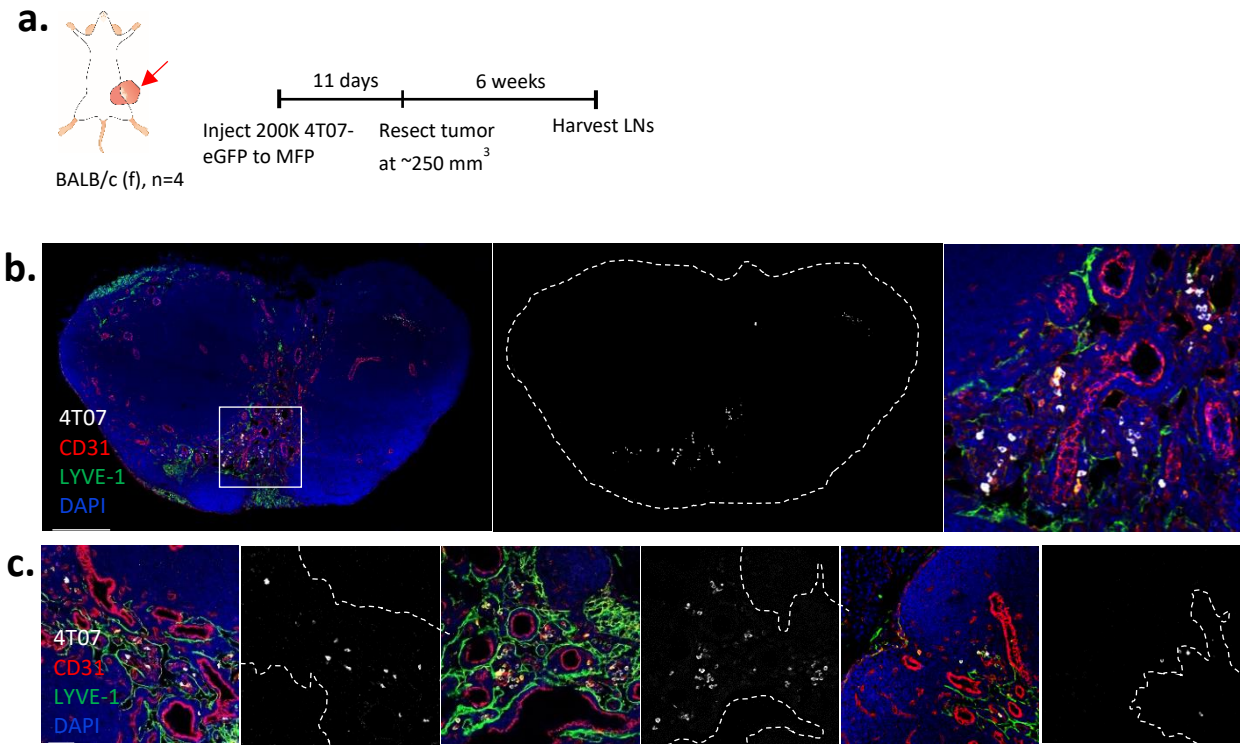

Fig. 7. An orthotopic model for spontaneous dissemination reveals that the lymph node harbors 4T07 DTCs in lymphovascular regions. a) Female BALB/c mice were orthotopically injected with $2x10^5$ syngeneic 4T07-eGFP mammary carcinoma cells (n=4). Primary tumors were resected 11 days later (V~250 mm^3). Axillary, brachial, and inguinal lymph nodes (LNs) were harvested six weeks post-resection. **b, c**) Representative tilescans of whole LNs showing DTC overlap to lymphovascular regions, stained with anti-GFP, anti-CD31, anti-LYVE1, and DAPI. Scale bar for whole LN tilescans (b): 200 μm. Scale bar for insets (c): 50 μm.

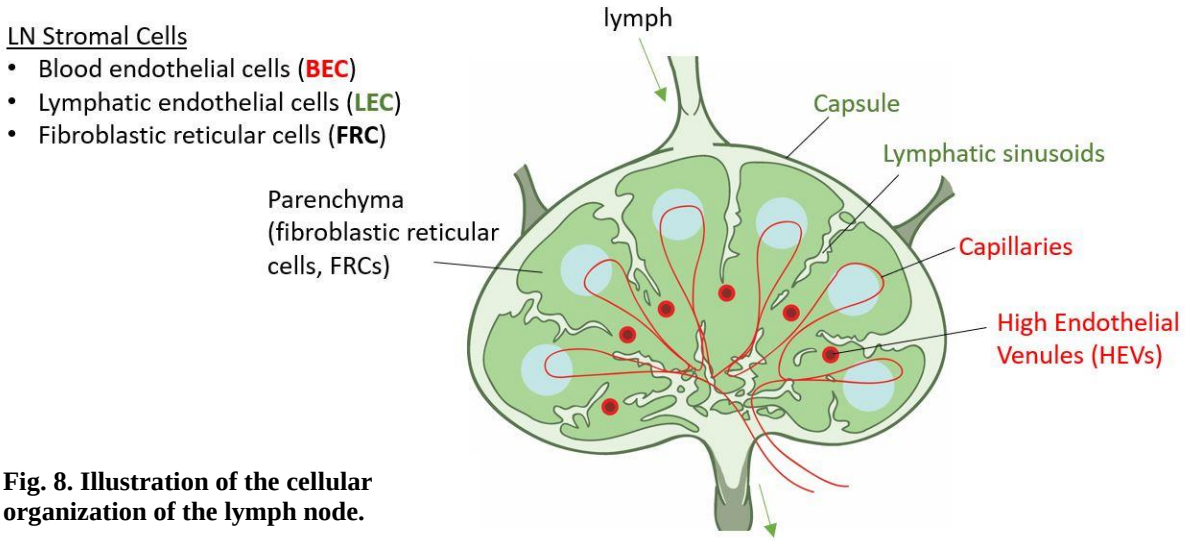

Fig. 8. Illustration of the cellular organization of the lymph node.

Intriguingly, there was a significant enrichment of Ki-67$^-$ DTCs in the BEC niche ($D_{BEC} \leq 10$ µm, $D_{LEC} \geq 10$ µm, P=0.0206) and a mild but non-significant enrichment of Ki-67$^+$ DTCs in the LEC niche ($D_{BEC} \geq 10$ µm, $D_{LEC} \leq 10$ µm, P=0.2809); no difference in localization was observed for cells residing within the 'pan-EC niche' (D_{BEC}, $D_{LEC} \leq 10$ µm, P=0.9886) or the 'non-EC niche' (D_{BEC}, $D_{LEC} \geq 10$ µm, P=0.8892) (one-way ANOVA followed by Sidak's multiple comparisons test between groups in each niche, **Fig. 9f**). These data indicate that BEC constitute the preferred niche for Ki-67$^-$ DTCs, in contrast to LEC. Further, Ki-67$^-$ DTCs were not enriched

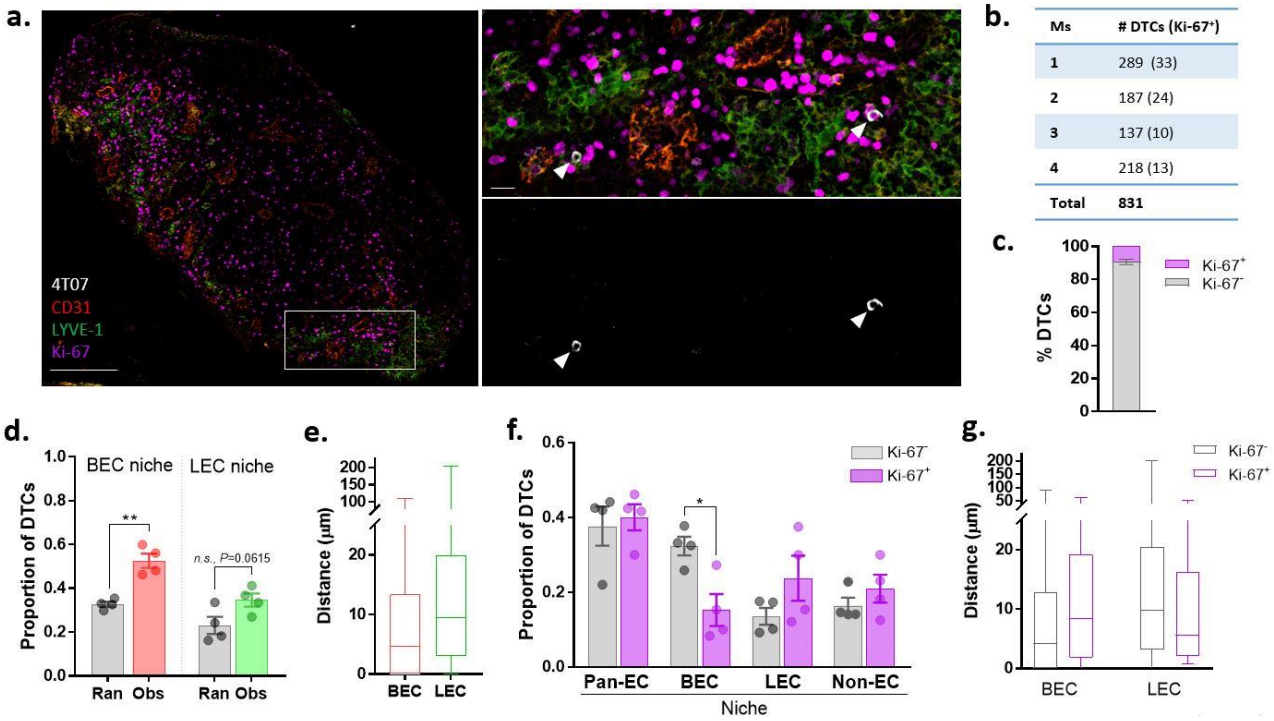

Fig. 9. Quiescent lymph node DTCs demonstrate a preference for the vascular niche. a) Representative tilescan of whole LNs stained for anti-GFP, anti-CD31, anti-LYVE1, and anti-Ki-67. Both Ki-67$^-$ and Ki-67$^+$ DTCs were detected (inset, arrows). Scale bar for whole LN tilescan: 200 µm. Scale bar for inset: 20 µm. **b**) The number of DTCs analyzed per mouse across LNs (number Ki-67$^+$ DTCs shown in parentheses). **c**) The percentage of Ki-67$^-$ DTCs detected was 90.6% ± 3.2% (n = 4 mice, mean ± S.D.) **d**) The proportion of observed ('Obs') DTCs versus random ('Ran') dots found within 10 µm of BEC or LEC (defined as the 'niche'. **P<0.01, *n.s.* indicates no significance; Student's *t* test for difference of proportions. **e**) Box-and-whisker plot showing the median distance of a DTC to BEC and LEC (n = 831 DTCs pooled; median D_{BEC} = 4.72 µm; median D_{LEC} = 9.51 µm). **f**) The proportion of Ki-67$^-$ versus Ki-67$^+$ DTCs residing in endothelial niches (pan-EC niche, P=0.9886; BEC niche, P=0.0206; LEC niche, P=0.2809; Non-EC niche, P=0.8892). *P<0.05; one-way ANOVA followed by Sidak's multiple comparisons test between groups in each niche. **g**) Box-and-whisker plot showing the median distance of Ki-67$^+$ and Ki-67$^-$ DTCs to BEC and LEC (n = 831 DTCs pooled; median Ki-67$^-$ D_{BEC} = 4.17 µm; median Ki-67$^+$ D_{BEC} = 8.43 µm; median Ki-67$^-$ D_{LEC} = 9.80 µm; median Ki-67$^+$ D_{LEC} = 5.64 µm).

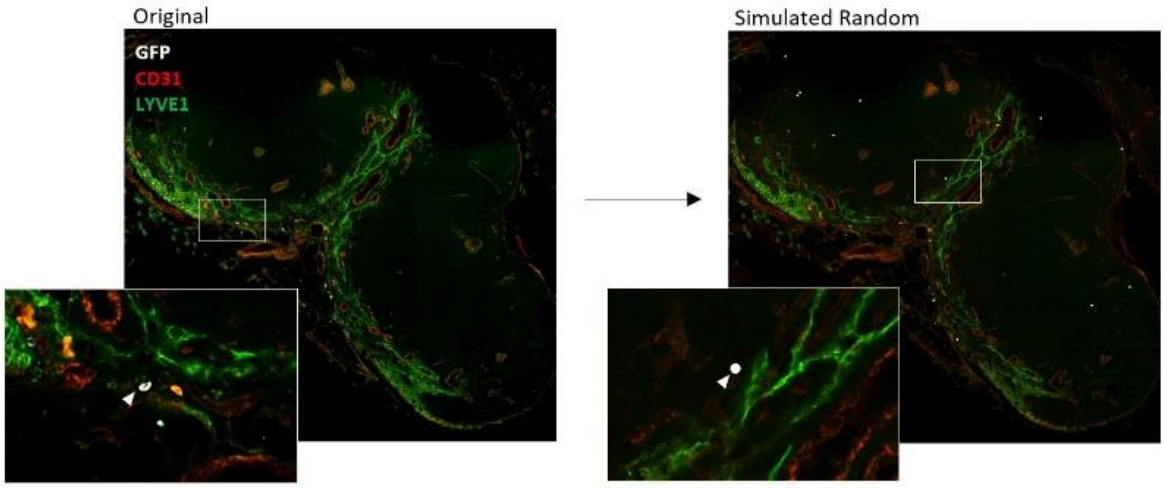

Fig. 10. A randomly generated point distribution serves as a null control for DTC localization in the lymph node. Representative images showing how a null distribution for DTCs in the lymph node (LN) was generated. A custom R program was used to apply a random distribution of dots representing DTCs to the same set of whole LN tilescan images analyzed for DTC distance to blood and lymphatic endothelia (BEC and LEC) (insets, white arrows). The number of dots applied was the average number of dots per section for each mouse. To generate the null distribution, the Euclidean distance from each dot to the nearest BEC and LEC was measured. The proportion of DTCs and dots within the BEC and LEC niches (within 10 μm) was compared to determine whether preferential localization to these landmark cell types existed *in situ*.

in the pan-EC niche (i.e., in close proximity to both BEC and LEC), indicating that LEC may counteract the BEC quiescent niche. The preference of Ki-67$^-$ DTCs for blood endothelium was reflected in the trend of aggregate distances to BEC and LEC (**Fig. 9g**).

4.2.2 *DTC-vascular association in a second orthotopic model*

To assess whether these findings applied to an secondary immune-competent model of mammary tumor cell dissemination and dormancy, we repeated the experiment using syngeneic D2.0R mammary carcinoma cells orthotopically implanted into female BALB/c mice [451] (**Fig. 11a**). Although fewer DTCs were detected in this model compared to the 4T07 model (mean ± S.D., 30.4 ± 19.6 DTCs, **Fig. 11b**), the majority of DTCs were again Ki-67$^-$ (mean ± S.D., 93.6% ± 6.4% Ki-67$^-$, n = 8 BALB/c mice, **Fig. 11b, c**). Compared to a random dot distribution, we observed a non-significant enrichment of D2.0R DTCs in the BEC niche (P=0.0666) and no DTC enrichment in the LEC niche (P=0.8610) (n = 8, paired Student's t test for difference of

proportions, **Fig. 11d**). The preference for the BEC niche was reflected in the aggregate distance of DTCs to each cell type (median D_{BEC} = 11.20 µm; median D_{LEC} = 21.11 µm, **Fig. 11e**).

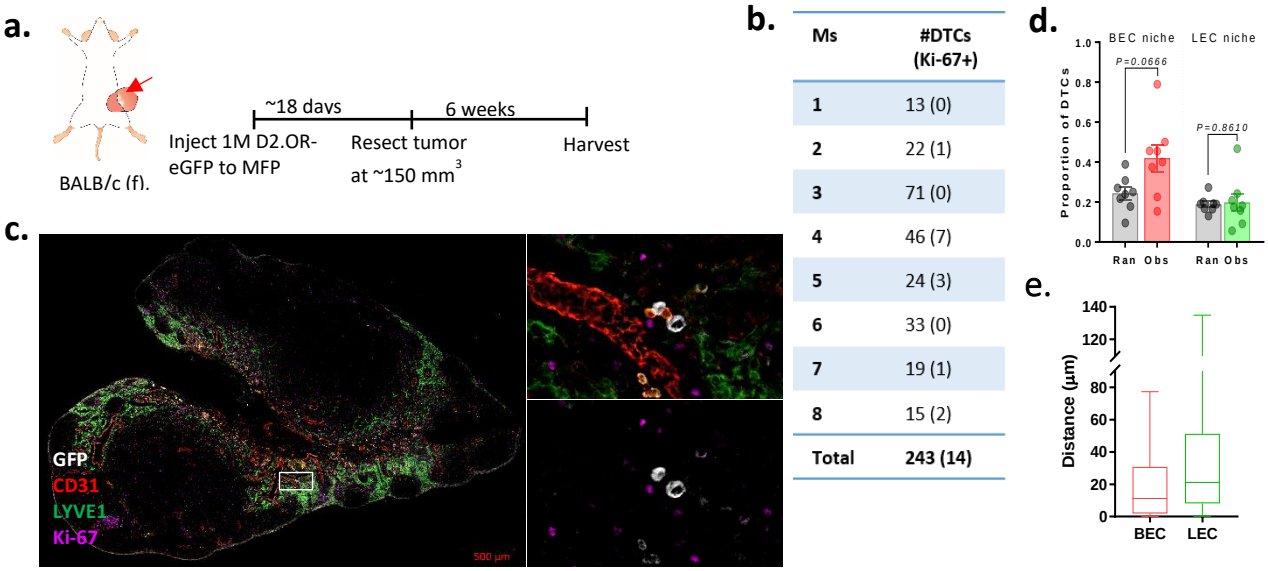

Ms	#DTCs (Ki-67+)
1	13 (0)
2	22 (1)
3	71 (0)
4	46 (7)
5	24 (3)
6	33 (0)
7	19 (1)
8	15 (2)
Total	243 (14)

Fig. 11. A second orthotopic model shows similar trends of blood vessel enrichment for D2.0R DTCs. a) Experimental schematic for a second model of spontaneous dissemination to the LN. Female BALB/c mice were orthotopically injected with $2x10^6$ syngeneic D2.0R-eGFP mammary carcinoma cells (n=8). Primary tumors were resected 18 days later (V~150 mm^3). Axillary, brachial, and inguinal lymph nodes (LNs) were harvested six weeks post-resection for immunostaining. b) The number of DTCs and Ki-67^+ DTCs (parenthesis) detected in the D2.0R model. c) Representative whole LN tilescan image showing solitary Ki-67^- D2.0R-eGFP DTCs at six weeks-post resection (insets). d) The proportion of D2.0R found in the BEC and LEC niches (within 10 µm of either structure), versus random dot distribution. n=8 mice, BEC niche P=0.0666, LEC niche P=0.8610, paired Student's t test. e) Box-and-whisker plot showing the aggregate distribution of distances from D2.0R DTCs to BEC and LEC. Median D_{BEC} = 11.2 µm; median D_{LEC} = 21.1

4.3 Discussion

Together, these orthotopic models demonstrate that the LN can sustain DTC quiescence and are the first to demonstrate in a dormancy setting that the blood endothelium form the primary niche for non-proliferating DTCs within LNs, in contrast the lymphatic endothelium. Despite its frequent colonization by metastasis, the LN microenvironment was growth suppressive in these models, agreeing with clinical observations of late recurrence in patients with $pN0_{(i+)}$-staging [402, 411]. This pattern implies isolated DTCs must overcome barriers to growth in order to progress to metastasis either through intrinsic adaption or through lowering

the external barriers to growth, which will be addressed in Chapter 6.

These results reinforce the notion that the perivascular niche is central to maintaining tumor quiescence across multiple organs [69]. The underlying cause may be a consequence of maintaining blood vessel integrity. Blood vessels are dynamic structures that respond to injury by activating and engaging in cell division and sprouting. Endothelia therefore secrete factors such as TSP-1 into the local environment, which stabilize the vessels in the absence of injury [452]. As DTCs extravasate into the tissue, they will encounter the basement membrane on the basal side of the vessels, including quiescence factors retained in the matrix. LN LEC also express thrombospondin family members and in fact secrete more ECM than LN BEC [453]. Therefore, the observed DTC stratification to BEC or LEC niches as a function of Ki-67 status may not be related to ECM, but other secreted factors (e.g., EGF and PDGF-BB as in [454]).

To define statistical enrichment in the niche, an artificial distribution of randomly generated dots was used a null control that did not presuppose preferential location. One limitation of this study is that the null distribution was simulated only once, due to the time-consuming nature of manual analysis. Further, an association between DTCs and non-endothelial perivascular cells was not investigated; however, these cells tend to make transient associations with the endothelia, whereas DTCs were consistently associate with blood vessels.

LN egress studies have shown that DTCs associate with $CD31^+$ vessels (HEV and/or capillaries) *en route* to leaving the LN [398, 399], and therefore it could be argued that the DTCs we located near endothelia were in transit. However, DTCs were not detected on the luminal side of the vessels, supporting the notion that the basal side was the biologically preferred niche. Intravital imaging would shed light on whether LN BEC localization is stable or transitory, and LN imaging windows have reportedly achieved stability for up to two weeks [455].

Chapter 5. DECONSTRUCTING THE LYMPH NODE ENDOTHELIAL NICHE

5.1 INTRODUCTION

Perennial interest lies in engineering organotypic models that capture a portion of tissue function for diverse uses, from transplant biology to studying complex interactions such as metastasis. Having identified the LN vasculature as a key niche for quiescent tumor cells, I set out to develop a tractable cell culture system that recapitulated endothelial-derived growth suppression of tumor cells and would allow mechanistic studies in a more reductionist setting than an animal. Previously, our lab used HUVEC-based vessel networks to model the bone and lung vascular niche. These "microvascular niches" (MVN) aided the identification of secreted angiocrine factors that contributed to tumor dormancy [456]. The goal was to adapt this format to model vascular and lymphatic endothelial vessels on a LN background and investigate tumor growth across combinatorial niches.

Two commercially available lines of endothelia were utilized: human umbilical vascular endothelial cells (HUVEC), which have been noted to form spontaneous vessel networks in the presence of mesenchymal stem cells [457] and various 3D matrices involving components of the ECM [458], and human dermal lymphatic endothelial cells from neonatal foreskin (hdLEC). The stromal compartment was represented by fibroblastic reticular cells (FRC), the main mesenchymal stromal cell within the LN that contribute ECM fibers to form the conduit network for nodal structure and antigen distribution [417, 459, 460]. FRC associate closely with endothelia and regulate LN function through a variety of roles supporting immune and stromal function at homeostasis and upon inflammation [459]. The murine FRC cell line BLS-4 was generously provided by H. Peinado (CNIO, Madrid) for these studies.

Differences have been noted between the optimal conditions for BEC and LEC tubule formation in culture. For example, LEC optimally organize in fibrin matrix while BEC networks prefer a mixed collagen-fibrin matrix [461]. Further, growth factors can be added to these systems to encourage differentiation, such as vascular endothelial growth factors (VEGFs), human growth factor, ascorbic acid, and others [462, 463]. Commercial Matrigel contains both matrix components and growth factors, and may interfere with LEC network formation since they deposit far less basement membrane than BEC [463]. Another consideration is that the LN MVN must be able to support tumor cells in the absence of serum to prevent rampant outgrowth. With these considerations in mind, a model was developed that captured the salient features of the *in vivo* LN endothelial niche for the purpose of investigating tumor dormancy.

5.2 RESULTS

5.2.1 *An organotypic co-culture model recapitulates tumor growth suppression observed in the lymph node.*

HUVEC were prepared for growth in serum-free media by transfection with the E4Orf1 vector [464]. To generate LN MVNs, $1x10^4$ human BEC (HUVEC-E4Orf1) and/or $1x10^4$ LEC (hdLEC) were admixed with $5x10^4$ murine FRC (BLS-4) in growth media containing 10 ng/ml VEGF-C in a 96-well plate format (**Fig. 12a**). As in previous models developed for the bone marrow and lung endothelium [69], the stromal cells instruct the endothelia to form vessel networks over 10 days, organizing into a vessel niche reminiscent of the murine lymphovasculature (**Fig. 12b**). VEGF-C has been shown to aid the formation of hdLEC tubule networks in 3D matrices [462, 463, 465] and was critical for LEC network formation in the absence of a 3D environment. After network formation, malignant human breast epithelial cells (including HMT-3522-T4-2 [T4-2] cells [466], MDA-MB-231, MCF7, T47D, D2.0R, 4T07,

4T1, and 66c14) expressing a fluorescent protein were seeded sparsely on LN MVNs (~50 cells per well) to avoid confounding growth effects from doublets or clusters (**Fig. 12c**). The murine cell lines grew abundantly in all LN MVN conditions, whereas most human tumor cell lines

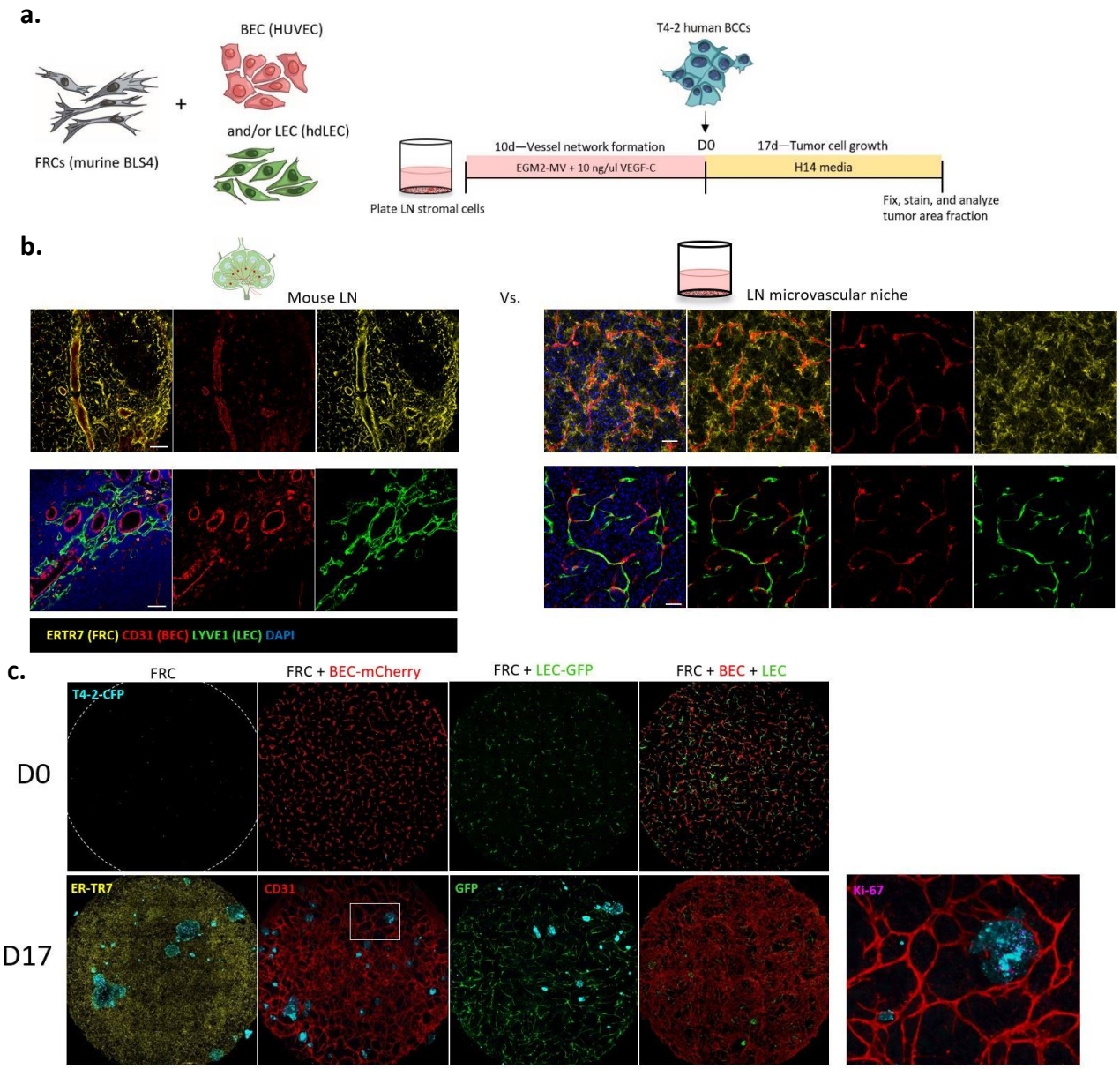

Fig. 12. An organotypic co-culture model of the lymph node endothelial niche. a) Schematic for generating lymph node (LN) microvascular niches (MVNs). After 10 days of growth in VEGF-C-containing media, tumor cells are sparsely seeded on the vessel networks and grow for 17 days before fixation. **b**) Representative images comparing FRC (ERTR7), BEC (CD31), and LEC (LYVE-1) organization in murine LNs to LN MVNs. Left panels, scalebar: 50 μm. Right panels, scalebar: 200 μm. **c**) Representative images of the LN MVNs at D0 (10 days of network formation) when T4-2-CFP cells are seeded, and at D17 after fixation and immunostaining. *Inset*, individual T4-2 cells and clusters could be visualized.

failed to establish growth, with the exception of T4-2 (**Fig. 13a, b**). Over 17 days in defined medium (i.e., no serum, minimal cytokines) T4-2 colonized the FRC-only niches whereas the presence of BEC and LEC suppressed T4-2 outgrowth (**Fig. 12c, 13b**). After this growth period, wells were fixed in 4% paraformaldehyde (PFA) and immunostained to quantify area fraction, normalized to the number of tumor cells seeded at Day 0. Area fraction analysis revealed that BEC and LEC individually suppress T4-2 outgrowth, though not in an additive manner (**Fig. 13b**). Growth suppression of tumor cells in the endothelial niches was not directly due to additional cells in these wells, as the T4-2 area fraction did not change with increasing number of FRC seeded per well (**Fig. 13c**). These data support the hypothesis that BEC promote DTC quiescence and demonstrate that the LN MVN model recapitulates the growth suppressive microenvironment of the LN.

5.2.2 *Characterization of lymph node niches via targeted ECM proteomics and transcriptomics*

The molecular basis for tumor growth suppression in LN MVNs was first investigated through targeted ECM proteomics. ECM proteins, particularly collagens and fibronectin, have been implicated in metastasis and progression from dormancy [68, 167, 467]. They are found at high density in the metastatic LN [468], suggesting a possible link between ECM organization and growth permissiveness in the LN niche.

LN MVNs were prepared sans tumor cells. Protein lysates were collected for FRC, FRC+BEC, FRC+LEC, and FRC+BEC+LEC conditions in triplicate and snap frozen in liquid nitrogen. Samples were sequentially fractionated into soluble and insoluble ECM and run separately by liquid chromatography-tandem mass spectrometry (LC-MS/MS). QconCat peptide probes were used to quantify functionally relevant ECM proteins and provide actual concentrations across

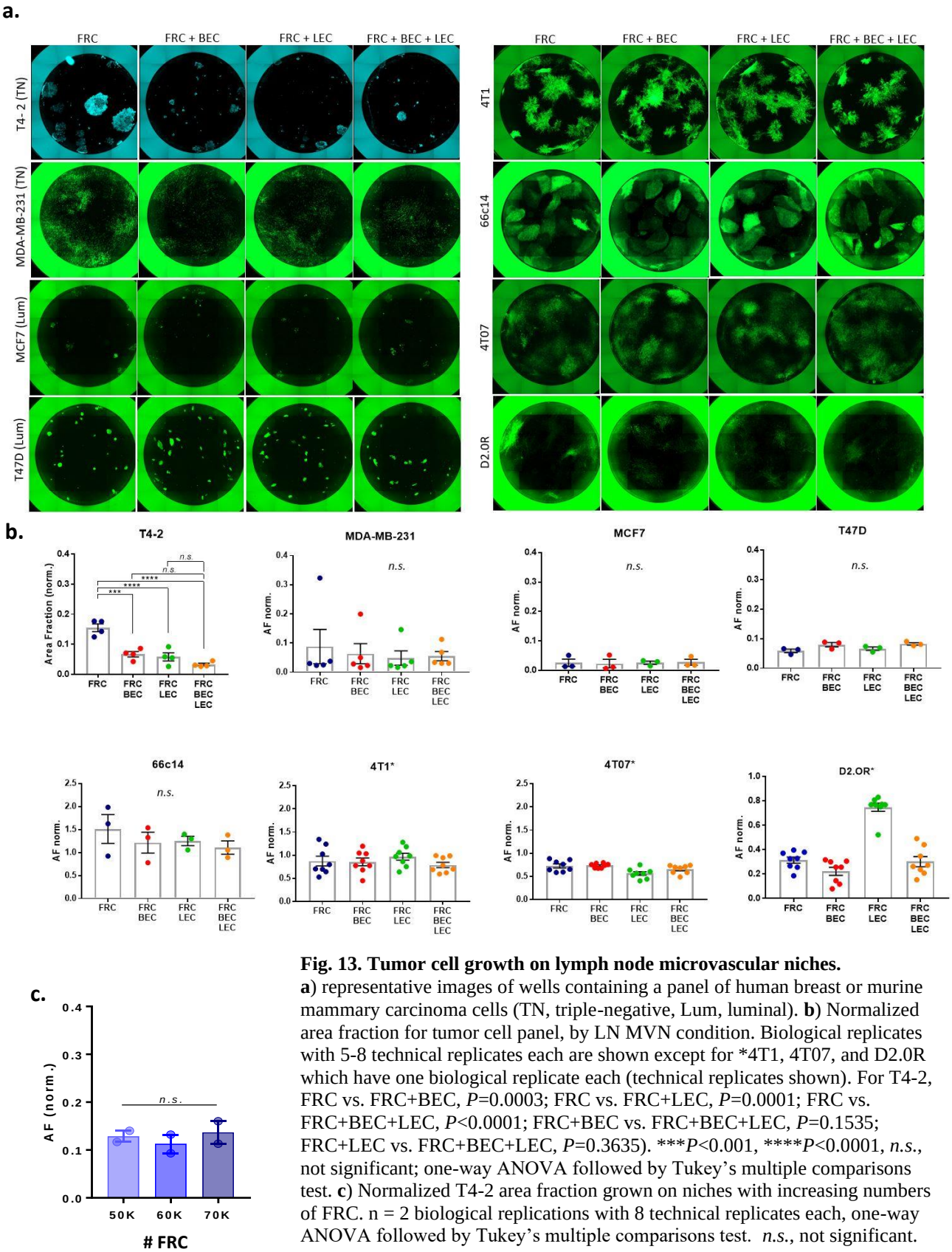

Fig. 13. Tumor cell growth on lymph node microvascular niches. **a**) representative images of wells containing a panel of human breast or murine mammary carcinoma cells (TN, triple-negative, Lum, luminal). **b**) Normalized area fraction for tumor cell panel, by LN MVN condition. Biological replicates with 5-8 technical replicates each are shown except for *4T1, 4T07, and D2.0R which have one biological replicate each (technical replicates shown). For T4-2, FRC vs. FRC+BEC, P=0.0003; FRC vs. FRC+LEC, P=0.0001; FRC vs. FRC+BEC+LEC, P<0.0001; FRC+BEC vs. FRC+BEC+LEC, P=0.1535; FRC+LEC vs. FRC+BEC+LEC, P=0.3635). ***P<0.001, ****P<0.0001, *n.s.*, not significant; one-way ANOVA followed by Tukey's multiple comparisons test. **c**) Normalized T4-2 area fraction grown on niches with increasing numbers of FRC. n = 2 biological replications with 8 technical replicates each, one-way ANOVA followed by Tukey's multiple comparisons test. *n.s.*, not significant.

conditions [469] (**Fig. 14**). Samples clustered within their condition (**Fig. 14a**). Several differentially expressed proteins of interest were found in the growth suppressive FRC+BEC+LEC niche, versus the FRC-alone niche, including collagens, and less well-established secreted factors such as tubulointerstitial nephritis antigen-like 1 (TINAGL1) and LGALS3 (**Fig. 14b**). The BEC-containing niches were associated with less unique deposition than expected (including fibronectin, FN1, and vimentin, VIM), whereas LEC niches contained a significant increase in fibrillar collagens (**Fig. 14c**). The source of this collagen is more likely to be FRC than LEC due to their role depositing ECM fibers within the LN, and lack of basement membrane around lymphatics [417].

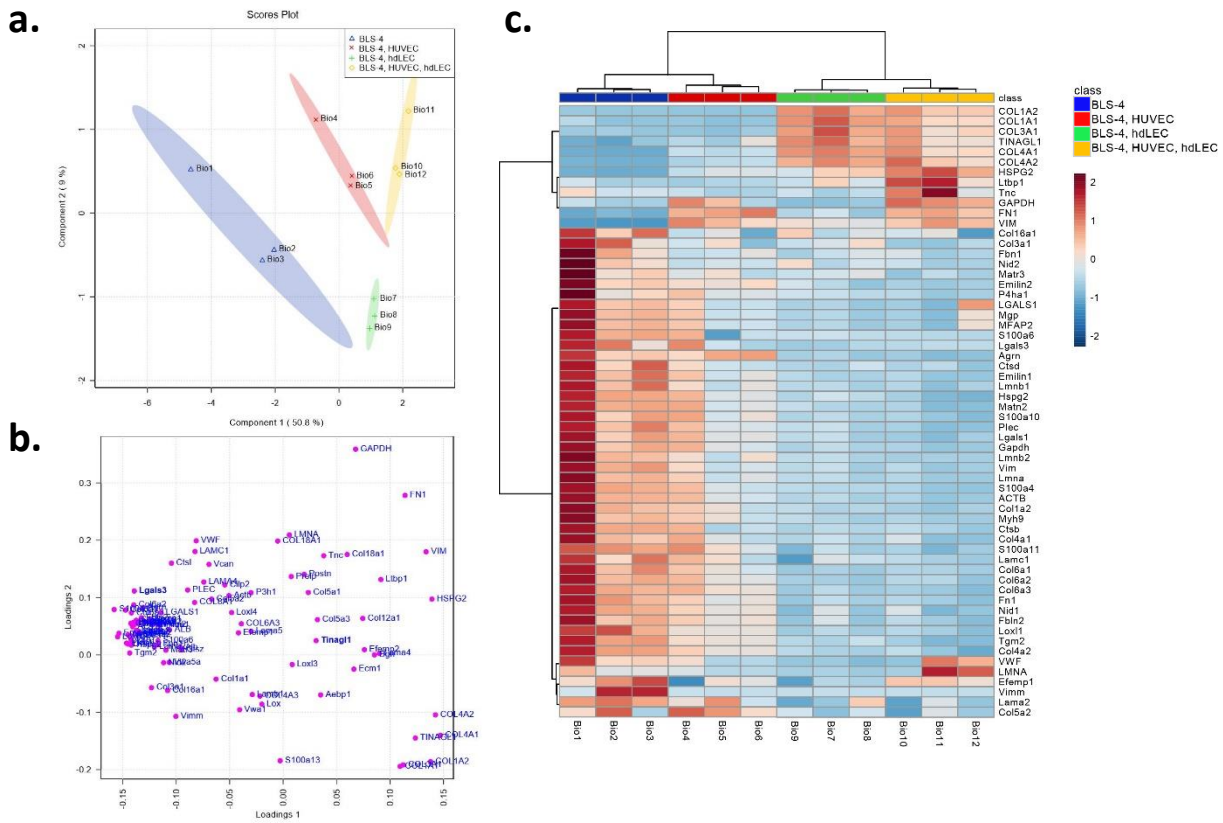

Fig. 14. Characterization of lymph node MVNs by targeted ECM proteomics. **a**) Sample replicates clustered closer to each other than across conditions. **b**) Volcano plot showing most differentially expressed ECM proteins in the BLS-4+HUVEC+hdLEC condition normalized to BLS-4 alone. Proteins of interest (TINAGL1, LGALS3, VIM) are circled. **c**) Heatmap showing unsupervised hierarchical clustering of LN MVN conditions. Arrows indicate selected targets of interest (TINAGL1, VIM, LGALS3).

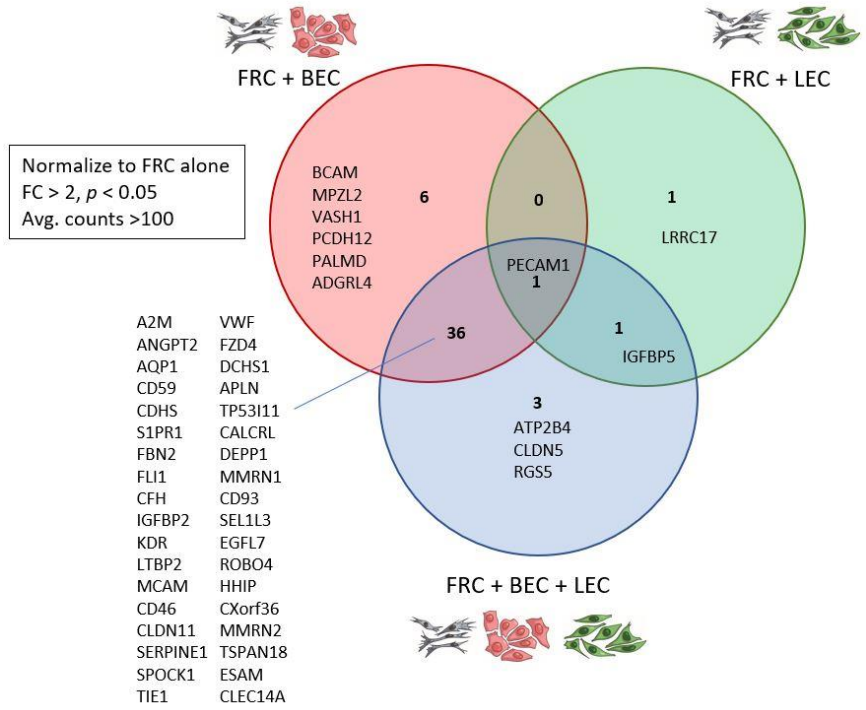

Fig. 15. RNAseq analysis of lymph node MVNs revealed differentially expressed targets in each endothelial condition, versus the FRC alone condition. The threshold was set at fold change (FC)>2, *P*<0.05, with greater than 100 average counts, for genes with murine and human orthologs to account for cross-species MVNs.

LN MVNs were also profiled by total RNA sequencing. RNA was collected from 10 wells of each condition in duplicate and sequenced on an Illumina HiSeq2500. Transcripts were annotated using both mouse and human ortholog sequences, in order to account for the cross-species model. Conditions were normalized to FRC-alone. Forty-eight gene products made the threshold of fold change greater than 2, *P*<0.05, and at least 100 counts in one of the replicates, most of them in BEC-containing niches **(Fig. 15**). The only transcript detected in all endothelial niches was PECAM1 (CD31), a characteristic marker of endothelia.

ECM and RNAseq targets of interest were manually curated for secreted molecules related to proliferation. Expression was validated in the LN MVNs by immunostaining **(Fig. 16**). The matricellular protein TINAGL1 was further explored in murine LNs. TINAGL1 has been identified as a metastasis suppressor in breast cancer by outcompeting fibronectin for binding

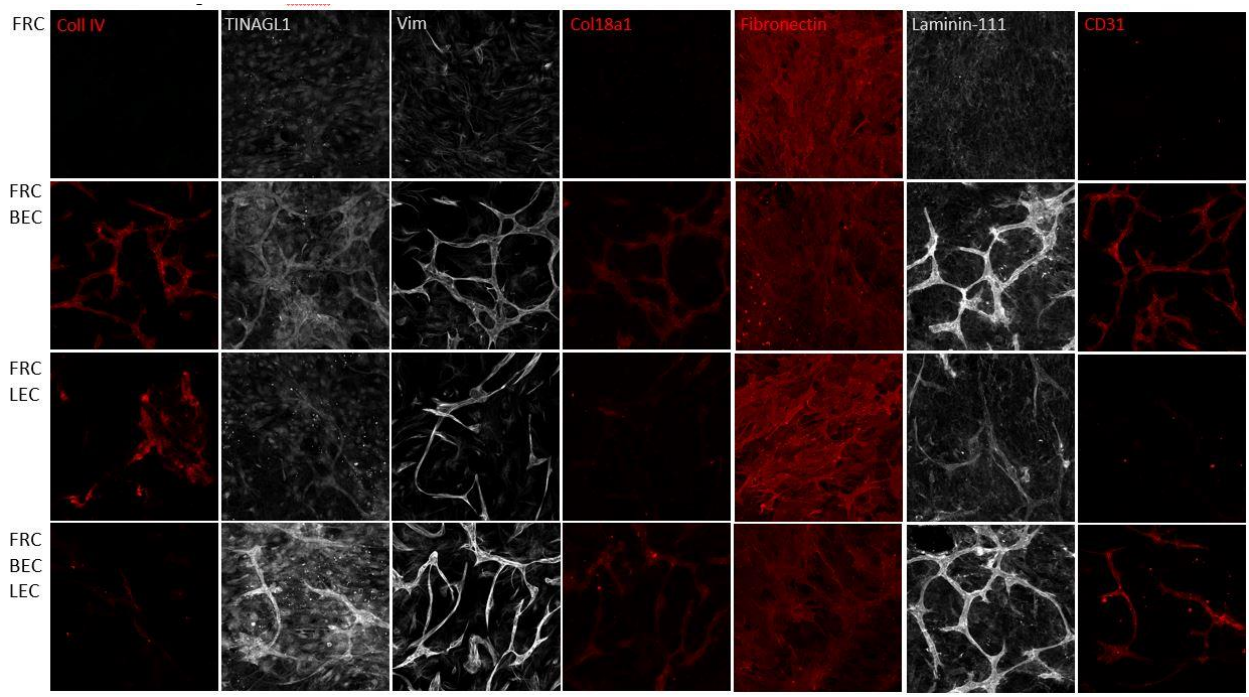

Fig. 16. Panel of ECM targets of interest that stained positively in lymph node MVNs. Several factors including the collagen IV, TINAGL1, vimentin, collagen 18a1, and laminin-111 were specific to the endothelia.

integrin receptors and preventing EGFR dimerization [470, 471]. Although ECM proteomics indicated that TINAGL1 was produced by LEC, staining revealed that it co-localized to blood endothelia and not lymphatic endothelia in mouse and human LNs (**Fig. 17a, b**). To our knowledge, this is the first report of TINAGL1 expression in the LN.

The functional role of these proteins in tumor dormancy was explored via knockdown in the endothelia using short-hairpin RNA constructs (pGIPz). Viral infection altered the structure of the HUVEC networks, even with only poor knockdown efficiency (**Fig. 18a**). Therefore, factors were overexpressed in the tumor growth permissive BLS-4 FRC cell line using the Broad hOrfeome library v8.1 [472]. It was hypothesized that overexpressing a growth suppressive factor would result in loss of tumor growth on the permissive BLS-4 stromal cells. The original pLX304 constructs with the CMV promoter were challenging to express in the murine BLS-4 cell line, so ORFs were Gateway cloned into the pLEX307 backbone (kindly provided by S. Beronja) with expression driven off the EF1a promoter. Overexpression was achieved in several

lines, using the V5 tag as a reporter (**Fig. 18b, c**). The overexpression lines were plated as in the LN MVNs, with T4-2 sparsely seeded for a 17-day growth period (**Fig. 18d**). T4-2 outgrowth significantly decreased with the SPOCK1 and LGALS3 lines and trended downward in all the tested lines, compared to empty vector control (**Fig. 18e**). These factors including SPOCK1, LGALS3, TINAGL1, VIM, MCAM, and EFEMP1 may therefore be growth-restricting factors since their overexpression in growth-permissive FRC niche hindered tumor cell growth.

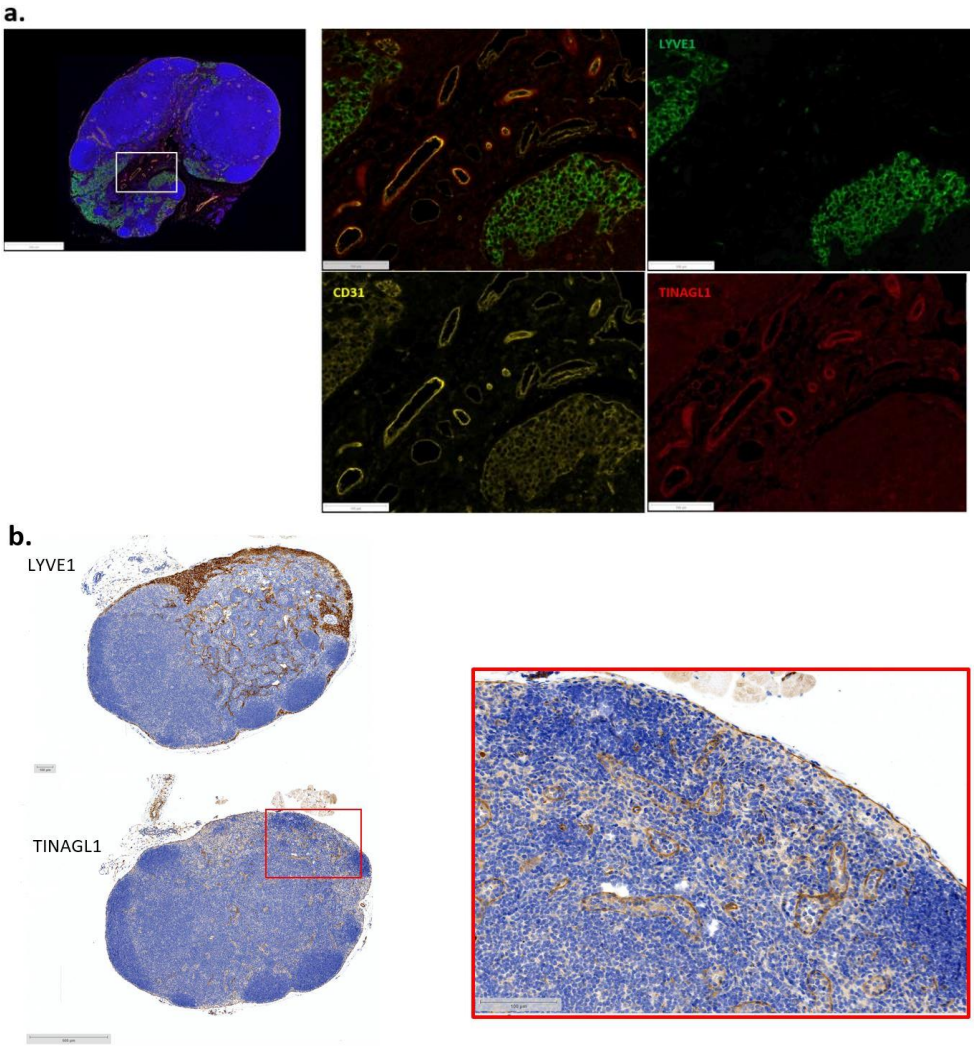

Fig. 17. TINAGL1 is expressed in the lymph node by blood endothelia. IHC staining of murine LN (a) and human LN (b) revealed that TINAGL1 localizes to CD31^{+} and not LYVE-1^{+} structures. **a**) Left, scale bar: 500 μm; insets, 100 μm. **b**) Left, scale bar: 500 μm; inset, 100 μm.

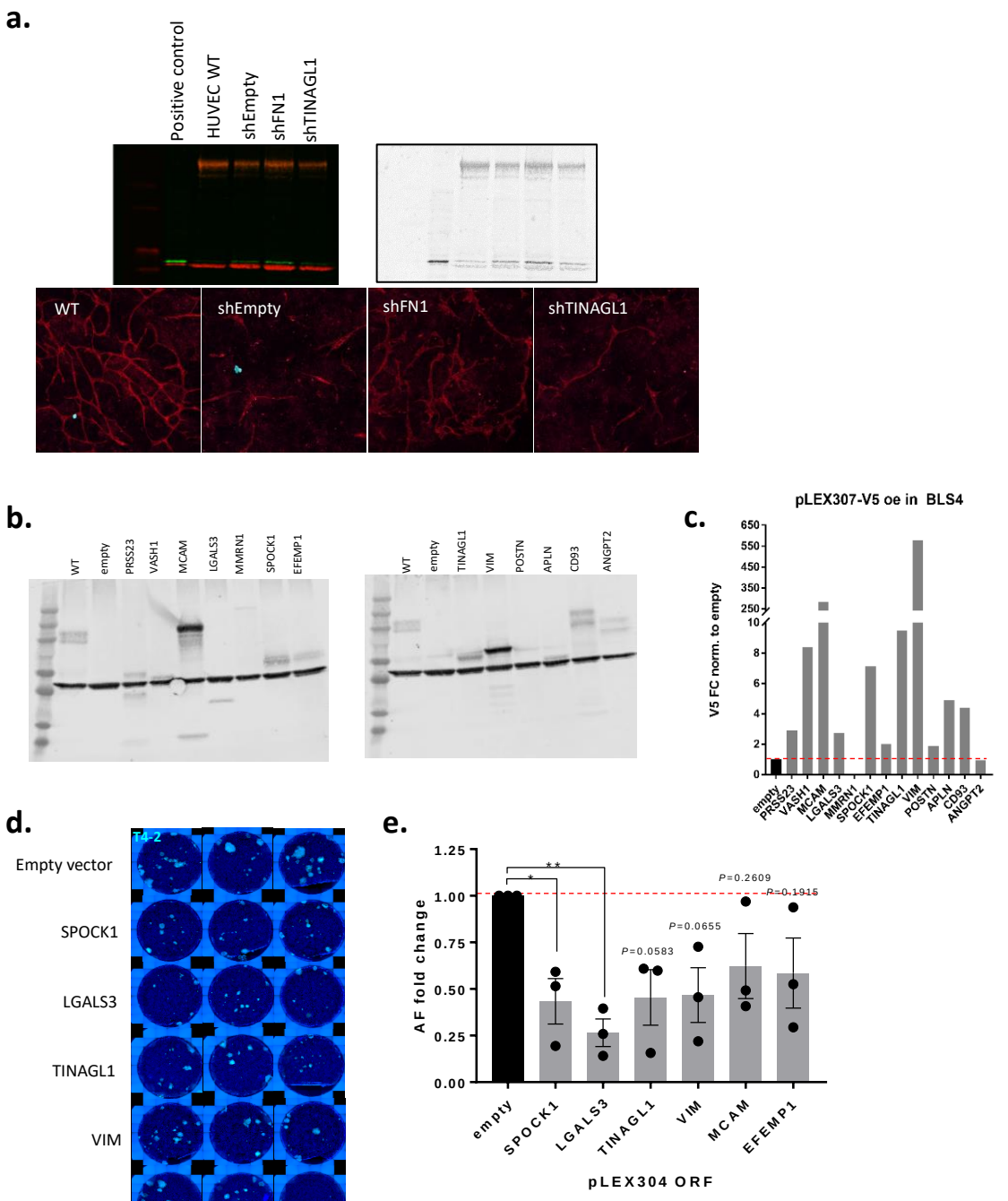

Fig. 18. Functional assessment of curated ECM factors in regulated tumor outgrowth. a) shRNA knockdown in HUVEC led to dysregulated vessel networks. **b, c**) Western blot and quantification of V5 tag signal from BLS-4 overexpression lysates. β-actin was used as a loading control. **d, e**) Representative images and quantification of T4-2 outgrowth on BLS-4 overexpression lines, normalized to empty control vector. n = 3 biological replications with 5-8 technical replicates each, one-way ANOVA with Dunnett's comparison to empty control*:* SPOCK1, *P*<0.0475; LGALS3, *P*<0.0091; TINAGL1, *P*<0.0583; VIM, *P*<0.0655; MCAM, *P*<0.2609; EFEMP1, *P*<0.1915.

5.2.3 *Functional studies indicate TGF-β1 is a BEC-specific growth suppressive factor*

In addition to investigating manually curated factors, the RNAseq data was assessed in an unbiased way through gene set enrichment analysis [473]. Differentially expressed genes were analyzed using the Hallmark gene set collection [474] to identify endothelial pathways that may be contributing to tumor growth suppression (**Fig. 19**). GSEA revealed the top differentially expressed pathways in the FRC+BEC condition vs. FRC, including EMT, TGFβ signaling, and inflammatory response (**Fig. 19b**); the top FRC+LEC pathways were oxidative phosphorylation, adipogenesis, and xenobiotic metabolism (**Fig. 19c**); and the top FRC+BEC+LEC pathways were coagulation, EMT, and TGFβ signaling (**Fig. 19d**). Since BEC were the primary quiescence niche *in vivo*, the TGFβ pathway was investigated further. TGF-β1 is a pleiotropic cytokine belonging to the TGFβ superfamily of ligands that includes three TGF-β ligands, bone morphogenic proteins (BMP), Nodal, activins, and growth and differentiation factors (GDF), among others. TGF-β1 is involved in a myriad of biological processes through membrane-to-nucleus signaling, including a context-dependent role as a tumor promotor or suppressor [154, 457, 475-478]. In addition to well-established pro-tumorigenic effects (EMT, angiogenesis, osteoclastic bone remodeling [155, 479], suppressing antitumor immunity [476]), TGF-β1 has also been linked to maintaining quiescence in early stage squamous cell carcinoma [83, 155, 479-481] and even some advanced metastatic breast cancer models [482] through modulating cell cycle protein expression [83, 153, 483]. In the bone marrow, autocrine TGF-β2 but not -β1 or -β3 induced dormancy of head and neck squamous cell carcinoma through p38α/β, revealing different family members may be under tissue-specific regulation [204]. TGF-β1 itself was enriched in FRC+BEC and FRC+LEC niches but not in FRC+BEC+LEC niches (**Fig. 20a)**, again indicating possible antagonism when both endothelia were present.

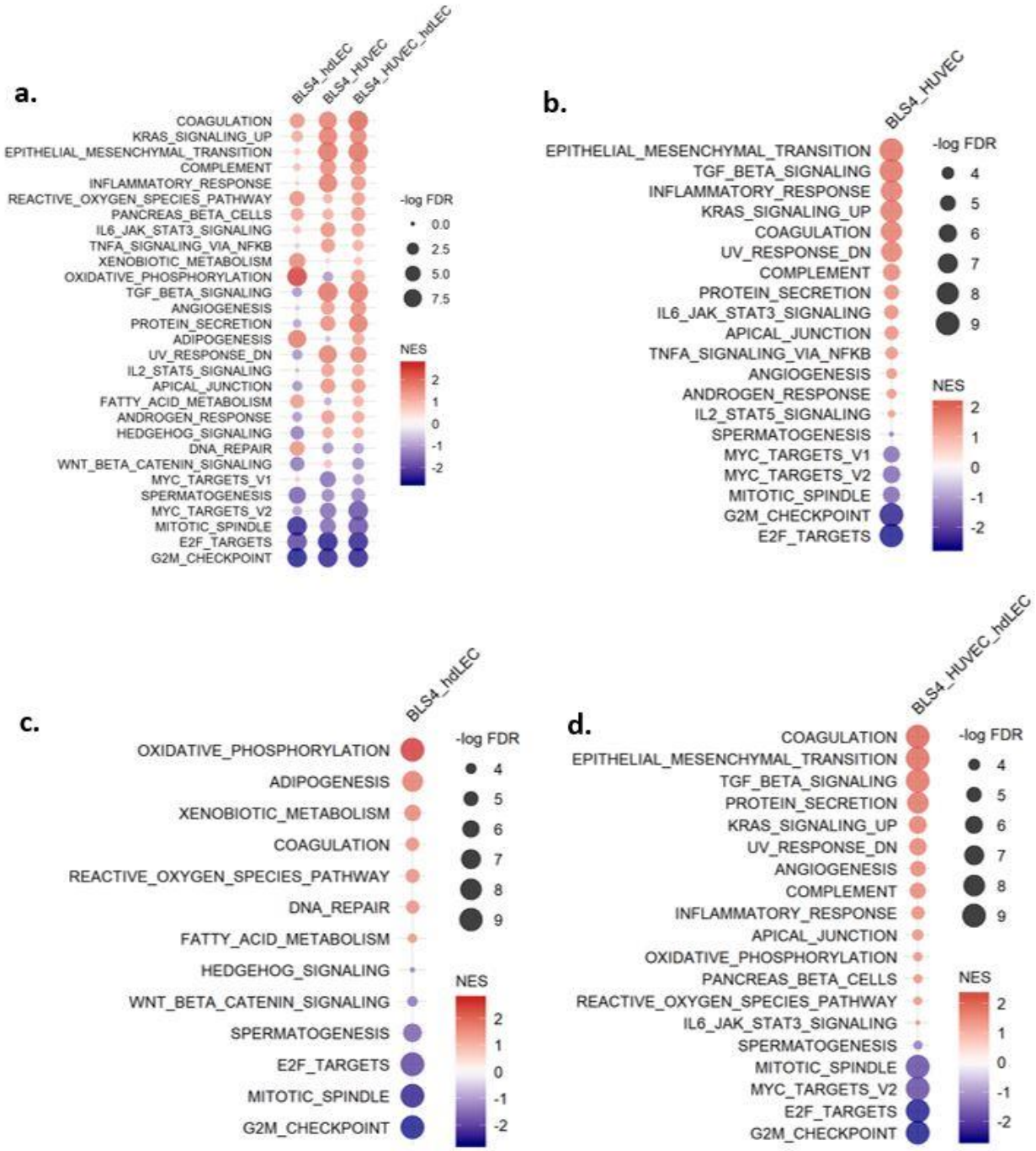

Fig. 19. Gene set enrichment analysis reveals top differentially expressed pathways among lymph node microvascular niches. **a**) Cross-niche comparison of differentially-expressed Hallmark pathways, ordered by normalized enrichment score (NES). **b-d**) Top pathways shown for FRC+BEC (b), FRC+LEC (c), and FRC+BEC+LEC (d).

TGF-β1 is first secreted in a latent form bound to carrier molecules and must be activated through cleavage by a variety of enzymes; although TGF-β1 expression was detected in both endothelial niches, several factors that affect TGF-β1 bioavailability were uniquely upregulated in the BEC-containing niches, including Tsp-1 [484] and Ltbp2 [485]. To determine whether functionally active TGF-β1 was present in the LN MVNs, the concentrations of latent and active human TGF-β1 from conditioned media were measured by ELISA. BEC-containing niches had significantly higher concentrations of both latent and active TGF-β1 versus FRC-only niches whereas elevated levels of TGF-β1 were not measured in FRC + LEC cultures (**Fig. 20b**), despite similar transcript levels (**Fig. 20a**). These results confirm that secreted, active TGF-β1 was uniquely bioavailable in the BEC-containing niches, indicating a potential mechanism for tumor cells quiescence in those niches.

To functionally test the effect of TGF-β1 on tumor growth within the LN MVNs, recombinant human TGF-β1 (rhTGF-β1) was added to FRC or FRC+BEC niches seeded with T4-2 cells (**Fig. 20c**, top panel). Increasing doses of rhTGF-β1 reduced T4-2 growth in the growth permissive FRC niches to baseline levels observed in the FRC+BEC niches (**Fig. 20c**, bottom left panel). TGF-β1 add-in had no effect on tumor cell outgrowth in the FRC+BEC condition, suggesting that TGF-β1-mediated suppression was effectively saturated where high concentration in the media was present (**Fig. 20c**, bottom left panel). rhTGF-β1 did not affect the Ki-67 status of single T4-2 cells in the FRC niche, which were already non-proliferative; conversely, it induced a dose-dependent loss of Ki-67 signal in T4-2 clusters, putting the brakes on dividing tumor cells by suppressing cell proliferation (**Fig. 20c**, bottom middle and right panels). Together, these data confirm that, (i) an organotypic LN-like co-culture system recapitulates vascular niche-driven quiescence seen *in vivo*, (ii) BEC-containing niches are rich

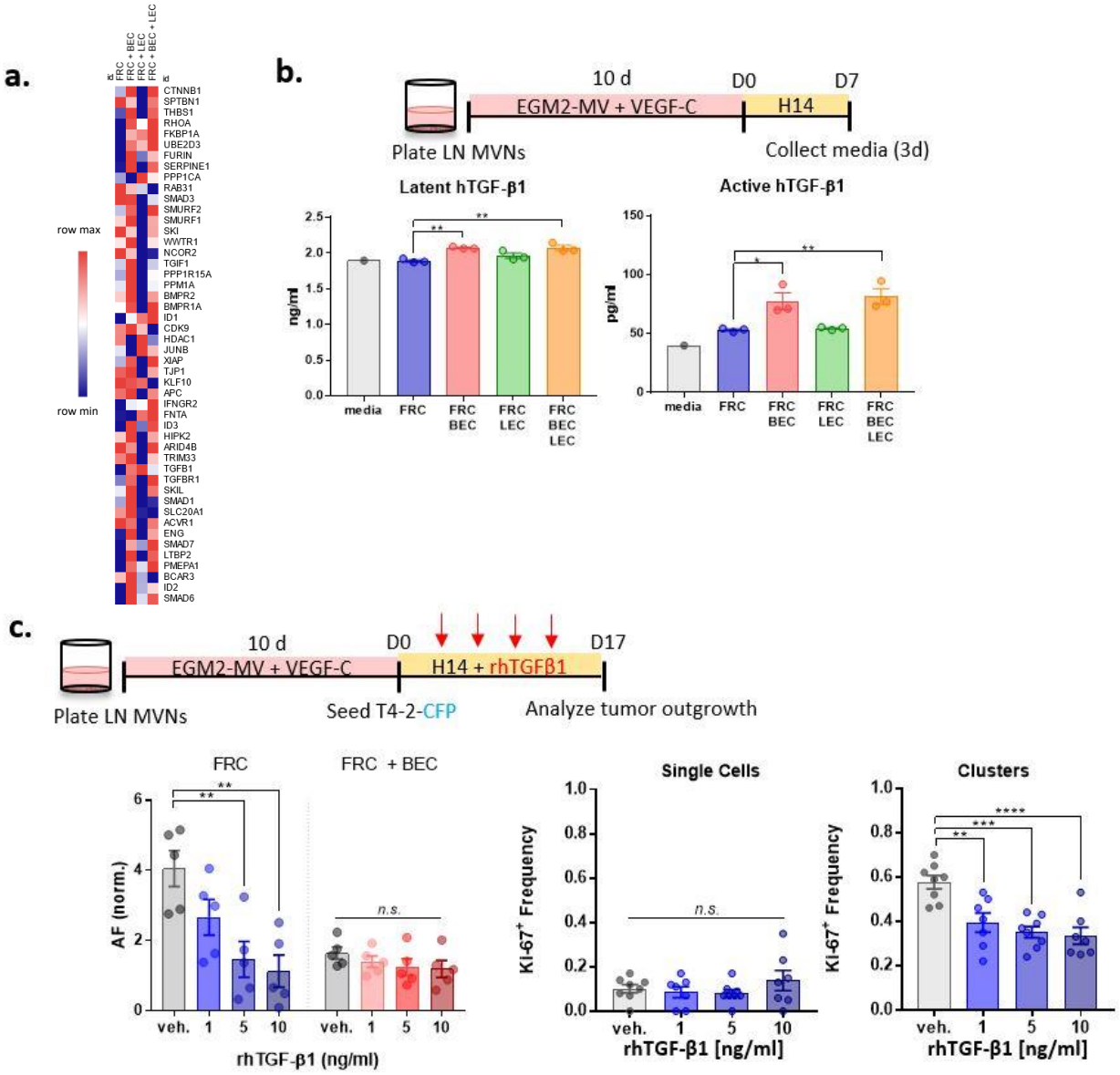

Fig. 20. Active TGF-β1 is present in BEC-containing niches and suppresses tumor growth. a) Heatmap showing row-normalized expression of genes in the Hallmark TGFβ signaling pathway, across LN MVN conditions. **b)** *Top panel*, schematic of conditioned media collection from LN MVNs to measure latent and active human TGF-β1 (hTGF-β1) by ELISA. n = 3 biological replicates with 8-10 technical replicates per condition. *Bottom left panel*, latent hTGF-β1: FRC vs. FRC+BEC, *P*=0.0037; FRC vs. FRC+LEC, *P*=0.2219; FRC vs. FRC+BEC+LEC, *P*=0.0037. *Bottom right panel*, active hTGF-β1: media vs. FRC vs. FRC+BEC, *P*=0.0187; FRC vs. FRC+LEC, *P*=0.9952; FRC vs. FRC+BEC+LEC, *P*=0.0083. **P*<0.05, ***P*<0.01, one-way ANOVA with Dunnett's multiple comparisons test to FRC control. **c)** *Top panel*, schematic of experiment to test whether add-in of recombinant human TGF-β1 (rhTGF-β1) suppresses T4-2 cell outgrowth on LN MVNs. *Bottom left panel*, T4-2 outgrowth on FRC and FRC+BEC MVNs with addition of rhTGF-β1, normalized to number of T4-2 cells seeded on D0. n = 5 biological replicates with 6-8 technical replicates per condition, one-way ANOVA with Dunnett's multiple comparisons test to vehicle (veh.): FRC, veh. vs. 1 ng/ml, *P*=0.1595, veh. vs. 5 ng/ml, *P*=0.0057, veh. vs. 10 ng/ml, *P*=0.0021; FRC+BEC, veh. vs. 1 ng/ml, *P*=0.7446, veh. vs. 5 ng/ml, *P*=0.4075, veh. vs. 10 ng/ml, *P*=0.3114. *Bottom middle and right panels*, representative graphs of Ki-67 analysis for single T4-2 cells and T4-2 clusters from rhTGF-β1 add-in experiments. n=5 biological replicates with 6-8 technical replicates per condition, one-way ANOVA with Dunnett's multiple comparisons test to veh.: Single cells, veh. vs. 1 ng/ml, *P*=0.9586, veh. vs. 5 ng/ml, *P*=0.8959, veh. vs. 10 ng/ml, *P*=0.6580; clusters, 1 ng/ml, *P*=0.0023, 5 ng/ml, *P*=0.0002, 10 ng/ml, *P*=0.0001. Clusters, veh. vs. 1 ng/ml, *P*=0.0023, veh. vs. 5 ng/ml, *P*=0.0002, veh. vs. 10 ng/ml, *P*=0.0001. **P*<0.05, ***P*<0.01, ****P*<0.001, *****P*<0.0001, *n.s.*, not significant.

in active TGF-β1, and (iii) increased doses of TGF-β1 are sufficient to suppress tumor cell colonization of growth-permissive FRC niches, functionally substituting for the presence of BEC. Having observed congruent results from decoupling inflammation and TGF-β1, it remained to be seen whether altering TGFβ signaling *in vivo* would be sufficient to impact metastatic outgrowth independent of inflammation.

5.3 DISCUSSION

Establishing the role of the LN microenvironment in tumor dormancy is crucial for preventing late relapse at this site and downstream vital organs. An organotypic model of the LN endothelial niche was developed to study the molecular mechanisms underlying tumor cell dormancy observed in this niche *in vivo*. MVNs combining murine FRC with human BEC and/or LEC faithfully recapture stroma-endothelial organization and reproducibly recapitulate tumor growth suppression for the human breast cancer cell line, triple-negative-like T4-2 (HMT-3522-T4-2) [466]. T4-2 resemble basal-like breast cancer by gene expression profiling and grow in a "mass"-type organization [486]. MCF-7 and T47D both fall under this growth category, yet neither cell line was able to colonize the LN MVNs. T4-2 display uniquely high levels of EGFR versus other human breast cancer lines [486], which may provide a clue for the signaling required to colonize the LN MVNs (and possibly the LN).

MVNs were characterized by targeted ECM proteomics and RNAseq, resulting in a clearer picture of molecular programs within each niche that could contribute to the effect on tumor cells. Although several secreted ECM factors related to proliferation were validated in the niches, functional studies proved challenging. ShRNA knockdown of targets in the primary human endothelia resulted in poor vessel network formation, a confounding factor in tumor growth. Overexpression of targets in the FRC trended towards suppressing tumor growth but did

not reach significance in two replicates.

However, GSEA using the RNA dataset for Hallmark pathways returned several differentially upregulated pathways of interest including TGFβ pathway in the growth suppressive BEC niche. TGF-β1 derived from the microenvironment has been shown to enhance breast cancer metastasis to the bone and lungs [69, 155, 479, 487] and melanoma progression [88], yet it also reversibly induces cell cycle arrest through activation of cyclin-dependent kinase inhibitors including $p15^{INK4B}$ and $p21^{CIP1}$ and inhibition of c-Myc [483]. These data show that active TGF-β1 is uniquely elevated in the BEC-containing niches and reduces tumor cluster proliferation in growth permissive FRC niches in a dose-dependent manner. Thus, TGF-β1 demonstrates a BEC-specific growth suppressive effect, which may be responsible for the tumor quiescence in the perivascular niche observed *in vivo.*

Several caveats may be mentioned here. First, only one of four human breast cancer lines was able to colonize the LN MVNs, indicating this is the exception in culture. The other human lines tested demonstrated minimal growth on any condition, suggesting they were unable to colonize the LN MVNs. Conversely, the mouse cancer lines displayed rampant outgrowth across the niches, which may point to their aggression or interspecies barriers to quiescent signaling. Second, differentially downregulated pathways were not explored. Third, the LN MVNs were a cross-species model, which may result in artificial barriers to signaling; however, we observed that murine FRC organized around the vessel tubules in a similar manner to murine tissue and supported spontaneous tubule network formation by the human endothelial cells (**Fig. 12b**). Additionally, human breast cancer cells were most successful at colonizing the FRC-only condition (**Fig. 13a, b**), implying conserved signaling mechanisms that facilitated tumor growth.

Chapter 6. TISSUE DYSREGULATION IN THE INFLAMED LYMPH NODE PRECEDES METASTATIC OUTGROWTH

6.1 INTRODUCTION

While the LN as a dormancy niche is under scrutiny, mechanisms of DTC awakening can be anticipated based on prior knowledge of awakening in the bone (Section 3.1.5), lungs (Section 3.2.2), and liver (Section 3.4.3). In each of these organs, structural remodeling and stromal activation are associated with tumor outgrowth as growth factors are released into the DTC microenvironment: bones undergo endosteal remodeling by osteoclasts and osteoblasts, releasing TGF-β1 and acidifying the niche [122]; the lungs respond to the inflammatory factor of tobacco smoke or bacterial infection by developing fibrosis and altered ECM organization [75, 237]; and liver responds to environmental insult by fibrosis as a result of activated stromal cells [343, 349], as well as the more controlled regeneration program [354]. Sprouting angiogenesis has been directly linked to dormant tumor cell awakening in two major organ sites, the bone and lungs, through loss of perivascular TSP-1 and introduction of mitogens such as POSTN into the microenvironment [69]. Thus, stromal remodeling in the context of physiological changes or fibrosis and injury change the cytokines within the milieu, activate the microenvironment, and may awaken resident quiescent DTCs as a secondary effect.

Despite the aforementioned conditions, adult tissues are generally resistant to acute physiological changes. A notable exception is peripheral immune organs including the LNs, which undergo swift and significant expansion upon inflammation in order to accommodate the influx of immune cells [417, 459, 488]. The initial phase of inflammation is regulated by $CD11c^+$ dendritic cells, and later expansion phases are maintained by B and T cells [489-491], although the exact cytokine program that fosters LN expansion and its cellular source is debated. A B cell-dependent, VEGF-independent expansion [492] as well as a B-cell independent program [493]

have both been described, and likely depend on timing post-immunization. Upon initial stimulation, activated dendritic cell CLEC-2 binds FRC podoplanin (PDPN), which relaxes the FRC network, allowing the LN to swell and expand [422, 494], and resident cells to proliferate [495]. The conduit network becomes leaky as FRCs loosen their attachments, exposing ECM components to the parenchyma. FRC expression of ECM components shifts, resulting in downregulation of netrin-1, which has been linked to quiescence factor TSP-1, and upregulation of metastatic niche components such as TNC and MMPs [417, 496]. Dendritic cells and FRCs coordinate secretion of VEGF-A and VEGF-C to induce BEC and LEC proliferation and angiogenesis and lymphangiogenesis [417, 489, 493, 497, 498]. Endothelial proliferation and cellularity peak five to seven days post-immunization [488, 490, 498-501] and LNs may remain enlarged more than 30 days post-immunization [499, 501].

The resulting inflamed LN is transcriptionally, morphologically, and functionally altered from homeostasis [417]. Given prior results showing loss of DTC quiescence around sprouting tip cells [69], it was hypothesized that such a dynamic response could result in loss of DTC-constraining mechanisms in the BEC niche as vessels activate and expand, leading to an investigation of tumor outgrowth from dormancy in the inflamed LN niche.

6.2 RESULTS

6.2.1 *Developing a model for inflammation-induced outgrowth from dormancy*

To examine whether disrupting the vascular architecture of the LN results in outgrowth of dormant DTCs, we leveraged the dramatic response of LNs to inflammation. We utilized bacterial lipopolysaccharide (LPS) from *Escherichia coli* to model a strong, sustained, and physiologically relevant inflammatory response in LN endothelia [501, 502]. First, the minimum dose of LPS that induced endothelial remodeling in draining LNs was determined by

subcutaneously injecting BALB/c mice with LPS near the lateral tail base over three consecutive days at a range of sublethal concentrations (**Fig. 21a**). This dosing scheme has been used to induce a sustained inflammatory response in prior studies, albeit in the lungs [75]. The draining axillary LNs [503] were collected seven days after the initial treatment and the three largest consecutive sections for each LN were analyzed. Using area as a surrogate for activation, we determined that 1 mg/kg LPS induced the most BEC growth without significantly affecting overall LN or LEC size, agreeing with previous reports that BEC are more responsive to LPS than LEC [488] (**Fig. 21b**). A timecourse was then performed using the 1 mg/kg LPS dose, with LNs harvested at 12 hours, four days, and seven days post-immunization (**Fig. 21c**). Total, $CD31^+$, and $LYVE\text{-}1^+$ areas increased by D4 post-treatment in agreement with prior immunization studies [488, 490, 504], although only the total area increase reached significance (**Fig. 21d)**. BEC expansion was likely related to cell division as opposed to enlargement of individual cells, as it was preceded by a significant increase in compartment-normalized $Ki\text{-}67^+$-area at 12 hours-post treatment (**Fig. 21e**).

For a model of LN metastasis, D2.0R cells were selected for their ability to re-emerge after extended periods (up to 240 days) of dormancy in the lungs [75]. Robust numbers of D2.0R in the LN were difficult to achieve via spontaneous dissemination from an orthotopic tumor (**Table 2, Fig. 22**), reflecting their noted slow growth kinetics [451]. To overcome these limitations, a direct injection route was explored. LN metastasis models have been limited by technical challenges related to confounding dissemination from primary tumors as well as accessing fragile lymph vessels [505]. Subcutaneous injection and spontaneous drainage to the nearest LN (e.g., footpad to popliteal LN) is commonly used but is most appropriate for melanoma, for which skin is the orthotopic site [503]. Direct LN injection has

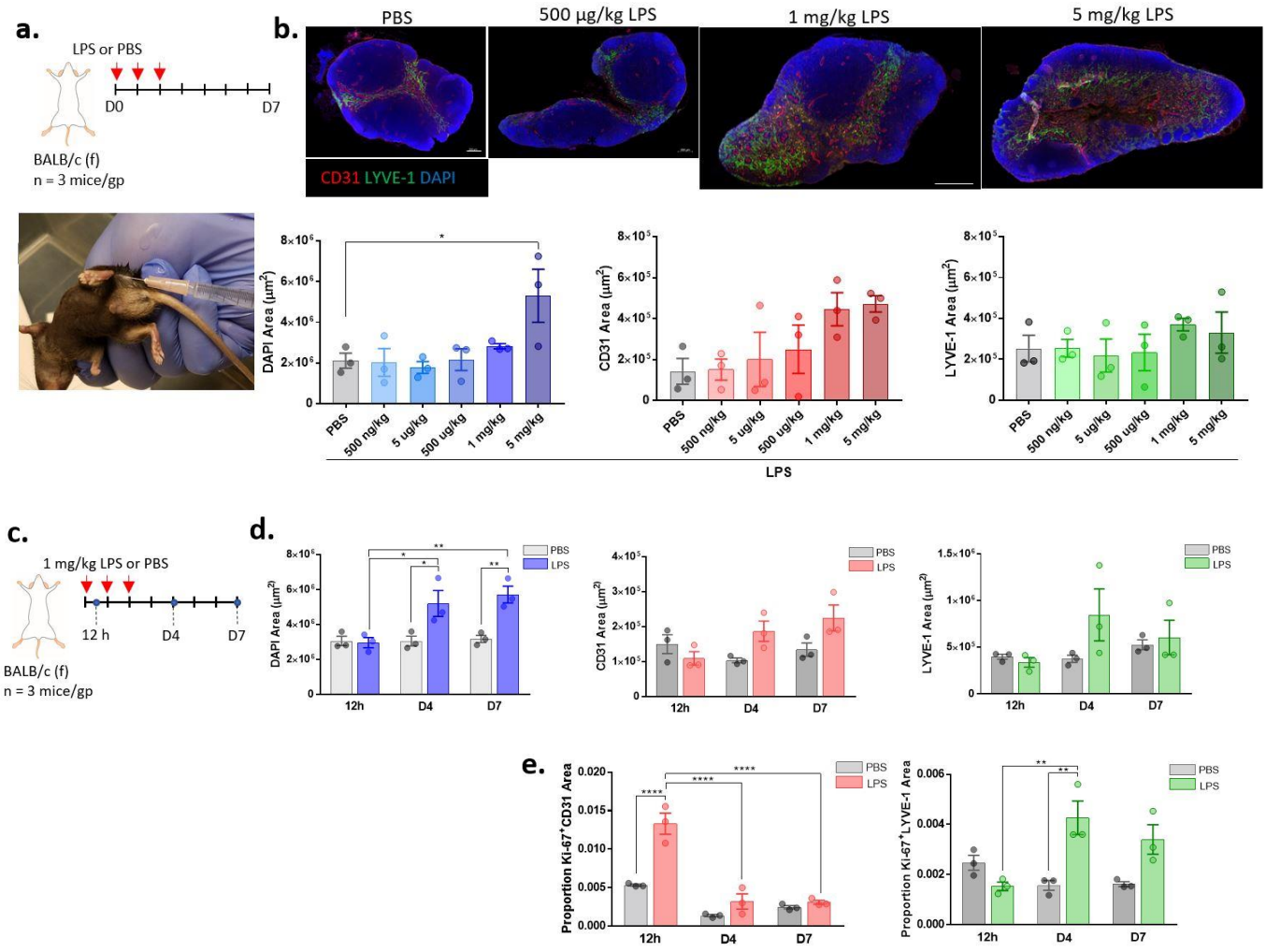

Fig. 21. Inflammation disrupts lymph node vasculature and triggers micrometastatic outgrowth.
a) Mice were treated over three consecutive days with increasing doses of lipopolysaccharide (LPS) to the lateral tail base (*bottom panel*) to determine optimal dosing. Draining axillary LNs were harvested on D7 from the initial treatment. **b**) Representative images of whole LN tilescans showing dose response to LPS. LNs were stained for anti-CD31, anti-LYVE1, and DAPI, shown to scale. Scale bar for PBS and 500 µg/kg LPS: 200 µm; scale bar for 1 mg/kg LPS and 5 mg/kg LPS: 500 µm. Total area of DAPI (*left panel*), CD31 (*center panel*), and LYVE-1 (*right panel*) as a function of LPS dose: DAPI, PBS vs. 5 mg/kg, P=0.0219. n = 3 sections per node for 3 mice per treatment, *P<0.05, one-way ANOVA followed by Dunnett's multiple comparisons test. **c**) Schematic of timecourse experiment. Draining axillary LNs were harvested at 12 hours, four days, and seven days after the initial treatment. **d**) DAPI (*left*), CD31$^+$ (*center*), and LYVE1$^+$ (*right*) areas over time. DAPI: D4 PBS vs. D4 LPS, P = 0.0314, D7 PBS vs. D7 LPS, P=0.0097, 12h LPS vs. D4 LPS, P=0.0238, 12h LPS vs. D7 LPS, P=0.0052. CD31: not significant. LYVE-1: not significant. N = 3 mice/group, *P<0.05, **P<0.01, one-way ANOVA followed by Sidak's multiple comparisons test. **e**) Proportion of Ki-67+ area normalized to CD31$^+$ (left) or LYVE-1$^+$ (right) area, over time. CD31: 12 h PBS vs. 12h LPS, P<0.0001, 12h LPS vs. D4 LPS, P<0.0001, 12h LPS vs. D7 LPS, P<0.0001. LYVE-1: D4 PBS vs. D4 LPS, P=0.0039, 12h LPS vs. D4 LPS, P=0.0035. N = 3 mice/group, **P<0.01, ****P<0.0001. one-way ANOVA followed by Sidak's multiple comparisons test.

been facilitated by intralymphatic vessel microinfusion [397] and transgenic models [32, 506] but requires specialized instruments or genetically engineered animals. More recently, direct injection of tumor into the robust mesenteric lymph duct [505], or popliteal [32] or inguinal LN[399], has enabled researchers to study spontaneously disseminating DTCs in downstream lymph vessels and LNs, successfully modeling intranodal metastasis.

To model intra-nodal metastases of mammary carcinoma D2.0R cells, the left inguinal LN was exposed through the overlying skin and D2.0R were injected directly into the LN (**Fig. 23a**). BLI signal showed that luciferase signal of injected D2.0R-ffLuc was lost over nine

Orthotopic injection (BALB/c)	Result
200K D2.OR parental	2/5 formed very small (nodule) tumors, regressed
1M D2.OR parental	2/5 formed tumors; D60 resected at ~300 mm^3. IP invasion.
1M D2.OR-eGFP	4/5 formed tumors; regressed around D9.
2M D2.OR-eGFP	8/10 formed tumors; D18 resected at ~150 mm^3. No IP invasion.

Table 2. Primary tumor growth kinetics from the D2.0R line injected to the orthotopic site. IP, intraperitoneal cavity.

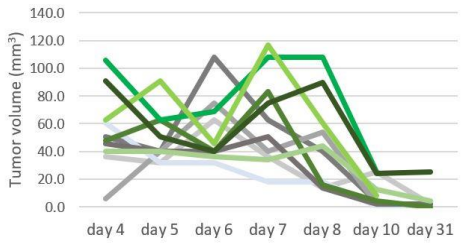

Fig. 22. Growth kinetics for D2.0R tumor cells injected orthotopically. Gray lines represent the parent line. Green lines represent eGFP-expressing lines. n = 5 BALB/c mice per group.

days, indicating dispersal of the cells (**Fig. 23b**). Low numbers of injected tumor cells ($1x10^5$) did not result in robust numbers of DTCs in downstream LNs but increasing the starting number up to $2x10^6$ D2.0R resulted in quantifiable DTCs with no primary tumor (**Table 3**). To determine whether D2.0R proliferated at secondary sites, a time course was conducted with systemic LN harvest at two to five weeks post-injection. At these time points, no overt metastases were detected, and single, Ki-67$^-$ D2.0R-eGFP cells were found in the medullary lymphovascular regions of systemic LNs (**Fig. 23c**), as in the 4T07 orthotopic model (**Fig. 7b**). Therefore, direct

LN injection recapitulated key characteristics of spontaneous dissemination to the LN with respect to quantity and localization of D2.0R LN DTCs.

6.2.2 *Inflammation disrupts lymph node vasculature and triggers micrometastatic outgrowth.*

Having optimized the model and treatment strategy, we set out to determine whether endothelial remodeling after LPS-induced inflammation resulted in metastatic outgrowth of dormant DTCs in the LN. $1x10^6$ D2.0R expressing eGFP and ffLuc were injected into the left inguinal LN of syngeneic BALB/c mice. Four weeks later, a timepoint shown to be sufficient to establish D2.0R dormancy *in vivo* [75] (**Fig. 23c**), mice were subcutaneously treated with three consecutive doses of 1 mg/kg LPS or PBS to the lateral tail base (**Fig. 24a**). Mice were

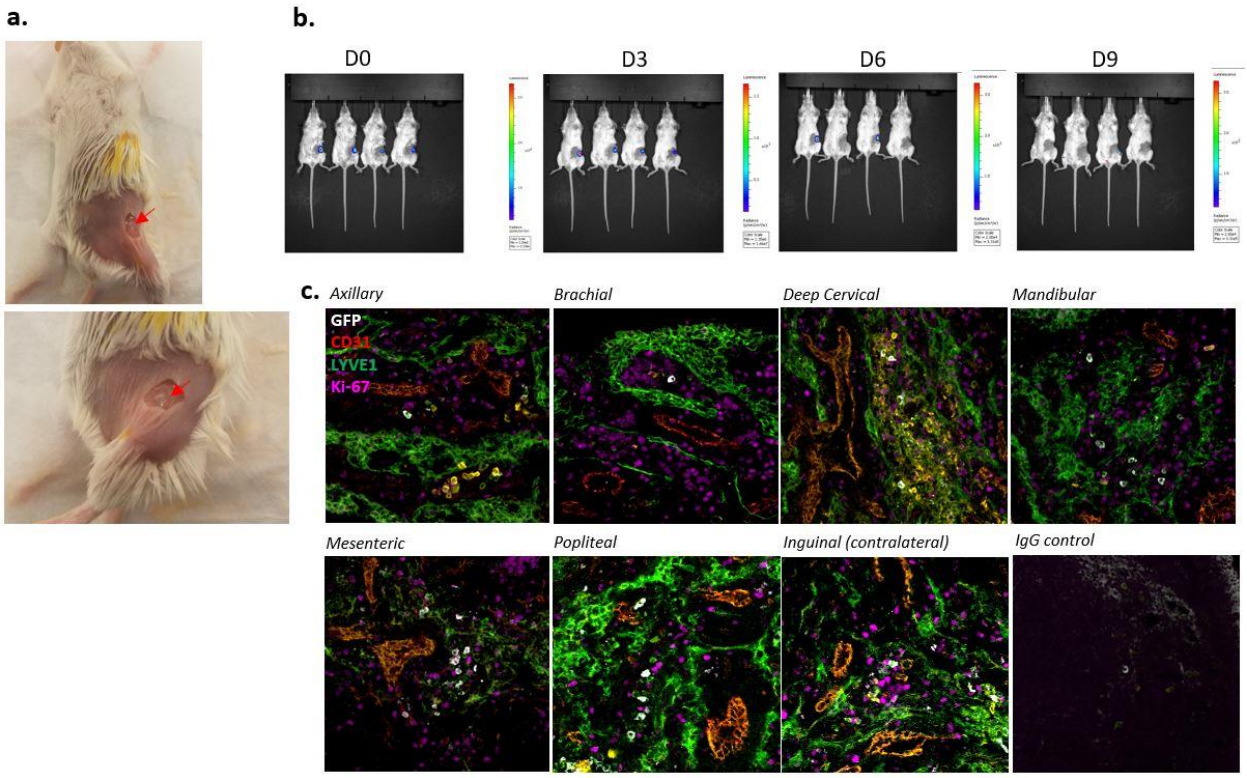

Fig. 23. Development of a model of syngeneic intranodal metastasis. a) The left inguinal LN was exposed and injected with tumor cells in a volume of 20 µl, causing the LN to swell (red arrows). **b)** Time course of intranodal injected D2.0R-ffLuc. Signal dispersed from the injection site by day nine. **c)** Representative images of D2.0R in systemic LNs at four weeks post intranodal injection. D2.0R were single and Ki-67$^-$, indicating minimum proliferation, and localized to the lymphovascular regions.

Intranodal injection (BALB/c)	Result
100K D2.OR parental	BLI thru D9; resected L Ing LN (enlarged). No tumor at injection site. Very few DTCs found in draining LNs.
100K D2.OR-ffLuc-eGFP	
100K 4T1-ffLuc-eGFP	
100K D2.OR-eGFP	Resect L Ing LN at D10 (enlarged). No tumor at injection site. Dormant DTCs found between 2 and 5 weeks post injection. More cells injected = more found in LNs.
200K D2.OR-eGFP	
500K D2.OR-eGFP	
1M D2.OR-eGFP	
2M D2.OR-eGFP	

Table 3. Intranodal injection with increasing doses of D2.0R. Increasing the number of injected D2.0R directly correlated with the frequency of DTCs that could be found in systemic LNs. 1M ($1x10^6$) D2.0R was selected as the number of cells for the inflammation experiment. 4T1 were used as a positive BLI signal control.

monitored weekly via bioluminescent imaging (BLI) for four weeks post-treatment, then the draining axillary and popliteal LNs [503] were harvested for immunostaining. No overt metastases or BLI signal was detected, so LNs were sectioned in their entirety to assess micrometastatic burden (**Fig. 24b**). Although micrometastases (defined as doublets to clusters of more than 20 cells) were detected in both LN sites and treatment groups, significantly more micrometastases were detected in the LNs of LPS-treated mice than control (total: mean ± S.D., 9.5 ± 10.32 micrometastases in PBS group vs. 120.7 ± 84.91 in LPS group; axillary: 7.6 ± 7.763 in PBS group vs. 67.3 ± 41.47 in LPS group; popliteal: 1.9 ± 3.381 micrometastases in PBS group vs. 54.4 ± 45.73 in LPS group, **Fig. 24c**). The number of micrometastases with at least one Ki-67^+ tumor cell in the cluster was also significantly greater in LPS-treated mice in total and in each LN analyzed (**Fig. 24d**), indicating enhanced proliferation with LPS treatment.

It has been reported that a combination of LPS and EGF induce proliferation in dormant MDA-MB-231 cells in culture [507]. To rule out the possibility that LPS directly stimulated D2.0R proliferation *in vivo*, a growth curve was generated for D2.0R treated with increasing doses of LPS in culture, with 4T07 as a comparison (**Fig. 24e**). After three days, at which point the cells reached confluency, no significant difference in cell number was detected, suggesting that the observed outgrowth of D2.0R with LPS treatment was related to cell-extrinsic factors.

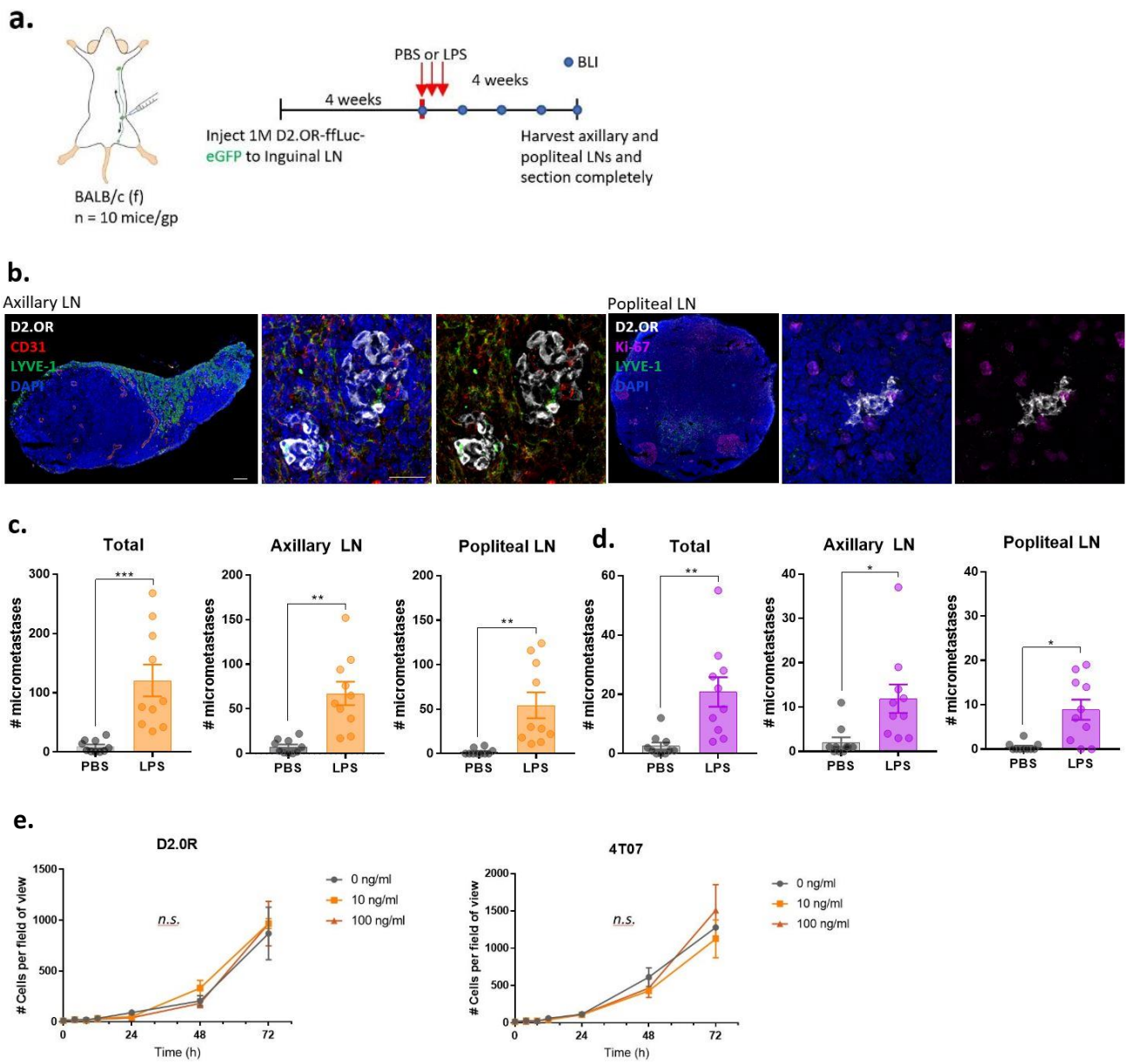

Fig. 24. Inflammation induces metastatic outgrowth of D2.0R in the lymph node. a) Female BALB/c mice were injected in the left inguinal LN with $1x10^6$ syngeneic D2.0R mammary carcinoma cells expressing eGFP-ffLuc. Four weeks after D2.0R inoculation, mice were treated over three consecutive days with PBS or 1 mg/kg LPS. Axillary and popliteal LNs were harvested four weeks after the initial treatment and sectioned completely. **b**) Representative images of micrometastases within the axillary (left) and popliteal (right) LNs of LPS-treated mice stained with anti-eGFP, anti-LYVE1, anti-Ki-67, DAPI, and anti-CD31. Scale bar for whole LN tilescans: 100 μm; scale bar for micrometastases: 20 μm. **c**) Number of micrometastatic clusters in the LNs of each treatment group, in total (*left panel*), axillary (*center panel*), and popliteal (*right panel*) LNs (n = 10 mice per treatment group, LNs sectioned completely through at 18 μm sections: total, P=0.0007; axillary, P=0.0003; popliteal, P=0.002). **P<0.001, ***P<0.0001; unpaired Student's t-test. **d**) Number of micrometastatic clusters with at least one Ki-67$^+$ nucleus, in total (*left panel*), axillary (*center panel*), and popliteal (*right panel*) LNs (n = 10 mice per treatment group, LNs sectioned completely through in 18 μm sections: total, P=0.0022; axillary, P=0.01; popliteal, P=0.0019). *P<0.05, **P<0.001; unpaired Student's t-test. **e**) Increasing doses of LPS did not directly stimulate D2.0R (*left*) or 4T07 (*right*) proliferation over 72 hours in culture. n=1 biological replicate, 3 fields of view per dose per timepoint, one-way ANOVA with Tukey's multiple comparisons test, *n.s.*, not significant.

6.2.3 *Single-cell RNAseq of LN stroma reveals loss of TGFβ signaling upon LPS treatment*

To identify molecular changes to the LN stroma induced by acute inflammation that potentially caused loss of tumor cell quiescence, we used single-cell (sc) RNAseq to profile LNSC from treated and untreated mice. ScRNAseq has identified subpopulations within murine and human LN FRC [508], BEC [509], and LEC [508, 510-512], and transcriptional changes following viral infection and inflammation [417, 501, 508]. We treated pairs of female BALB/c mice with PBS or 1 mg/kg LPS, injected subcutaneously over three consecutive days (**Fig. 25a**). LN pairs from six locations (axillary, brachial, mandibular, deep cervical, inguinal, and popliteal; 12 LN total) were harvested on day four following the initial treatment, a timepoint guided by previous observations of LNSC activation (**Fig. 21c**) and prior studies indicating maximum activation at three to six days post-immunization [488, 501, 513, 514]. We also wanted to ensure any transcriptional changes measured in BEC were associated with inflammatory activation and not merely entering the cell cycle, which occurred ~12 hours post-treatment (**Fig. 21d**).

After harvesting, LNs were enzymatically and mechanically digested, then pooled LNSC were enriched by FACS (FRC: $CD45^-CD31^-PDPN^+$; BEC: $CD45^-CD31^+PDPN^-$; LEC: $CD45^-CD31^+PDPN^+$) (**Fig. 25a**). The experiment was carried out in triplicate, using the 10X Chromium single-cell 3' kit (v3.1) to generate libraries. The numbers of FRC, BEC, and LEC that were analyzed for each replicate are reported in **Fig. 25b**. FRC were the most abundant cell type in each sample, followed by BEC, LEC, and a small population of B cells that were excluded from further analysis (**Fig. 25c, d**). Unsupervised clustering was used to delineate cell populations (**Fig. 25d**), and cluster identities were assigned using characteristic markers for FRC, BEC, and LEC (**Fig. 26**). Unsupervised clustering within each LNSC population revealed shifting transcriptional profiles with LPS treatment (**Fig. 27a-c**). The most consistent change was

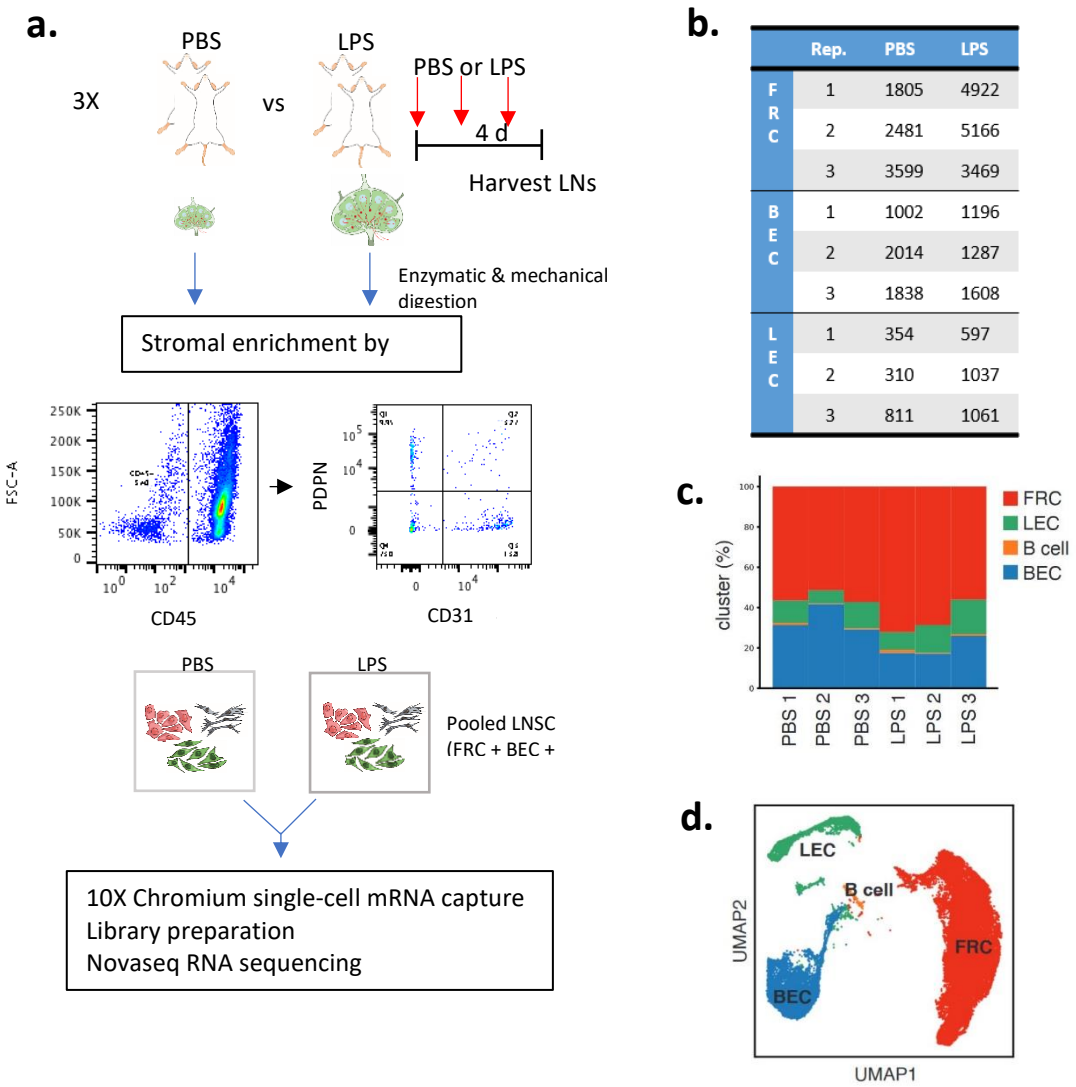

	Rep.	PBS	LPS
FRC	1	1805	4922
	2	2481	5166
	3	3599	3469
BEC	1	1002	1196
	2	2014	1287
	3	1838	1608
LEC	1	354	597
	2	310	1037
	3	811	1061

Fig. 25. A single-cell RNAseq approach to profiling inflamed lymph node stromal cells. a) Experimental workflow for murine lymph node stromal cell (LNSC) enrichment for single-cell RNAseq. Three biological replicates using pairs of mice for each treatment condition (PBS or 1 mg/kg LPS) were harvested and processed under identical conditions. LNSC were mechanically and enzymatically isolated from LNs (paired axillary, brachial, deep cervical, mandibular, inguinal, and popliteal, 12 LNs total) and enriched by FACS (FRC: $CD31^{-}PDPN^{+}$, LEC: $CD31^{+}PDPN^{+}$, BEC: $CD31^{+}PDPN^{-}$). Libraries of pooled LNSC were prepared for each replicate, frozen, and then sequenced simultaneously. **b**) Counts of LNSC per treatment group and replicate. **c**) Relative distribution of cells per treatment and replicate. **d**) UMAP plot showing unsupervised clustering of LNSC from all three replicates (including both PBS and LPS treatment groups). The number of cells represented are: 21,442 FRC; 8,945 BEC; 4,170 LEC; and 288 B cells, which were excluded from downstream analysis.

in the BEC, with cells shifting from cluster 0 (blue) to cluster 2 (green) with treatment (**Fig. 27d**). Closer analysis of the Reactome pathways upregulated in cluster 2 include platelet degranulation, leukocyte adhesion, and complement cascade (**Fig. 27e**), indicating cluster 2 may be activated HEVs that support immune trafficking to the inflamed LN.

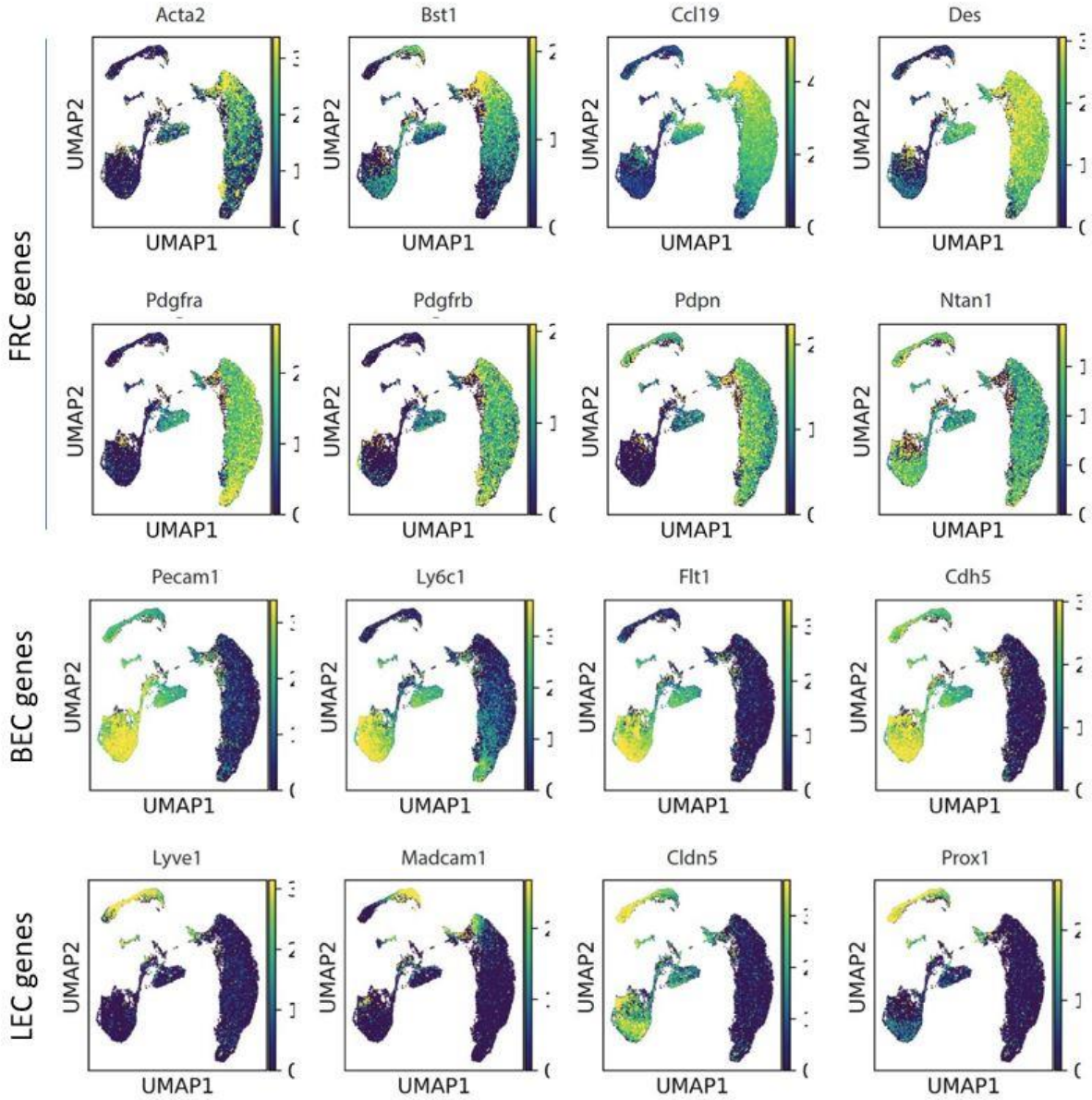

Fig. 26. Identification of lymph node stromal cell identities among unsupervised clusters using characteristic genes. FRC genes: smooth muscle alpha-2 actin (Acta2), bone marrow stromal cell antigen 2 (Bst2), C-C motif chemokine ligand 19 (Ccl19), desmin (Des), platelet-derived growth factor alpha and beta (Pdgfra, Pdgfrb), podoplanin (Pdpn), N-terminal asparagine amidase(Ntan1/PNAD). BEC genes: platelet and endothelial cell adhesion molecule (PECAM1), lymphocyte antigen 6C1 (Ly6c1), Fms related receptor tyrosine kinase 1 (Flt1), and cadherin 5 (Cdh5). LEC genes: lymphatic vessel endothelial hyaluranon receptor 1 (LYVE1), mucosal addressin cell adhesion molecule 1 (Madcam1), claudin 5 (Cldn5), and Prospero-homeobox protein 1 (Prox1).

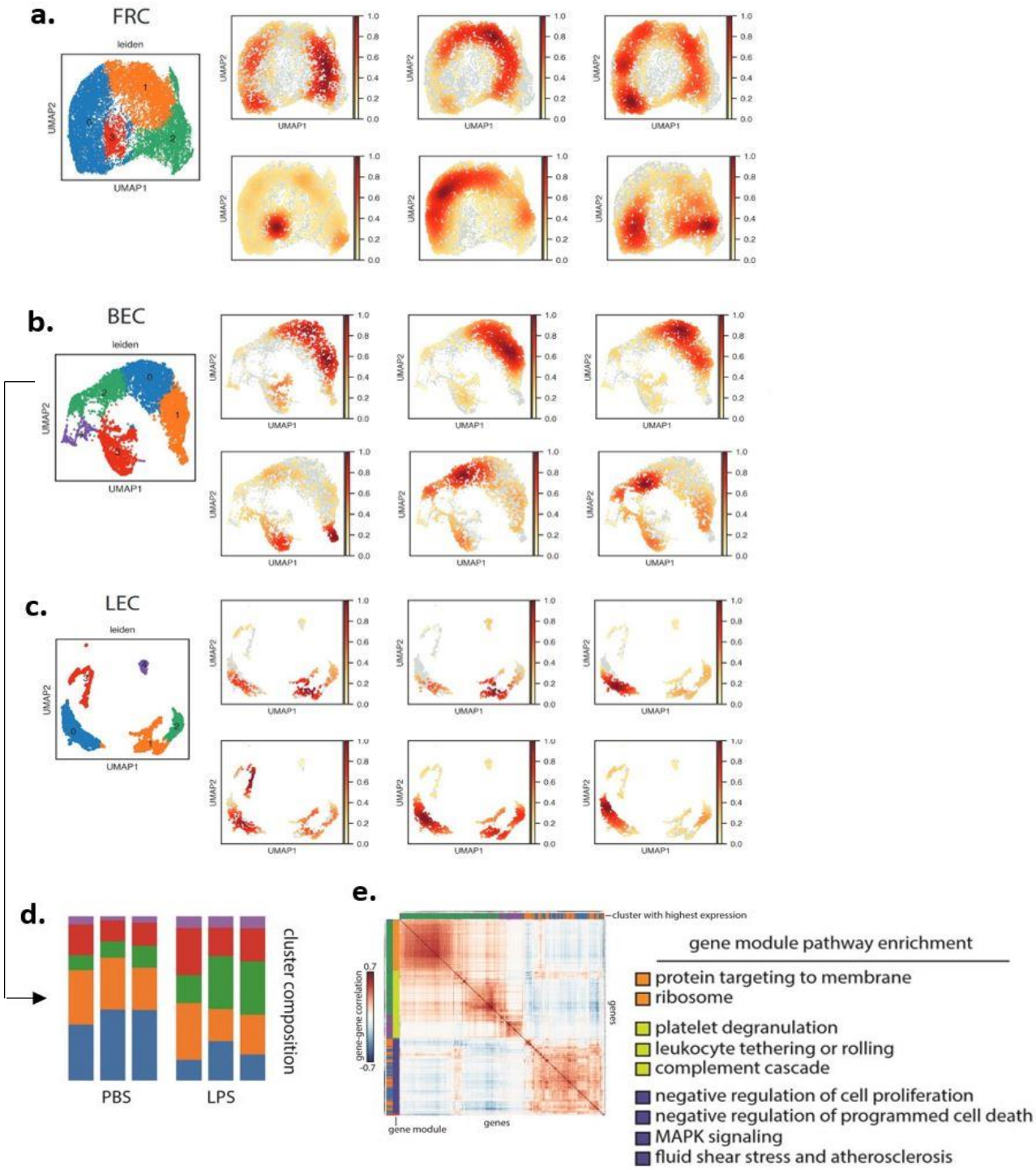

Fig. 27. Lymph node stromal cells shift transcriptional profiles with inflammatory treatment. UMAP plots of **i**ntra-group clustering for each LNSC with treatment: a) FRC, **b**) BEC, **c**) LEC. *Top panels*, PBS control; *bottom panels*, LPS treatment. **d**) Proportion of BEC populating each cluster across treatments and replicates. **e**) Heatmap and gene set enrichment showing differential expression of Reactome pathways for BEC clusters.

Unpaired analysis of PBS vs. LPS-treated LNSC initially revealed several LPS-responsive genes were upregulated including MHCI antigen presentation molecules (H2-K1, H2-D1) and anti-microbial factor lipocalin 2 (Lcn2) [515] which Malhotra *et al.,* identified as a marker of inflamed LNSC at 12 h post-immunization[417]. This indicated that the LNSC in our model were responding to LPS-induced inflammation with the sustained three day-treatment.

Next, the top differentially expressed (DE) genes ($log_2FC > 0.5$) between treatments were identified for each LNSC within replicate pairs, resulting in 79 DE genes for FRC, 61 DE genes for BEC, and 44 DE genes the passed the FDR ≤ 0.5 threshold in at least one replicate (**Fig. 28a**). We confirmed upregulation of inflammatory response genes such as interferon regulatory factor 7 (Irf7) [516, 517] in all three LNSC populations and Cxcl9 [518] in BEC and LEC, as well as loss of anti-inflammatory cytokine IL-6 [519, 520] in FRC, in agreement with the emerging immune modulatory role of the stroma [516, 517, 521]. BEC displayed an upregulation of cell cycle protein Cdk1, confirming active proliferation upon treatment. Fos and Jun, which form the activator-protein-1 complex, were consistently lost across LNSC, which is a prognostic indicator for tumor progression and increased LN metastasis in gastric [522] and ovarian cancer[523]. Several changes to secreted extracellular matrix molecules among LNSC were observed (upregulation of versican and downregulation of fibronectin 1, collagen1a1, periostin, tenascin C, and angiopoietin 2) accompanied by variation in MMP and TIMP expression. Although these changes reflect a dynamically evolving microenvironment, many of the downregulated ECM molecules typically belong to a *pro*-metastatic stromal signature [69, 167, 241, 524-527]. Thus, their loss was unexpected given the phenotypic outcome of LPS treatment (**Fig. 24**), leading us to rule out these ECM factors as central regulators of metastatic outgrowth upon inflammation.

In addition to changes in ECM molecule expression, we noted that several TGFβ pathway-related genes were consistently downregulated in BEC and LEC upon treatment (Tgfb1, Tgfbr2, Smad4, Smad7, Tsp-1, Tgif, Smurf2, Ski, Ltbp2) (**Fig. 28a**). The apparent loss of TGFβ family members with treatment, combined with the observation that several pro-metastatic DE ECM molecules responded in the *opposite* trend from expected, led us to speculate whether endothelial TGFβ signaling could be responsible for DTC quiescence under homeostatic conditions and subsequently lost upon inflammation-induced activation. Using comparative pathway analysis, we found that the BEC TGFβ pathway score decreased with treatment (especially in replicates 2 and 3), in contrast to FRC and LEC (**Fig. 28b**). Pooling replicates confirmed that the TGFβ pathway score significantly decreased in all three LNSC populations (FRC, $P<0.003$; BEC, $P<2e^{-9}$; LEC, $P<1e^{-11}$, **Fig. 28c**). TGF-β1 was expressed in a large proportion of BEC and LEC, and mean expression in each population decreased upon LPS treatment (**Fig. 28c**). Compared to TGF-β1, TGF-β2 and -β3 demonstrated low population expression, indicating that TGF-β1 is the dominant pro-quiescent cytokine in the LN (in contrast to TGF-β2 in the bone marrow [157]). Other individual pathway members including Smad2, -3, -4, -7, Tsp-1, and Ltbp2 demonstrated mild loss of expression with treatment, albeit in a relatively small proportion of cells. Thus, we focused our attention on TGF-β1 as a potential LN-specific angiocrine quiescent factor.

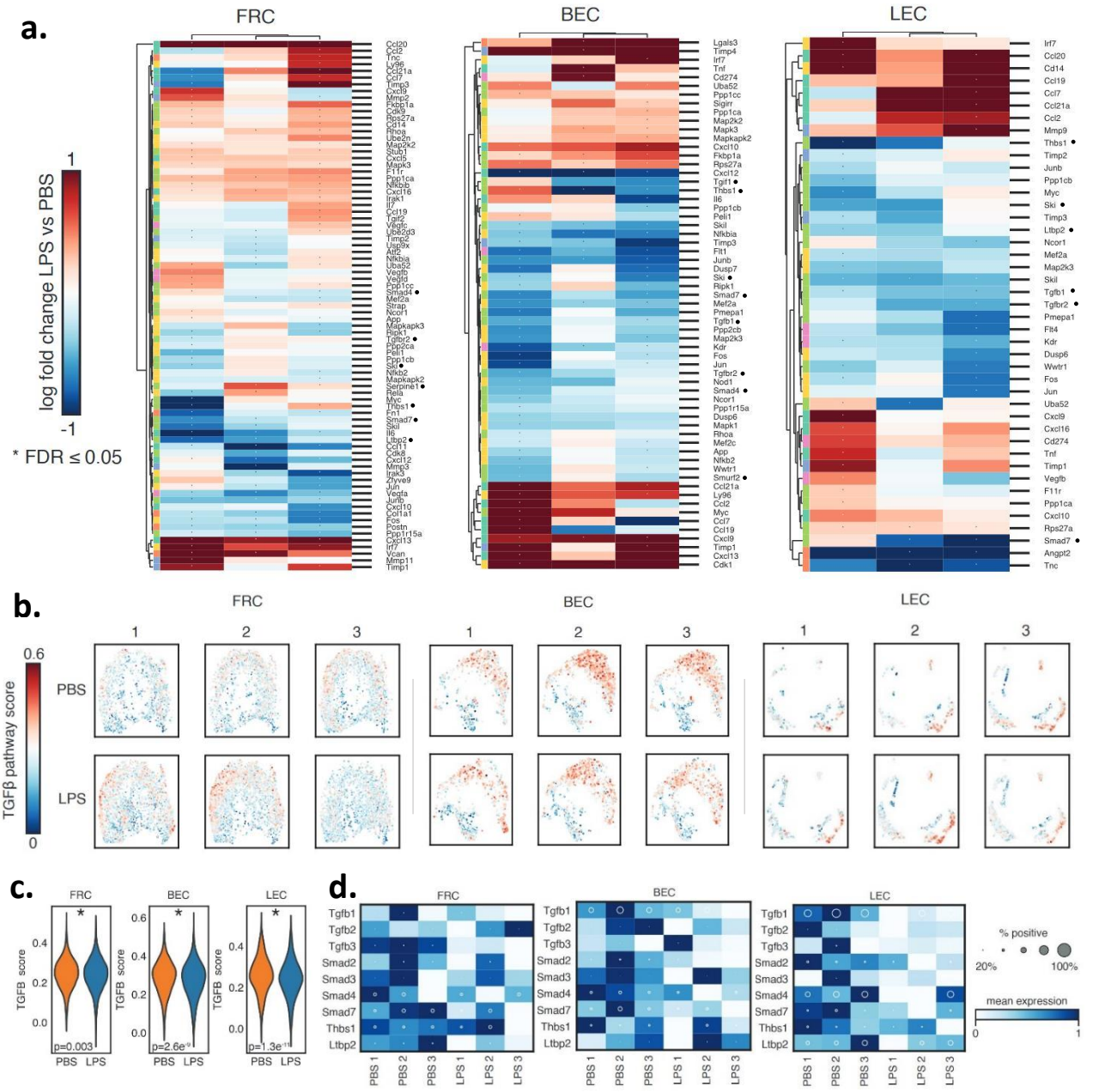

Fig. 28. Single-cell RNAseq reveals a loss of TGFβ signaling in lymph node stromal cells upon inflammation. a) Heatmaps of pairwise comparisons showing $\log_2$ fold changes in gene expression between treatments for respective LNSC replicates. Asterisk indicates FDR ≤ 0.05. Dots indicate proteins related to TGFβ signaling. **b**) Single-cell TGFβ pathway scores overlaid on cell type UMAPs showing changes between treatments for respective LNSC replicates. **c**) Violin plots showing significant decrease in TGFβ pathway score in LNSC (pooled replicates). **d**) Heatmaps showing relative mean expression (color) and population penetrance (dot size) of individual TGFβ pathway members for each LNSC and treatment replicate.

6.2.4 *TGFβ signaling is required for lymph node DTC dormancy in vivo.*

TGF-β1 ligand binds to a heterodimer of type I and II transmembrane serine/threonine protein kinases, TGF-βR1 (TβR1) and TGF-βR2 (TβR2). Upon binding, TβR2 phosphorylates TβR1, which in turn phosphorylates SMAD2 and 3, allowing them to complex with SMAD4 and translocate to the nucleus to enact transcription factor function [476].

It was hypothesized that interrupting this signaling axis would release D2.0R from quiescence induction by the vascular niche and effect micrometastatic outgrowth. TβR2 was knocked down in D2.0R-ffLuc cells using pLKO.1 shRNA constructs [528]. Out of five shRNA clones screened, two resulted in substantial knockdown of TBR2 to 5.9% and 9.7% of expression by the non-targeting (NT) vector line, by Western blot (**Fig. 29a**). BALB/c mice were injected in the left inguinal LN with D2.0R expressing either the Sh #1 or NT control vector (n = 4/group, **Fig. 29b**). BLI was used to monitor metastatic outgrowth weekly. Although no BLI signal was detected after four weeks, previous experiments with D2.0R indicated that differences might be observed at the micrometastatic level (**Fig. 24**). Axillary LNs were harvested and immunostained for eGFP (D2.0R), CD31, Ki-67, and DAPI (**Fig. 29c**). Micrometastatic clusters of at least two cells were counted throughout the same tissue volume for each mouse spanning approximately half the total volume of the node. TβR2 KD in tumor cells resulted in a significant 1.75-fold increase in micrometastases compared to NT control cells (P=0.0313, Student's t test; mean ± SD, KD vs. NT, 429.3 ± 63.09 vs. 246 ± 114.8 micrometastases, **Fig. 29e**), and significantly more Ki-67$^+$ clusters were detected in the knockdown group (P=0.0112, Student's t test; mean ± SD, KD vs. NT, 59.75 ± 13.2 vs. 31 ± 8.91 micrometastases, **Fig. 29f**). It is interesting to note that TβR2 KD did not alter the vascular association of clusters (**Fig. 29g**), indicating that loss of TGF-β1 signaling allowed outgrowth in the suppressive perivascular niche.

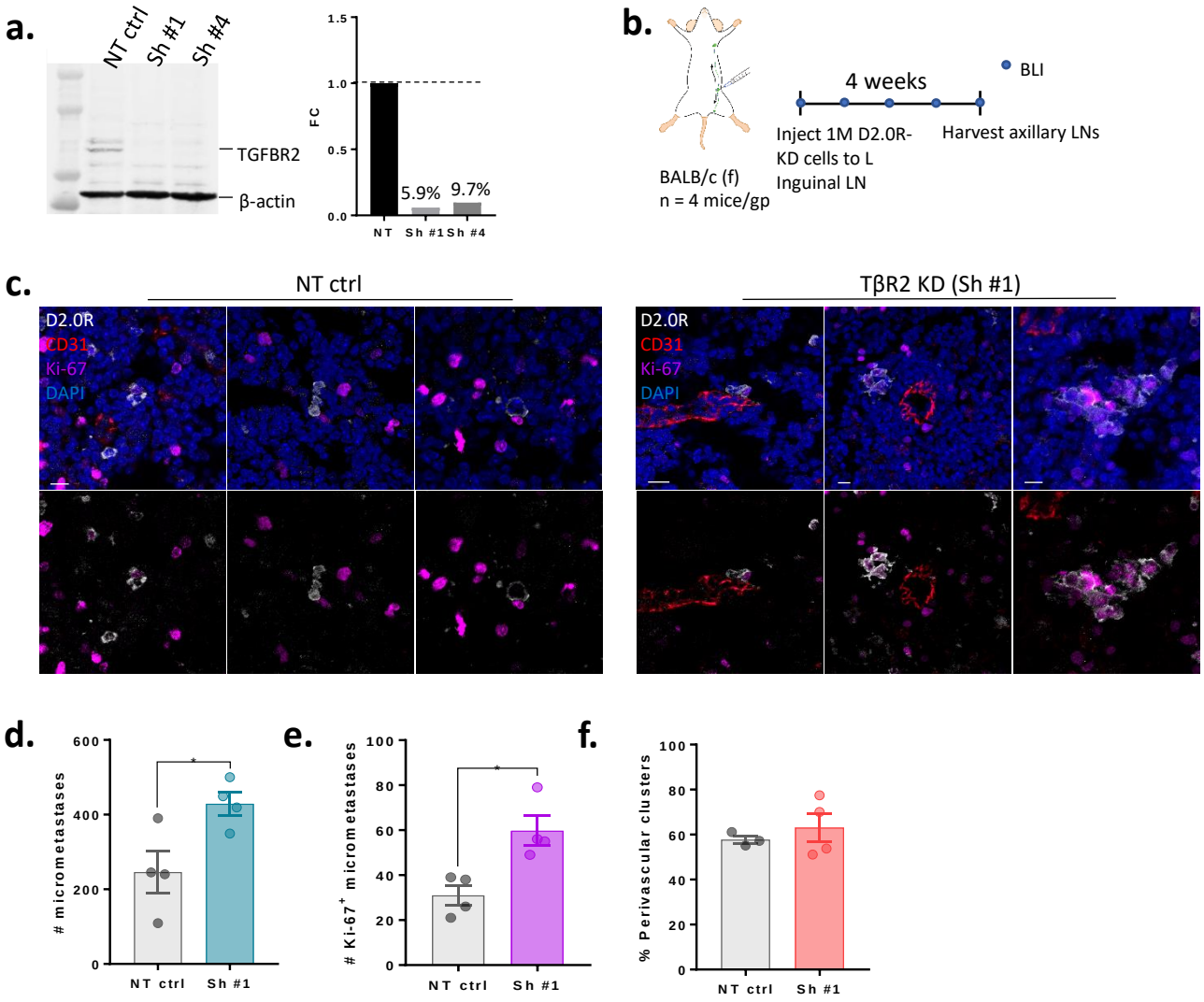

Fig. 29. Disrupting the TGF-β1-TβR2 axis results in D2.0R outgrowth in the lymph node. a) Murine lymph node (LN) stained for anti-SMAD2, anti-CD31, and anti-LYVE-1. **b**) TβR2 was knocked down in D2.0R-ffLuc cells using shRNA. *Left panel*, Western blot of lysates from non-targeting (NT) control-infected cells and two shRNA KD cell lines showing loss of TβR2 (~70 kDa) protein levels. β-actin (~45 kDa) was used as a loading control. *Right panel*, fold change in TβR2 protein levels normalized to NT control. **c**) Experimental schematic for injection of D2.0R-KD cells to the left inguinal LN, followed by weekly BLI monitoring for metastatic outgrowth. After four weeks, axillary LNs were harvested, fixed, and sectioned for immunostaining (n = 4 mice per group). **d**) Representative images of D2.0R clusters in the axillary LNs of BALB/c mice four weeks after intranodal injection. LN sections were immunostained for anti-GFP (D2.0R), anti-CD31, anti-Ki-67, and DAPI. *Left panel*, NT control. Scale bar: 10 μm. *Right panel*, TβR2 KD Sh#1. Scale bar: 10 μm. **e**) The number of clusters with at least two cells was counted in axillary LNs. 21 sections at 18 μm thickness were examined per node. n = 4 mice, P=0.0313, Student's unpaired t test. *P<0.05. **f**) The number of clusters with at least one Ki-67$^+$ nucleus between. n = 4 mice, P=0.0112, Student's unpaired t test. *P<0.05. **g**) The percent of clusters within 10 μm of a CD31$^+$ blood vessel, normalized to the total number of clusters. n = 4 mice, P=0.5195, unpaired Student's t test, not significant.

6.3 DISCUSSION

These results show that acute inflammation results in rapid loss of vascular homeostasis, downregulation of endothelial TGFβ signaling, and metastatic outgrowth within the LN. More broadly, these data provide *in vivo* evidence for the paradigm that loss of vascular homeostasis compromises the mechanisms enforcing DTC dormancy, which is especially relevant to the LN but could be postulated for any tissue or physiological condition in which vascular remodeling occurs.

For the LN, tissue dysregulation occurs through natural encounters with pathogens, eliciting an immune response and coordinated stromal activation. An animal model was carefully developed to assess the effect of inflammation on the LN and resident DTCs. Injection route, dose and timing of activation were considered in order to mimic a patient with residual LN disease who sustains a bacterial infection. The results were surprisingly dramatic, with more than 10-fold increase in average number of micrometastases per mouse found in the LPS-treated group. The absence of large metastases or BLI signal suggests some form of immune selection, possibly against proliferating and/or exogenous antigen-expressing metastases (GFP, ffLuc). Although patient data demonstrating that late relapse follows infection could not be identified, it is a realistic scenario that patients might encounter. However, if the effect indeed holds true in patients, then any kind of inflammatory insult could activate dormant residual disease, resulting in ample metastases. Since this is not apparently the case in the clinic, additional layers of biological suppression such as the immune system likely control rampant metastatic outgrowth. Further, it may be fruitful to study the magnitude and specific stimulus (e.g., bacterial, viral, chemical) of inflammation-induced remodeling required for metastasis, which could underlie the frequency of LN metastases and micrometastases.

Since the endothelia were identified as the preferential niche for quiescent DTCs (See Chapter 3), the LN stroma were profiled at homeostasis and inflammation using scRNAseq. The TGFβ pathway was downregulated in blood and lymphatic endothelia with treatment, suggesting that it may contribute to loss of perivascular DTC quiescence. This hypothesis was functionally validated by knocking down its critical receptor, TBR2, resulting in increased micrometastatic burden in the LN. Stromal TGF-β1 has been shown to promote melanoma progression [88] and breast cancer metastasis to the bone and lungs [69, 155, 479, 529] and, yet it also reversibly induces cell cycle arrest through activation of cyclin-dependent kinase inhibitors including $p15^{INK4B}$ and $p21^{CIP1}$, and inhibition of c-Myc [483]. Our data showing that interrupting the TGF-β1-TβR2 signaling axis results in significantly increased micrometastatic outgrowth within the murine LN agrees with prior reports showing that: (i) TGF-β1 stimulation led to cell cycle withdrawal of squamous cell carcinoma (SCC) in a TβR2-dependent manner [83]; and (ii) loss of TβR2 resulted in spontaneous SCC [480]. Moreover, TGF-β2 is a dormancy effector derived from perivascular MSCs in the marrow [78, 158], and other TGFβ family members such as BMP7 and BMP4 are noted pro-quiescence factors in the bone marrow and lungs [160, 222]. Thus, these results place the LN in context with other more commonly studied sites of tumor dormancy, but show the subtleties of regulation by TGFβ signaling change in a fashion specific to the LN.

Multiple inflammation-related mechanisms could have contributed to metastatic reawakening: for instance, activated neutrophils have been noted to enable tumor outgrowth from dormancy through altering the ECM [75], and the LN has been described as an immune-suppressive environment [530-532]. Future studies will be needed to clarify the role of the immune system in context of LN dormancy, which in our model allowed for emergence of

micrometastases. Another limitation of our study was exclusion of the “double negative” pericyte population [417] and immune cells from single-cell transcriptional analysis. However, tumor growth suppression in the organotypic co-culture model (**Figs. 12, 13**) did not require either cell type in the system to recapitulate this effect.

Chapter 7. CONCLUSIONS AND FUTURE DIRECTIONS

Compared to vital organs such as the bone and lungs, we know relatively little about mechanisms of dormancy regulation in the LN. This dissertation contributes to remedying this deficiency by establishing a dominant role for LN vasculature in the dormant niche of spontaneously disseminated dormant DTCs. Further, I provide evidence that short, sustained bacterial inflammation is sufficient to induce micrometastatic outgrowth in a site of peripheral immunity, which coincides with loss of TGF-β1 in the endothelial compartment upon inflammation. I go on to show that TGF-β1 signaling is necessary for tumor cell quiescence in the LN, revealing a LN-specific mechanism of tumor dormancy. Thus, in the face of pathogenic insult, the LN shifts from a tumor growth suppressive to a growth permissive niche. These results reveal a critical and previously undescribed relationship between inflammation, LN remodeling, and resident tumor cell outgrowth through loss of endothelial TGF-β1 in the vascular niche (**Fig. 30**).

This dissertation provides the first description of cellular DTC dormancy within the LN, along with evidence that the physiological response of the LN to inflammation triggers micrometastatic outgrowth. Further, it offers *in vivo* support for the paradigm that maintenance of vascular homeostasis is key to preventing the emergence of dormant DTCs [59, 69].

7.1 THE LYMPH NODE NICHE FOR DORMANT DISSEMINATED TUMOR CELLS

It has been reported by our lab and others that dormant, disseminated breast tumor cells associate with vascular niches in lung and bone marrow [49, 59, 69, 158, 533]. This biology likely reflects co-optive mechanisms employed to maintain tissue-specific cell populations within this niche (see Chapter 2) [138-140, 224, 534], and the paradigm that divergent

endothelial states and even populations within an organ differentially regulate stem cell proliferation and differentiation trajectories has emerged [140, 175, 535].

I employed spatial analysis to demonstrate a non-random enrichment of quiescent 4T07 DTCs to LN BEC but not LEC (and a non-significant trend towards the same with D2.0R). The preference of quiescent DTCs for BEC but not LEC underlies functional and transcriptional differences between these two endothelia, despite their common progenitor [536]. As blood endothelial subpopulations are defined at higher resolution through scRNAseq and other methods [500, 509], it will be interesting to see whether specific subpopulations disproportionally contribute to the tumor dormancy niche. This is already hinted at by a recent study showing that inflamed LN endothelial remodeling is driven by clonal expansion along the lines of tip-stalk cell coordination, demonstrating that even in the same tissue, not all endothelial cells are created equal [500].

Although this work focused on the contribution of BEC, it would be interesting to determine whether LEC contribute mitogenic factors to the niche. LEC have been documented to promote tumor growth through secreted EGF and PDGF-BB [442]; whether single DTCs elicit a similar paracrine response from lymphatic sinuses within the LN is unknown.

7.2 AN ORGANOTYPIC CO-CULTURE MODEL OF THE LYMPH NODE ENDOTHELIAL NICHE CAPTURES *IN VIVO* TUMOR GROWTH SUPPRESSION

To investigate the contribution of the vascular niche on DTC quiescence more deeply, I adapted the organotypic model developed by our lab for lung and bone [69, 457] to the LN as a tri-culture system. LN MVNs recapitulate the *in vivo* LN tissue architecture including FRCs directly supporting BEC tubules and interactions between BEC and LEC. This model provides a reductionist approach to teasing apart cellular contributions of LN stroma while retaining

complex cell-cell interactions.

Of the eight tumor cell lines tested, the human breast cancer cells were generally unsuccessful at colonizing the LN MVNs, whereas the murine mammary carcinoma lines grew rampant across conditions. T4-2 are a unique cell breast cancer cell line, having gained malignancy through spontaneous immortalization of breast epithelium and subsequent passaging through mice until a tumor developed [466]. They express high levels of EGFR, so it would be interesting to explore whether this pathway is required for LN metastasis. Given that TINAGL1, an EGFR inhibitor [471], is differentially upregulated in the LN MVNs containing endothelia (**Fig. 14a**) (as well as expressed by blood vasculature in the LN tissue, **Fig. 17a**), T4-2 may be uniquely poised to exhibit growth suppression in a model of the LN endothelial niche.

LN niches were characterized by ECM proteomics and total RNA sequencing. An overexpression screen identified several endothelial proteins of interest that may be responsible for suppressing tumor growth (including LGALS3, SPOCK, and TINAGL1), and these might be of interest for future studies. Using GSEA, the TGFβ pathway as a prospective tumor suppressor in the BEC niche. However, other pathways upregulated in the BEC niches (EMT, complement cascade) and LEC niches (oxidative phosphorylation, adipogenesis, xenobiotic metabolism, and ROS generation) may be fruitful to explore. In particular, they suggest the LEC niche experiences more metabolic stress and ROS, which is pro-metastatic in the bone marrow sinusoid niche for activated HSCs [175].

The LN MVN model is a simple co-culture system without Cultrex. Although the stromal and endothelial cells deposit basement membrane (**Fig. 18**), a true 3D matrix may enhance the model further, provided the LEC can adapt to higher concentrations of basement membrane. Other LN culture models such as a LN ‘slice’ model [537] have been developed to study

immunity, but may be beneficial for validating the role of the LN stroma in future dormancy studies with additional complexity.

7.3 LYMPH NODE INFLAMMATION INDUCES METASTATIC OUTGROWTH AND LOSS OF ENDOTHELIAL-DERIVED TGF-B1, A TUMOR SUPPRESSIVE FACTOR

In this work, I provide proof-of-principle evidence that common bacterial inflammation is sufficient to drive loss of endothelial TGF-β1 and subsequent metastatic outgrowth. The changes that occur to the LN stroma under inflammation are well-documented but have not been considered in the light of disrupting tumor dormancy as a secondary effect. The dramatic increase in micrometastatic burden that was observed in LPS-treated animals is noteworthy given the tissue's activation *against* pathological invasion. Within this heightened immune environment, tumor cell outgrowth was tolerated, although maintained below outright metastasis. The former conclusion indicates that some form of immune suppression was present; the latter indicates that immune cells could still have been actively editing growing metastatic clusters. Many studies have highlighted an immunoregulatory role for FRC and LEC, which oppose auto-reactive T cells [538-540]. Repeating this experiment in immune-compromised animals or with neutralizing antibodies—for instance, against CD4 or CD8 (T cells), CD20 (B cells), Ly6C (monocytes), Ly6G (neutrophils), or NK1.1 (natural killer cells)—may help clarify how anti-tumor immunity impacts DTC outgrowth within an activated environment.

In support of this surprising result, we present a scRNAseq analysis of the three major LN stromal cell types at homeostasis and upon inflammation to better understand the mechanistic changes that occur with LN stromal activation. The interesting observation that pro-metastatic ECM fibers decreased in endothelia with treatment led us to focus on loss of TGFβ signaling. Functional testing revealed that interrupting the TGF-β1-TβR2 signaling axis in tumor

cells allowed greater micrometastatic growth, even in the perivascular niche. This result agrees with prior reports showing that TGF-β1 stimulation led to cell cycle withdrawal of squamous cell carcinoma (SCC) in a TβR2-dependent manner [83, 483], and loss of TβR2 resulted in spontaneous SCC [480]. Moreover, TGF-β2 is a dormancy effector derived from perivascular MSCs in the bone marrow [78, 158], and other TGFβ family members such as BMP4 are noted pro-quiescence factors in the lungs [222]. Thus, these results place the LN in context with other dormancy tissues, including a LN-specific mechanism of DTC quiescence. More broadly, these results strengthen the emerging paradigm of tissue disruption as a mechanism of dormant DTC awakening.

It is unknown whether short-term inflammation precedes metastatic outgrowth from latency in human patients, but if true, this implies that LN metastasis poses a serious potential risk. The danger of awakening LN DTCs is not so much destruction of a single node but rather the risk of activated DTCs spreading to vital organs and initiating secondary distant metastases: phylogenetic studies indicate that up to 35% of distant liver metastases are more closely related to LN metastases than the primary colorectal tumor [107], so it is of great interest to eradicate residual LN disease and minimize potential spread. The LN has been described as a hub for DTCs that go on to metastasize [106, 415]; therefore, it is more critical than ever to uncover ways to target LN DTCs specifically. It may be speculated that reducing inflammation through NSAIDs may stabilize the stromal architecture and reduce metastatic outgrowth [376], even restricting dissemination from the LN to other sites, at the cost of restraining the antigen-specific immune response. These questions remain open for future studies.

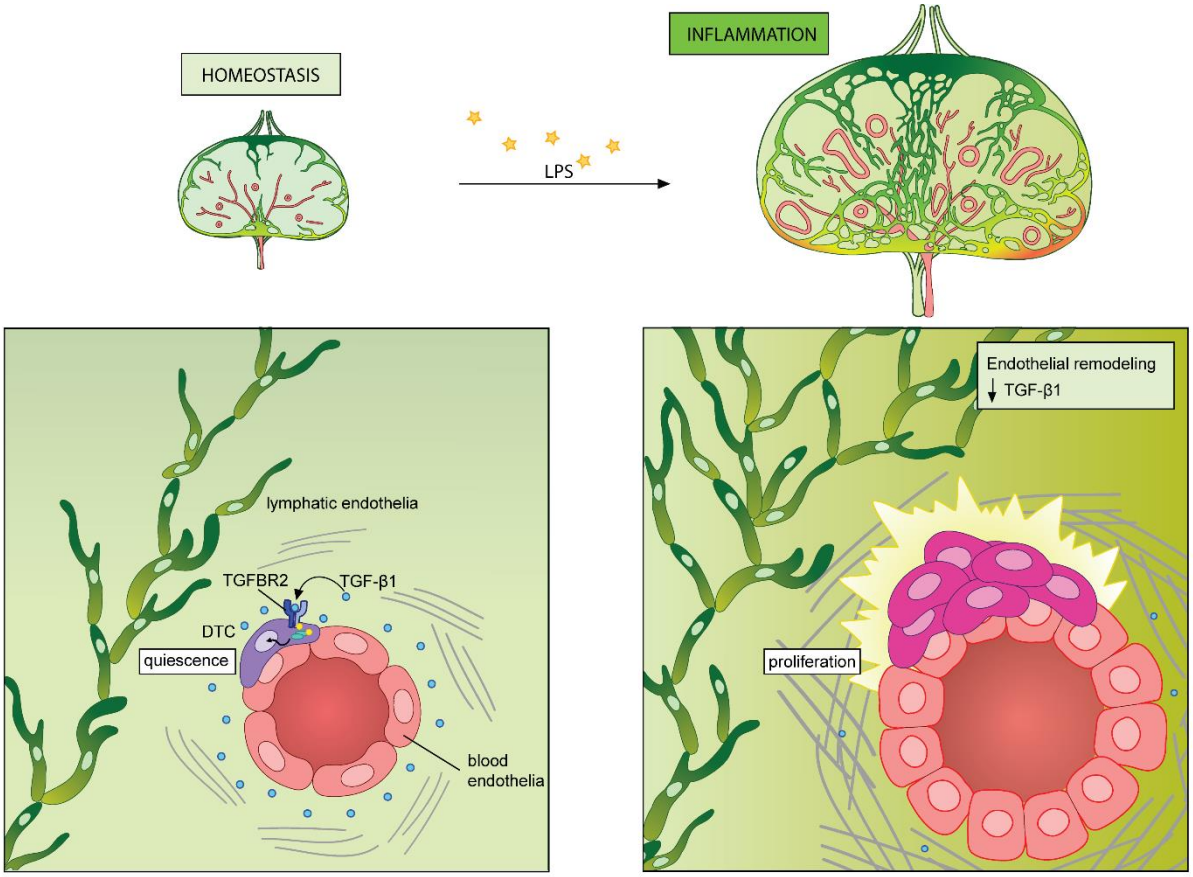

Fig. 30. Model for DTC dormancy and inflammation-induced awakening in the lymph node vascular niche.

Chapter 8. MATERIALS AND METHODS

8.1 ANIMAL STUDIES

All animal work was performed under Fred Hutchinson IACUC protocols and AAALAS guidelines and ethical regulations. Female BALB/c mice were purchased from Charles River and used for experiments at 7 weeks old.

8.1.1 *Spontaneous dissemination model*

Mice were injected with tumor cells into the fourth inguinal mammary fat pad. $2x10^5$ 4T07-eGFP or $2x10^6$ D2.0R-eGFP were suspended in a 20 ul volume of sterile 1:1 PBS to collagen I rat Cultrex (R&D, 3447-020-01) mixture, and kept on ice. After isoflurane (2% v/v) anesthetization, the mouse was secured on its back, depilated from the midline to the left hip joint, and sterilized using alternating betadine and ethanol wipes. A 1 cm vertical incision was made between the midline and hip, and subdermal fascia cleared using surgical scissors. The fourth mammary fat pad was gently retrieved through the incision using J-forceps and the tumor cell mixture injected into the fat pad using a 28-gauge needle. Successful injection was confirmed by fat pad swelling. The fat pad was tucked back into the inguinal region and the incision closed with silk sutures. Animals were allowed to recover under mild heat and slow-release buprenorphine analgesic.

8.1.2 *Intranodal injection model*

Mice were injected with tumor cells into the left inguinal lymph node (LN)with $1x10^6$ D2.0R cells suspended in 20 µl sterile PBS in a 26-g syringe. After isoflurane anesthetization, the mouse was secured on its back, depilated around the hip joint, and sterilized using alternating

betadine and ethanol wipes. The inguinal lymph node (LN) was visible through the skin as a gray dot about 1 mm^2 in size. A 1 cm horizontal incision was made across the skin of the hip joint directly over the LN, which was then visible as a translucent dot within the opaque adipose tissue. J-forceps were used to gently scoop up the LN and the syringe needle was carefully inserted into the LN. Successful injection caused the LN to swell with minimal leakage. The incision was closed using silk sutures. Animals were allowed to recover under mild heat and slow-release buprenorphine analgesic.

8.1.3 *Acute inflammation model*

Mice were treated with ultrapure *E.coli* lipopolysaccharide (LPS) O111:B4 (Invivogen TLRL-3PELPS) injected subcutaneously to the left of the base of the tail. LPS was resuspended in endotoxin-free H_2O according to the manufacturer's instructions, aliquoted, and stored at -20^oC for up to three months. Aliquots were freshly thawed for each treatment. Thawed LPS stock solution was diluted in sterile PBS to the concentrations indicated in a final injectate volume of 20 ul. Mice were anesthetized with isoflurane and placed on their right side. The left hind leg was sprayed with 70% ethanol and hair between the tail and knee matted to each side until a straight line of skin was exposed. The needle was inserted at the base of the tail and pushed subdermally under the line of exposed skin toward the back of the knee. Before reaching the muscle, the injectate was expelled behind the knee, which caused an apparent swelling. The needle was removed and the mouse allowed to recover under mild heat. Mice were treated once daily for three consecutive days.

8.2 CELL CULTURE

Murine fibroblastic reticular cell line BLS-4 was graciously provided by Dr. Hector Peinado, CNIO Madrid. BLS-4 were cultured in high-glucose Dulbecco's Modified Eagle's Medium (DMEM)/10% heat-inactivated FBS (Gibco 16140089**)** without antibiotics and used between passages 16-30. Primary human umbilical vascular endothelial cells (HUVEC, generously provided by Dr. Andrew Putnam, University of Michigan) were lentivirally infected with E4-Orf1 [464] and selected in serum-free medium (Ghajar et al, NCB 2013). HUVEC were cultured in EGM-2 media (Lonza, CC-3162) and used between passages 8-10. Human dermal lymphatic endothelial cells derived from neonatal foreskin (hdLEC-dLy-Neo, Lonza CC-2812) were cultured in EGM2-MV media (CC-3202) and used between passages 8-11. T4-2 were generously gifted by Mina Bissell, Lawrence Berkeley National Laboratory and cultured in H14 media [466] on PureCol (Advanced Biomatrix 50360230)-coated flasks and used between passages 50-60. To normalize seeding counts in LN MVNs, T4-2 were lentivirally transfected with pcDNA3-CFP (Addgene 13030).

For all cells, standard subculturing practices were used: before reaching confluence, cells were washed in PBS, 0.05% trypsin was added for 4 minutes at 37^{o}C, and neutralized with either defined trypsin inhibitor (for T4-2, Fisher R007100) or DMEM/10% FBS (all other cells). Cells were spun down at 200xg for 5 minutes then resuspended at the desired concentration.

8.2.1 *Lentivirus transfection*

HEK293FT were subcultured 2-3 times prior to plating for transfection. 1x10^{6} HEK293FT were seeded in 8 ml DMEM/10% FBS in a 10 cm plate to reach 50% confluence by the next day. When cells reached the correct confluence, 3 µg psPAX2, 2 µg pMDS-G-VSV, and 5 µg plasmid of interest were added to a mixture of 3:1 FuGENE 6 transfection reagent

(Promega E2691) to DNA (v/w) in Opti-MEM media (Gibco 51985034**),** dropwise. The plasmid mixture was incubated for 15 minutes at room temperature and 1 mL added to each 10 cm plate dropwise. After a 24 hour incubation at 37^{o}C, media was changed to 13 mL DMEM/10% FBS. 48 hours after the first media change (3 days post-transfection), media was collected and replaced. The collected supernatant was spun down at 500 x g for 10 minutes and filtered through a 0.45 um surfactant-free cellulose acetate filter.

Lenti-X concentrator (Clontech 631232) was added at 1:3 Lenti-X:media (v/v), gently mixed, and stored at 4^{o}C. Viral collection was repeated a second time 24 hours after the first collection and stored at 4^{o}C overnight. The next day, both the first and second viral collections were spun down at 1500 x g for 45 minutes at 4^{o}C to concentrate virus. The supernatant was carefully drained off the viral pellet resuspended in sterile PBS at 200X media concentration. The first and second collection resuspensions were mixed together and 25 µL aliquots were stored at -80^{o}C.

8.2.2 *Lentivirus transduction*

5x10^{4} cells to be infected were plated in a 12-well plate the night before. The next day, when cells were ~50% confluent, 500 µL of the respective growth media plus 8 ug/ml polybrene was changed and incubated for at least 1 hour prior to infection. One 25 µL aliquot of lentivirus was thawed on ice and added dropwise to the cells. Cells with lentivirus were incubated for 8 hours at 37^{o}C. Then the viral medium was removed and fresh growth medium added. After two to three days, cells were checked for fluorescence, if present. If selection was to be carried out, selection agent was added to the media from day three post infection until wildtype parental cells were killed (usually within seven days) at a concentration determined by a death curve titration.

8.2.3 *Lentiviral-mediated shRNA knockdown in HUVEC*

The following pGIPz constructs from the Open Biosystems library (Thermo Fisher) were obtained from the shRNA core in Fred Hutch Shared Resources.

ORF	**Clone**
FN1	V3LHS_314138, V3LHS_314140
TINAGL1	V3LHS_314921

Empty pGIPz vector was used as the control. HUVEC were infected as in Section 8.2.2. Three days after infection, cells were selected in 1 µg/ml puromycin and continually grown in selection media until right before the experiment. Cells were washed abundantly in PBS before harvest for LN injection to remove antibiotics.

8.2.4 *Lentiviral-mediated overexpression in BLS-4 lines*

The following constructs from the Broad hOrfeome v8.1 library [472] were generously provided by P. Paddison and cloned from the pLX304 to the pLEX307 backbone (Addgene plasmid #41392, generously provided by S. Beronja) via Gateway cloning:

ORF	**Clone**
ANGPT2	CCSBBroad304_121D1
SPOCK1	CCSBBroad304_149D1
APLN	CCSBBroad304_050D1
VIM	CCSBBroad304_006D1
LGALS3	CCSBBroad304_135D1
MCAM	CCSBBroad304_078D1
CD93	CCSBBroad304_111D1
PRSS23	CCSBBroad304_047D1
TINAGL1	CCSBBroad304_065D1
VASH1	CCSBBroad304_151D1
POSTN	CCSBBroad304_035D1
MMRN1	CCSBBroad304_158D1
EFEMP1	CCSBBroad304_144D1

Empty pLEX307 vector was used as the control. BLS-4 cells were infected as in Section 8.2.2. Three days after infection, cells were selected in 1 μg/ml puromycin for up to one week until uninfected control cells were killed.

8.2.5 *Lentiviral shRNA-mediated knockdown of TβR2 for* in vivo *metastasis experiment*

The following pLKO.1 constructs from The RNAi Consortium shRNA library[528] (generously provided by S. Beronja) were used to generate lentivirus to knock down TβR2 in D2.0R cells (bolded constructs #1 and #4 were selected for metastasis experiments):

	Sequence	**Clone**
#1	**CCGGCGACCTGTTGTTGGTCATTATCTCGAGATAATGACCAACAACAGGTCGTTTTT**	**NM_009371.2-801s1c1**
#2	CCGGCCATCCACGTAAGCTGTAATACTCGAGTATTACAGCTTACGTGGATGGTTTTT	NM_009371.2-377s1c1
#3	CCGGGCTCGCTGAACACTACCAAATCTCGAGATTTGGTAGTGTTCAGCGAGCTTTTT	NM_009371.2-2009s1c1
#4	**CCGGCCAGATCGTGTGTGAGACTTTCTCGAGAAAGTCTCACACACGATCTGGTTTTT**	**NM_009371.2-1857s1c1**
#5	CCGGCCATCCATCCACTGAAACATTCTCGAGAATGTTTCAGTGGATGGATGGTTTTT	NM_009371.2-401s1c1

Non-targeting (NT) vector was used as the control. Three days after infection, D2.0R were selected in 1 μg/ml puromycin and continually grown in selection media until right before the experiment. Cells were washed abundantly in PBS before harvest for LN injection to remove antibiotics.

8.2.6 *Gateway cloning*

Cloning ORFs from pLX304 to pLEX307 was performed via the Gateway cloning method according to the manufacturer's protocol, using BP Clonase II (Fisher 11789020) and LR Clonase II (Fisher 11791020) enzyme mix.

8.3 CELL CULTURE ASSAYS

8.3.1 *Lymph node microvascular niche model*

For each well in a 96-well, cell culture-treated, flat-bottom microplate (Falcon, 353072), $5x10^4$ BLS-4 were seeded or admixed with $1x10^4$ HUVEC and/or $1x10^4$ hdLEC in EGM-2MV + 10 ng/ml recombinant human VEGF-C (R&D, 9199-VC-025, prepared according to manufacturer instructions, aliquoted, and kept frozen at -20°C until used). Media was changed every third day. 10 days after plating, breast cancer cells were sparsely seeded (50 cells) in each well in H14 media, which was changed every third day for 17 more days. Wells were fixed in 4% PFA for 20 minutes at room temperature, washed 3 x 10 minutes in PBS, and stored in 0.5M glycine/PBS for up to 2 weeks at 4°C before immunostaining.

8.3.2 *TGF-β1 add-in*

Recombinant human TGF-β1 (R&D, 240-B-002) was reconstituted at 20 μg/mL in sterile 4 mM HCl with 1 mg/mL bovine serum album per the manufacturer's instructions. Aliquots were frozen at -20°C and thawed fresh for each experiment. Once thawed, aliquots were kept at 4°C for no longer than one month. After network formation (10 days), tumor cells were seeded in H14 media containing rhTGF-β1 at the indicated concentrations. H14/ TGF-β1 media was changed every third day for 17 days before fixation.

8.3.3 *ELISA*

Conditioned media was collected from LN MVNs at Day 7 in H14. Media was conditioned by MVNs for three days (D4-7) before supernatant was collected, spun down at 500xg for 5 minutes to remove cell debris, filtered through 0.45 um filters, and stored at -80°C.

When samples were collected in triplicate, one ELISA was run for each target, with technical duplicates: human latent TGF-β1 (Biolegend, 432907) and human active TGF-β1 (Life Technologies, BMS249-4), according to manufacturer instructions. Colorimetric quantification and analysis was carried out using a Molecular Devices Spectramax M5 multi-detection microplate reader.

8.4 Analysis of lymph node microvascular niches via LC-MS/MS.

8.4.1 *Sample preparation*

LN microvascular niche co-cultures were established for 10 days in EGM-2MV/10 ng/ml VEGF-C. Cultures were washed extensively with PBS to remove medium, incubated in 0.1% Triton X-100/PBS with protease inhibitor cocktail (Roche 04693159001) for 30 min, then carefully collected using a p10 pipette tip into 1.5 ml Eppendorf tubes, and flash frozen prior to storage at −80°C.

8.4.2 *Mass spectrometry analysis*

Sample digestion and LC-MS/MS analysis for LN MVNs were carried out as previously described[69]: 30 micrograms of protein from each experimental condition were proteolytically cleaved by modified, sequencing-grade trypsin (Promega) in 50 mM NH_4 (HCO_3) digestion buffer containing 1 μg trypsin and 2 mM $CaCl_2$ for 16 h at 37 °C. Reactions were then acidified with 90% formic acid (2% final) to stop proteolysis. Samples were centrifuged for 30 min at 16,100*g* to remove insoluble material, and then subjected to LC–MS/MS analysis as previously described [541].

8.1 RNA SEQUENCING OF LN MICROVASCULAR NICHES

Total RNA for LN microvascular niche cultures was extracted from two independent biological replicates of 10 wells per condition using the RNeasy Plus Mini Kit (Qiagen, 74134) according to manufacturer's instructions and frozen at -80^{o}C. RNA-seq libraries were constructed from 1 μg total RNA using the Illumina TruSeq Stranded mRNA LT Sample Prep Kit (Illumina 20020594) according to the manufacturer's protocol. Barcoded libraries were pooled and sequenced on the Illumina HiSeq 2500 generating 50 bp paired end reads. Sequencing reads were mapped to the hg38 human and mm10 mouse genomes using TopHat v2 [542]. Mouse and human specific reads were separated as previously described [543]. Gene level abundance was quantified from the filtered human alignments in R using the GenomicAlignments Bioconductor package [544]. Differential expression was assessed using transcript abundances as inputs to the edgeR [545] and limma [546] Bioconductor packages in R, filtered for a minimum expression level of at least 1 count per million reads (CPM) in at least two samples prior to testing, and using the Benjamin-Hochberg false discovery rate (FDR) adjustment. Gene expression results were ranked by their limma statistics and used to conduct Gene Set Enrichment Analysis (GSEA) [473] to determine patterns of pathway activity utilizing the curated pathways from within the MSigDBv7.2.

8.2 SINGLE-CELL RNA SEQUENCING OF LN STROMAL CELLS

8.2.1 *LN Dissociation*

Axillary, inguinal, and popliteal LNs were harvested into digestion buffer (DMEM, 1.2 mM $CaCl_2$, 2% FBS), carefully opened using two 28-G needles, and enzymatically dissociated with agitation in digestion buffer plus collagenase IV (220 U/ml, Worthington Biomedical

LS004188) and DNase (>80 U/ml, Sigma-Aldrich 11284932001) for 30 min at 37°C. The supernatant was discarded and remaining LN stromal tissue was subjected to a second round of dissociation in digestion buffer plus collagenase D (0.7854 U/ml, Sigma-Aldrich 11088866001) and DNase (>80 U/ml, Sigma-Aldrich 11284932001) for 5 minutes at 37°C with agitation, pipetted 10 times, then returned to 37°C incubation for 10 minutes. EDTA was added to a final concentration of 5 mM (pH 7.2), then the suspension was pipetted 100 times. The single-cell suspension was filtered through a 70-um pore nylon cell strainer and spun down at 1500 x g for 5 minutes at 4°C, counted, and resuspended at 1 x 10^{6-7} cells/mL in FACS buffer for immunostaining.

8.2.2 *Flow Cytometry*

Single-cell suspensions were blocked with CD16/32 for 20 min at 4°C, then incubated with primary antibodies for 1 hour in the dark at 4°C. Samples were washed three times with FACS buffer and filtered through a 70-um pore nylon cell strainer. UltraComp beads (Fisher, 01-2222-42), unstained sample, single-stain and fluorescence-minus-one (FMO) controls were used to set up the gating strategy for each fluorophore.

All data were acquired using the Aria 2 flow cytometer with a 100 µm nozzle. Pooled LNSC were sorted into cold DMEM/10% FBS in 5 ml Eppendorf tubes pre-coated with 5% BSA/PBS. Flow data was analyzed using FlowJo Software (TreeStar Inc.).

8.2.3 *Single-cell RNA sequencing preparation*

Single-cell RNA libraries were prepared using the 10x Chromium NEXT GEM Single Cell 3′ kit, v3.1 (10X Genomics, 1000128) following the manufacturer's protocol. Briefly, single cells were partitioned into gel beads in emulsion in the 10X Chromium Controller instrument

followed by cell lysis, barcoded reverse transcription of RNA, amplification, shearing and 5′ adapter and sample index attachment. Samples from the two treatment groups (PBS, LPS), in triplicate, were loaded separately onto the Chromium Next GEM Chip G (10X Genomics, 1000127) for indexing before libraries were combined for paired-end sequencing on the Illumina Miseq 300v2 kit to determine the number of cells recovered per sample. The libraries were then combined proportional to the number of recovered cells to normalize reads per sample. The pool was then sequenced on the Illumina NovaSeq 6000 S1 resulting in 2.2 billion reads total.

8.3 IMMUNOFLUORESCENCE

8.3.1 *OCT-embedded murine tissue lymph nodes*

Mice were sacrificed by CO_2 asphyxiation and PBS-perfused through the left ventricle of the heart. Tissues were fixed in 4% PFA/PBS for 2 hours rocking at room temperature, then switched to 30% sucrose/PBS and rocked at 4^{o}C overnight. The next day, tissues were switched to a mixture of 1:1 30% sucrose/PBS to optimal cutting temperature (Thermo Fisher Scientific 23-730-571) for 45 minutes rocking at room temperature before embedding in OCT (TissueTek, 4583) and flash-frozen in liquid nitrogen. Tissues were stored at -80^{o}C. Frozen tissue sections 18 um thick were cut on a Leica cryostat. Slides were incubated at 37^{o}C for 15 minutes, then rehydrated in PBS, permeabilized in 0.5% Triton-X-100 for 20 minutes and washed 3 x 10 minutes in PBS. Tissues were blocked in 5% bovine serum albumin/5% goat serum/0.1% Triton-X-100/PBS for 1 hour at room temperature, then primary antibodies were added in 5% BSA/PBS (filtered) and left overnight at 4^{o}C. The next day, tissues were washed 5 x 30 minutes in PBS, then secondary antibodies were added in 5% BSA/PBS (filtered) for 1 hour at room temperature. Tissues were washed for 5 minutes, 10 minutes, 30 minutes, and overnight at 4^{o}C before being mounted on Superfrost Plus slides (VWR) in Fluoromount-G and imaged on a Zeiss LSM 700

confocal microscope using either a 0.55NA 20x objective for whole LN tilescanning or a 1.4NA 63x oil-immersion objective for micrometastasis quantification. For area analysis after LPS treatment, whole LN tilescans were imaged on a Zeiss Celldiscoverer 7 automated microscope using the 10X objective.

For the LPS treatment experiment, the entire volume of the axillary and popliteal nodes was analyzed; for the TβR2 knockdown experiment, 21 sections representing approximately half the volume of each axillary LN were analyzed.

8.3.2 *Three-plex OPAL staining of formalin-fixed paraffin-embedded murine lymph nodes*

Formalin-fixed paraffin-embedded tissues were sectioned at 4 microns onto positive-charged slides and baked for 1 hour at 60°C. The slides were then dewaxed and stained on a Leica BOND Rx stainer (Leica, Buffalo Grove, IL) using Leica Bond reagents for dewaxing (Dewax Solution), antigen retrieval and antibody stripping (Epitope Retrieval Solution 2), and rinsing after each step (Bond Wash Solution). A high stringency wash was performed after the secondary and tertiary applications using high-salt TBST solution (0.05M Tris, 0.3M NaCl, and 0.1% Tween-20, pH 7.2-7.6).

Antigen retrieval and antibody stripping steps were performed at 100°C with all other steps at ambient temperature. Endogenous peroxidase was blocked with 3% H_2O_2 for 8 minutes followed by blocking with 5% mouse serum in TCT buffer (0.05M Tris, 0.15M NaCl, 0.25% Casein, 0.1% Tween 20, pH 7.6 +/- 0.1) for 30 minutes. The first primary antibody (position 1) was applied for 60 minutes followed by the secondary antibody application for 10 minutes and the application of the tertiary TSA-amplification reagent (PerkinElmer OPAL fluor) for 10 minutes. The primary and secondary antibodies were stripped with retrieval solution for 20 minutes before repeating the process with the second primary antibody (position 2) starting with

a new application of 3% H_2O_2. The process was repeated until all three positions were completed; however, there was no stripping step after the third position. Slides were then stained with Spectral DAPI (Sigma D8417)) for 3 minutes, rinsed for 5 minutes, and coverslipped with Prolong Gold Antifade reagent (Invitrogen/Life Technologies, Grand Island, NY).

Slides were cured for 24 hours at room temperature, then representative images from each slide were acquired on Aperio FL Automated Imaging System. Images were exported to HaloLink and Halo for analysis.

8.3.3 *Microvascular Niches*

Wells were fixed for 20 minutes in 4% PFA, washed in PBS, neutralized in 0.5M glycine, and stored at 4^{o}C for no longer than 2 weeks. Before staining, wells were washed once in PBS, permeabilized in 0.3% Triton-X-100 for 20 minutes, washed 3 x 10 minutes in PBS, and blocked in 5% BSA/PBS for 1 hour at room temperature, rocking. Primary antibodies were added in 5% BSA/PBS overnight at 4^{o}C, rocking. The next day, wells were washed 5 x 30 minutes in PBS. Secondary antibodies including DAPI were added for 45 minutes at room temperature, rocking. Wells were washed 5 x 10 minutes in PBS and left rocking at 4^{o}C overnight in PBS. Wells were imaged the next day.

8.4 IMMUNOHISTOCHEMISTRY

Formalin-fixed paraffin-embedded human lymph nodes (archived tissues from Experimental Histopathology Shared Resource, Fred Hutch) were sectioned at 4 microns onto positively charged slides and incubated for 1 hour at 60°C. The slides were then dewaxed and stained on a Leica BOND Rx autostainer (Leica, Buffalo Grove, IL) using Leica Bond reagents for dewaxing (Dewax Solution). Antigen retrieval was performed at 100°C for 20 minutes using

Leica Epitope Retrieval Solution 1. Endogenous peroxidase was blocked with 3% H_2O_2 for 5 minutes followed by protein blocking with 3% mouse serum in TCT buffer (0.05M Tris, 0.15M NaCl, 0.25% Casein, 0.1% Tween 20, pH 7.6 +/- 0.1) for 10 minutes. The primary LYVE-1 antibody (Novus #NBP1-43411) was applied at 1:1000 for 60 minutes. The secondary HRP rat-specific polymer (Vector) was applied for 60 minutes followed by 3,3'-diaminobenzidine (DAB, Dako) for 10 minutes. Sections were counter-stained with hematoxylin (Dako) for 3 minutes and then coverslipped. Concentration matched isotype control slides were performed for each antibody on each tissue sample.

8.5 WESTERN BLOT

Cells were lysed in 2% SDS plus cOmplete protease inhibitor cocktail (Roche, 04693159001) and PhosStop phosphatase inhibitor cocktail (Roche, 04906837001). Protein concentration was determined by BCA protein assay (Pierce 23225) and analyzed on a Molecular Devices Spectramax M5 multi-detection microplate reader. For protein agarose gel electrophoresis (SDS-PAGE), 30 ug of lysate were loaded per well of a Novex Wedgewell 4-20% Tris-Glycine gel (Life Technologies, Inc., XP04200BOX) in Trizma buffer (Sigma-Aldrich, T6066) with Kaleidoscope ladder (Biorad, 1610375). SDS-PAGE was run at 40V for 20 minutes followed by 100V for ~1.5 hours. Gel was transferred to nitrocellulose membrane overnight at 10V, 120 mA at 4^{o}C. Successful transfer was checked with Ponceau S staining (0.1% w/v in 5% v/v acetic acid). The membrane was blocked in 5% non-fat milk for 1 hour at room temperature. Primary antibodies diluted in 5% non-fat milk were added overnight at 4^{o}C. After washing in PBST, secondary antibodies were added for 1 hour at room temperature, rocking. After washing in PBST, blots were imaged on the Li-Cor Odyssey CLx system.

8.6 IMAGE ANALYSIS

8.6.1 *DTC distance analysis*

The distance from each DTC to the nearest $CD31^+$ BEC and $LYVE\text{-}1^+$ LEC was quantified manually using built-in Zeiss Zen Black software. To generate the random dot distribution, whole tilescan LN images were batch exported without the GFP (DTC) channel and processed using a custom R script that generated a random dot overlay on each image. The size of the dots was calibrated to approximate the diameter of DTCs. The number of dots placed was based on the average number of DTCs per image. After exporting the LN tilescans with random dot overlays, the same distance measurements from each dot to nearest BEC and LEC was conducted manually in the Zen Black program.

8.6.2 *Quantification of area fraction for LPS-treated LNs*

LN sections stained for CD31, LYVE-1, Ki-67, and DAPI were imaged on the Zeiss Celldiscoverer 7 automated microscope using the 5x objective to capture a tilescan of the whole LN. $CD31^+$ area, $LYVE\text{-}1^+$ area, DAPI area, and number of Ki-67 nuclei were quantified by channel using the built-in Zeiss blue analysis software. Areas and Ki-67 counts were averaged for the n=3 sequential sections for each of the mice. The proportion of Ki-67 nuclei per endothelial compartment was calculated by normalizing the number of Ki-67 nuclei within a masked region to the area of that region.

8.6.3 *Quantification of normalized area fraction for LN microvascular niches*

96-well plates were imaged on the Zeiss Celldiscoverer 7 automated microscope using the 5x objective to capture a tilescan of 100% of the well. Wells were imaged within one hour

after seeding fluorescent tumor cells (D0) and after fixation and immunostaining on D17. Zeiss Blue analysis software was used to quantify the number of tumor cells seeded on D0 and the area fraction of the fluorescent tumor channel after fixation. The D17 area fraction was normalized to the number of tumor cells seeded at D0 to account for seeding variations among the wells. Area fraction measurements for each condition were averaged (technical replicates) and subsequently normalized to the vehicle-treated control as indicated.

For Ki-67 status, tumor cells or clusters were manually recorded if they contained at least one cells with strong nuclear Ki-67 signal. The proportion of Ki-67$^+$ cells/clusters was calculated by dividing the number of Ki-67$^+$ cells/clusters with the total number of tumor cells plus clusters per well.

8.6.4 *Quantification of micrometastases in LPS-treated and TβR2 knockdown metastasis assays*

LN sections stained for eGFP (tumor cells), CD31, LYVE-1, Ki-67, and/or DAPI were imaged on the Zeiss LSM 700 confocal microscope. The number of eGFP$^+$ clusters containing at least two cells was counted manually by scanning through the tissue using the 63x oil-immersion objective. Images of each micrometastatic cluster were captured for Ki-67 and vascular association analysis. Clusters were considered Ki-67+ if at least one cell within the cluster displayed strong nuclear Ki-67 signal. Vascular association was defined as the cluster residing within 10 μm of a CD31$^+$ vessel.

8.7 Statistical Analysis

Statistical analyses were performed using GraphPad Prism 7. Unpaired and paired Student's *t* tests were used to compare two groups. One-way ANOVA was used for multiple

group comparisons, with Sidak's, Dunnett's, or Tukey's post-hoc test where appropriate, provided in Prism. $P<0.05$ was considered significant, shown by asterisks. All experiments were performed independently at least three times unless indicated otherwise, and cumulative or representative data are presented as indicated. Error bars represent standard error of the mean (SEM). Details may be found in each figure legend.

8.8 ANTIBODIES

Further information on all antibodies employed in this study for immunostaining, flow cytometry and western blotting are provided in the following tables:

Immunofluorescence: Primary antibodies						
Target	**Host sp.**	**Target sp.**	**Clone**	**Dilution**	**Manufacturer**	**Cat no.**
GFP	Chicken	Jellyfish	-	1:500	Abcam	ab13970
CD31	Mouse	Human	HC1/6	1:400	Millipore	CBL468
CD31	Hamster	Mouse	2H8	1:400	Millipore	mab1398z
LYVE1	Rat	Mouse	223322	1:400	R&D	MAB-2125
Ki-67	Rabbit	Mouse	-	1:400	Abcam	ab15580
Ki-67-AF647	Mouse	Human	B56	1:200	BD Biosciences	562899
Pan-cytokeratin	Rabbit	Mouse	-	1:400	Abcam	ab9377
ER-TR7	Rat	Mouse	S68	1:300	Bio-Rad	MCA2402
pSMAD2 (Ser465/467)	Rabbit	Mouse	138D4	1:400	Cell Signaling	3108
For OPAL:						
TINAGL1	Rabbit	Mouse	-	1:300	Novus	NBP2-13434

CD31	Rabbit	Mouse	D8V9E	1:1000	Cell Signaling	776995
LYVE-1	Rat	Mouse	ALY7	1:5000	Novus	NBP1-43411

Immunofluorescence: Secondary antibodies					
Target	**Host sp.**	**Fluorophore**	**Dilution**	**Manufacturer**	**Cat no.**
Chicken	Goat	AlexaFluor 488	1:400	Abcam	ab150169
Mouse	Goat	AF488	1:400	Invitrogen	A11029
		AF568	1:400	Invitrogen	A11031
		AF647	1:400	Invitrogen	A21235
Armenian hamster	Goat	AF488	1:400	Abcam	ab173003
		AF647	1:400	Abcam	ab173004
Rat	Goat	AF568	1:400	Abcam	Ab175710
		AF647	1:400	Life Tech.	A21247
Rabbit	Goat	AF405	1:400	Life Tech.	A31556
		AF488	1:400	Invitrogen	A11008
		AF568	1:400	Invitrogen	A11011
		AF647	1:400	Invitrogen	A21244
DAPI	-	-	1:1000	Invitrogen	
For OPAL:					
Vector rat polymer		Opal 520	1:50	Akoya Bio.	FP1487001KT
Power Vision rabbit polymer		Opal 570	1:50	Akoya Bio.	FP1488001KT
Power Vision rabbit polymer		Opal 650	1:50	Akoya Bio.	FP1496001KT

Immunohistochemistry: Primary antibodies						
Target	**Host.**	**Target sp.**	**Clone**	**Dilution**	**Manufacturer**	**Cat no.**
TINAGL1	Rabbit	Mouse	-	1:200	Novus	NBP2-13434
LYVE-1	Rabbit	Mouse	-	1:200	Millipore	AB2988

Flow cytometry

Target	Host sp.	Clone	Fluorophore	Dilution	Manufacturer	Cat no.
CD45	Rat	30-F11	AF488	1:400	Biolegend	103122
CD31	Rat	MEC13.3	APC	1:800	Biolegend	102510
Gp38/PDPN	Syrian Hamster	8.1.1	PE	1:100	Life Tech.	12-5381-821
CD16/32	Rat	93	-	1:400	Biolegend	101320

Western Blot					
Target	**Host sp.**	**Clone**	**Dilution**	**Manufacturer**	**Cat no.**
TGFβR2	Rabbit	-	1:400	Invitrogen	PIPA535076
β-actin	Mouse	AC-15	1:5000	Sigma Aldrich	A5441

Bibliography

1. Dasgupta, A., A. Lim, and C. Ghajar, *Circulating and disseminated tumor cells: Harbingers or initiators of metastasis?* Mol Oncol, 2017. **11**(1): p. 40-61.
2. Coleman, R., et al., *Adjuvant denosumab in early breast cancer (D-CARE): an international, multicentre, randomised, controlled, phase 3 trial.* The Lancet Oncology, 2020. **21**(1): p. 60-72.
3. DeSantis, C.E., et al., *Breast cancer statistics, 2019.* CA Cancer J Clin, 2019. **69**(6): p. 438-451.
4. Narod, S.A., J. Iqbal, and A.B. Miller, *Why have breast cancer mortality rates declined?* Journal of Cancer Policy, 2015. **5**: p. 8-17.
5. Tevaarwerk, A.J., et al., *Survival in patients with metastatic recurrent breast cancer after adjuvant chemotherapy: little evidence of improvement over the past 30 years.* Cancer, 2013. **119**(6): p. 1140-8.
6. Dillekås, H., M.S. Rogers, and O. Straume, *Are 90% of deaths from cancer caused by metastases?* Cancer medicine, 2019. **8**(12): p. 5574-5576.
7. Brewster, A., et al., *Residual risk of breast cancer recurrence 5 years after adjuvant therapy.* J National Cancer Institute, 2008. **100**(16): p. 1179-83.
8. Stingl, J., et al., *Deciphering the Mammary Epithelial Cell Hierarchy.* Cell Cycle, 2006. **5**(14): p. 1519-1522.
9. Ernster, V.L., et al., *Detection of Ductal Carcinoma In Situ in Women Undergoing Screening Mammography.* JNCI: Journal of the National Cancer Institute, 2002. **94**(20): p. 1546-1554.
10. Li, C.I., et al., *Trends in Incidence Rates of Invasive Lobular and Ductal Breast Carcinoma.* JAMA, 2003. **289**(11): p. 1421-1424.
11. Jamal, S., et al., *Carcinoma of the male breast: a study of 141 cases from northern Pakistan.* Asian Pac J Cancer Prev, 2006. **7**(1): p. 119-21.
12. Abdelwahab Yousef, A.J., *Male Breast Cancer: Epidemiology and Risk Factors.* Semin Oncol, 2017. **44**(4): p. 267-272.
13. Larsen, M.J., et al., *Hereditary breast cancer: clinical, pathological and molecular characteristics.* Breast cancer : basic and clinical research, 2014. **8**: p. 145-155.
14. Shiovitz, S. and L.A. Korde, *Genetics of breast cancer: a topic in evolution.* Annals of oncology : official journal of the European Society for Medical Oncology, 2015. **26**(7): p. 1291-1299.
15. Chlebowski, R.T., et al., *Estrogen plus progestin and breast cancer incidence and mortality in postmenopausal women.* JAMA, 2010. **304**(15): p. 1684-1692.
16. Momenimovahed, Z. and H. Salehiniya, *Epidemiological characteristics of and risk factors for breast cancer in the world.* Breast cancer (Dove Medical Press), 2019. **11**: p. 151-164.
17. Waks, A.G. and E.P. Winer, *Breast Cancer Treatment: A Review.* JAMA, 2019. **321**(3): p. 288-300.
18. Harris, L., et al., *American Society of Clinical Oncology 2007 update of recommendations for the use of tumor markers in breast cancer.* J Clin Oncol, 2007. **25**(33): p. 5287-312.
19. Perou, C.M., et al., *Molecular portraits of human breast tumours.* Nature, 2000. **406**(6797): p. 747-752.

20. Park, S., et al., *Characteristics and outcomes according to molecular subtypes of breast cancer as classified by a panel of four biomarkers using immunohistochemistry.* Breast, 2012. **21**(1): p. 50-7.
21. van Maaren, M.C., et al., *Ten-year recurrence rates for breast cancer subtypes in the Netherlands: A large population-based study.* Int J Cancer, 2019. **144**(2): p. 263-272.
22. Voduc, K.D., et al., *Breast cancer subtypes and the risk of local and regional relapse.* J Clin Oncol, 2010. **28**(10): p. 1684-91.
23. Kennecke, H., et al., *Metastatic behavior of breast cancer subtypes.* J Clin Oncol, 2010. **28**(20): p. 3271-7.
24. Recamier, J., *Recherches sur la Traitment du Cancer sur la Compression Methodique Simple ou Combinee et sure l'Histoire Generale de la Meme Maladie.* 1829. **2nd ed.**
25. Wong, S.Y. and R.O. Hynes, *Lymphatic or hematogenous dissemination: how does a metastatic tumor cell decide?* Cell Cycle, 2006. **5**(8): p. 812-7.
26. Kim, Y.N., et al., *Anoikis resistance: an essential prerequisite for tumor metastasis.* Int J Cell Biol, 2012. **2012**: p. 306879.
27. Heerboth, S., et al., *EMT and tumor metastasis.* Clinical and translational medicine, 2015. **4**: p. 6-6.
28. Chiang, S.P.H., R.M. Cabrera, and J.E. Segall, *Tumor cell intravasation.* American journal of physiology. Cell physiology, 2016. **311**(1): p. C1-C14.
29. Kerjaschki, D., et al., *Lipoxygenase mediates invasion of intrametastatic lymphatic vessels and propagates lymph node metastasis of human mammary carcinoma xenografts in mouse.* J Clin Invest, 2011. **121**(5): p. 2000-12.
30. Roussos, E.T., J.S. Condeelis, and A. Patsialou, *Chemotaxis in cancer.* Nature reviews. Cancer, 2011. **11**(8): p. 573-587.
31. Fidler, I.J., *Metastasis: quantitative analysis of distribution and fate of tumor emboli labeled with 125 I-5-iodo-2'-deoxyuridine.* J Natl Cancer Inst, 1970. **45**(4): p. 773-82.
32. Ubellacker, J.M., et al., *Lymph protects metastasizing melanoma cells from ferroptosis.* Nature, 2020. **585**(7823): p. 113-118.
33. Herman, H., et al., *Paracellular and transcellular migration of metastatic cells through the cerebral endothelium.* Journal of cellular and molecular medicine, 2019. **23**(4): p. 2619-2631.
34. Gunasinghe, N.P.A.D., et al., *Mesenchymal–epithelial transition (MET) as a mechanism for metastatic colonisation in breast cancer.* Cancer and Metastasis Reviews, 2012. **31**(3): p. 469-478.
35. Klein, C.A., *Cancer progression and the invisible phase of metastatic colonization.* Nature Reviews Cancer, 2020. **20**(11): p. 681-694.
36. Nagrath, S., et al., *Isolation of rare circulating tumour cells in cancer patients by microchip technology.* Nature, 2007. **450**(7173): p. 1235-9.
37. Conway, A.-M., et al., *Molecular characterisation and liquid biomarkers in Carcinoma of Unknown Primary (CUP): taking the 'U' out of 'CUP'.* British Journal of Cancer, 2019. **120**(2): p. 141-153.
38. Ilie, M., et al., *"Sentinel" circulating tumor cells allow early diagnosis of lung cancer in patients with chronic obstructive pulmonary disease.* PLoS One, 2014. **9**(10): p. e111597.
39. Rhim, A.D., et al., *EMT and dissemination precede pancreatic tumor formation.* Cell, 2012. **148**(1-2): p. 349-61.

40. Hüsemann, Y., et al., *Systemic spread is an early step in breast cancer.* Cancer Cell, 2008. **13**(1): p. 58-68.
41. Klein, C.A., *Parallel progression of primary tumours and metastases.* Nat Rev Cancer, 2009. **9**(4): p. 302-12.
42. Collins, V.P., R.K. Loeffler, and H. Tivey, *Observations on growth rates of human tumors.* Am J Roentgenol Radium Ther Nucl Med, 1956. **76**(5): p. 988-1000.
43. Kuukasjärvi, T., et al., *Genetic Heterogeneity and Clonal Evolution Underlying Development of Asynchronous Metastasis in Human Breast Cancer.* Cancer Research, 1997. **57**(8): p. 1597.
44. Yates, L.R., et al., *Genomic Evolution of Breast Cancer Metastasis and Relapse.* Cancer Cell, 2017. **32**(2): p. 169-184.e7.
45. Liang, Y., et al., *Metastatic heterogeneity of breast cancer: Molecular mechanism and potential therapeutic targets.* Seminars in Cancer Biology, 2020. **60**: p. 14-27.
46. Turashvili, G. and E. Brogi, *Tumor Heterogeneity in Breast Cancer.* Frontiers in Medicine, 2017. **4**(227).
47. Jones, S.E., *Metastatic Breast Cancer: The Treatment Challenge.* Clinical Breast Cancer, 2008. **8**(3): p. 224-233.
48. Priedigkeit, N., et al., *Intrinsic Subtype Switching and Acquired ERBB2/HER2 Amplifications and Mutations in Breast Cancer Brain Metastases.* JAMA Oncol, 2017. **3**(5): p. 666-671.
49. Carlson, P., et al., *Targeting the perivascular niche sensitizes disseminated tumour cells to chemotherapy.* Nat Cell Biol, 2019. **21**(2): p. 238-250.
50. Harris, C.A., et al., *The efficacy of HER2-targeted agents in metastatic breast cancer: a meta-analysis.* Annals of Oncology, 2011. **22**(6): p. 1308-1317.
51. Ding, L., et al., *Genome remodelling in a basal-like breast cancer metastasis and xenograft.* Nature, 2010. **464**(7291): p. 999-1005.
52. Bardia, A., et al., *Efficacy and Safety of Anti-Trop-2 Antibody Drug Conjugate Sacituzumab Govitecan (IMMU-132) in Heavily Pretreated Patients With Metastatic Triple-Negative Breast Cancer.* J Clin Oncol, 2017. **35**(19): p. 2141-2148.
53. Schmid, P., et al., *Atezolizumab and Nab-Paclitaxel in Advanced Triple-Negative Breast Cancer.* N Engl J Med, 2018. **379**(22): p. 2108-2121.
54. Cortes, J., et al., *KEYNOTE-355: Randomized, double-blind, phase III study of pembrolizumab + chemotherapy versus placebo + chemotherapy for previously untreated locally recurrent inoperable or metastatic triple-negative breast cancer.* Journal of Clinical Oncology, 2020. **38**(15_suppl): p. 1000-1000.
55. Demicheli, R., et al., *Time distribution of the recurrence risk for breast cancer patients undergoing mastectomy: further support about the concept of tumor dormancy.* Breast Cancer Research and Treatment, 1996. **41**: p. 177-185.
56. Karrison, T.G., D.J. Ferguson, and P. Meier, *Dormancy of mammary carcinoma after mastectomy.* J Natl Cancer Inst, 1999. **91**(1): p. 80-5.
57. Pan, H., et al., *20-Year Risks of Breast-Cancer Recurrence after Stopping Endocrine Therapy at 5 Years.* The New England journal of medicine, 2017. **377**(19): p. 1836-1846.
58. Braun, S., et al., *A pooled analysis of bone marrow micrometastasis in breast cancer.* N Engl J Med, 2005. **353**(8): p. 793-802.
59. Ghajar, C.M., *Metastasis prevention by targeting the dormant niche.* Nature Reviews Cancer, 2015. **15**(4): p. 238-247.

60. Goddard, E.T., et al., *Dormant tumour cells, their niches and the influence of immunity.* Nat Cell Biol, 2018. **20**(11): p. 1240-1249.
61. Willis, R.A., *The spread of tumours in the human body*. 1934, London: J. & A. Churchill Ltd.
62. Paget, S., *The distribution of secondary growths in cancer of the breast.* The Lancet, 1889. **133**: p. 571-573.
63. Fuchs, E., *Das Sarkom des Uvealtractus.* Archiv für Ophthalmologie, 1882. **XII**(2): p. 233.
64. Hadfield, G., *The dormant cancer cell.* British Medical Journal, 1954. **2**(4888): p. 607-610.
65. Wu, Q., et al., *Breast cancer subtypes predict the preferential site of distant metastases: a SEER based study.* Oncotarget, 2017. **8**(17): p. 27990-27996.
66. Holmgren, L., M.S. O'Reilly, and J. Folkman, *Dormancy of micrometastases: balanced proliferation and apoptosis in the presence of angiogenesis suppression.* Nat Med, 1995. **1**(2): p. 149-53.
67. Schofield, R., *The relationship between the spleen colony-forming cell and the haemopoietic stem cell.* Blood Cells, 1978. **4**(1-2): p. 7-25.
68. Aguirre-Ghiso, J.A., et al., *Urokinase receptor and fibronectin regulate the ERK(MAPK) to p38(MAPK) activity ratios that determine carcinoma cell proliferation or dormancy in vivo.* Mol Biol Cell, 2001. **12**(4): p. 863-79.
69. Ghajar, C., et al., *The perivascular niche regulates breast tumour dormancy.* Nat Cell Biol, 2013. **15**: p. 807-817.
70. Gimbrone, M.A., Jr., et al., *Tumor dormancy in vivo by prevention of neovascularization.* The Journal of experimental medicine, 1972. **136**(2): p. 261-276.
71. Blagosklonny, M.V., *Cell cycle arrest is not senescence.* Aging, 2011. **3**(2): p. 94-101.
72. Wells, A., et al., *The dormancy dilemma: quiescence versus balanced proliferation.* Cancer Res, 2013. **73**(13): p. 3811-6.
73. Nakamura-Ishizu, A., H. Takizawa, and T. Suda, *The analysis, roles and regulation of quiescence in hematopoietic stem cells.* Development, 2014. **141**(24): p. 4656.
74. Coller, H.A., L. Sang, and J.M. Roberts, *A new description of cellular quiescence.* PLoS Biol, 2006. **4**(3): p. e83.
75. Albrengues, J., et al., *Neutrophil extracellular traps produced during inflammation awaken dormant cancer cells in mice.* Science, 2018. **361**(6409): p. eaao4227.
76. Pommier, A., et al., *Unresolved endoplasmic reticulum stress engenders immune-resistant, latent pancreatic cancer metastases.* Science (New York, N.Y.), 2018. **360**(6394): p. eaao4908.
77. Goodison S, et al., *Prolonged dormancy and site-specific growth potential of cancer cells spontaneously disseminated from nonmetastatic breast tumors as revealed by labeling with green fluorescent protein.* Clin Cancer Res, 2003. **9**(10): p. 3808-3814.
78. Bragado, P., et al., *TGF-β2 dictates disseminated tumour cell fate in target organs through TGF-β-RIII and p38α/β signalling.* Nat Cell Biol, 2013. **15**(11): p. 1351-1361.
79. Montagner, M., et al., *Crosstalk with lung epithelial cells regulates Sfrp2-mediated latency in breast cancer dissemination.* Nature Cell Biology, 2020. **22**(3): p. 289-296.
80. Sosa, M.S., et al., *NR2F1 controls tumour cell dormancy via SOX9- and RARβ-driven quiescence programmes.* Nature Communications, 2015. **6**: p. 6170-6170.

81. Miller, I., et al., *Ki67 is a Graded Rather than a Binary Marker of Proliferation versus Quiescence.* Cell Reports, 2018. **24**(5): p. 1105-1112.e5.
82. Sobecki, M., et al., *The cell proliferation antigen Ki-67 organises heterochromatin.* eLife, 2016. **5**: p. e13722.
83. Brown, J.A., et al., *TGF-β-Induced Quiescence Mediates Chemoresistance of Tumor-Propagating Cells in Squamous Cell Carcinoma.* Cell Stem Cell, 2017. **21**(5): p. 650-664.e8.
84. Lee, E., et al., *Growth Arrest-Specific 6 (GAS6) Promotes Prostate Cancer Survival by G(1) Arrest/S Phase Delay and Inhibition of Apoptosis During Chemotherapy in Bone Marrow.* Journal of cellular biochemistry, 2016. **117**(12): p. 2815-2824.
85. Yumoto, K., et al., *A novel method for monitoring tumor proliferation in vivo using fluorescent dye DiD.* Cytometry. Part A : the journal of the International Society for Analytical Cytology, 2014. **85**(6): p. 548-555.
86. Naumov, G.N., et al., *Persistence of Solitary Mammary Carcinoma Cells in a Secondary Site.* Cancer Research, 2002. **62**(7): p. 2162.
87. Kienast, Y., et al., *Real-time imaging reveals the single steps of brain metastasis formation.* Nat Med, 2010. **16**(1): p. 116-22.
88. Taniguchi, S., et al., *Tumor-initiating cells establish an IL-33-TGF-β niche signaling loop to promote cancer progression.* Science, 2020. **369**(6501).
89. Yuan, R., L.L. Peters, and B. Paigen, *Mice as a mammalian model for research on the genetics of aging.* ILAR journal, 2011. **52**(1): p. 4-15.
90. Vera-Ramirez, L., et al., *Autophagy promotes the survival of dormant breast cancer cells and metastatic tumour recurrence.* Nature communications, 2018. **9**(1): p. 1944-1944.
91. Naumov, G.N., et al., *Ineffectiveness of doxorubicin treatment on solitary dormant mammary carcinoma cells or late-developing metastases.* Breast Cancer Res Treat, 2003. **82**(3): p. 199-206.
92. Dai, Y., et al., *Activation of anaphase-promoting complex by p53 induces a state of dormancy in cancer cells against chemotherapeutic stress.* Oncotarget, 2016. **7**(18): p. 25478-25492.
93. Acharyya, S., et al., *A CXCL1 paracrine network links cancer chemoresistance and metastasis.* Cell, 2012. **150**(1): p. 165-78.
94. Schardt, J.A., et al., *Genomic analysis of single cytokeratin-positive cells from bone marrow reveals early mutational events in breast cancer.* Cancer Cell, 2005. **8**(3): p. 227-39.
95. Hosseini, H., et al., *Early dissemination seeds metastasis in breast cancer.* Nature, 2016. **540**(7634): p. 552-558.
96. Harper, K.L., et al., *Mechanism of early dissemination and metastasis in Her2(+) mammary cancer.* Nature, 2016. **540**(7634): p. 588-592.
97. Noltenius, C. and H. Noltenius, *Dormant tumor cells in liver and brain: An autopsy study on metastasizing tumors.* Pathology - Research and Practice, 1985. **179**(4): p. 504-511.
98. Buell, J.F., et al., *Donor transmitted malignancies.* Ann Transplant, 2004. **9**(1): p. 53-6.
99. Tjensvoll, K., et al., *Detection of disseminated tumor cells in bone marrow predict late recurrences in operable breast cancer patients.* BMC Cancer, 2019. **19**(1): p. 1131.
100. Demicheli, R., et al., *Late effects of adjuvant chemotherapy adumbrate dormancy complexity in breast cancer.* Breast (Edinburgh, Scotland), 2020. **52**: p. 64-70.

101. Naume, B., et al., *Clinical outcome with correlation to disseminated tumor cell (DTC) status after DTC-guided secondary adjuvant treatment with docetaxel in early breast cancer.* J Clin Oncol, 2014. **32**(34): p. 3848-57.
102. Suzuki, M., et al., *Dormant cancer cells retrieved from metastasis-free organs regain tumorigenic and metastatic potency.* American Journal of Pathology, 2006. **169**: p. 673-681.
103. Oshima, G., et al., *Imaging of tumor clones with differential liver colonization.* Scientific Reports, 2015. **5**(1): p. 10946.
104. Yamamoto, N., et al., *Determination of clonality of metastasis by cell-specific color-coded fluorescent-protein imaging.* Cancer Res, 2003. **63**(22): p. 7785-90.
105. Tang, Y.J., et al., *Tracing Tumor Evolution in Sarcoma Reveals Clonal Origin of Advanced Metastasis.* Cell Reports, 2019. **28**(11): p. 2837-2850.e5.
106. Reiter, J.G., et al., *Lymph node metastases develop through a wider evolutionary bottleneck than distant metastases.* Nature genetics, 2020. **52**(7): p. 692-700.
107. Naxerova, K., et al., *Origins of lymphatic and distant metastases in human colorectal cancer.* Science, 2017. **357**(6346): p. 55-60.
108. Disibio, G. and S. French, *Metastatic patterns of cancers: Results from a large autopsy study.* Arch Pathol Lab Med, 2008. **132**(6): p. 931-939.
109. Shiozawa, Y., et al., *GAS6/AXL axis regulates prostate cancer invasion, proliferation, and survival in the bone marrow niche.* Neoplasia, 2010. **12**(2): p. 116-27.
110. Crist, S.B. and C.M. Ghajar, *When a House Is Not a Home: A Survey of Antimetastatic Niches and Potential Mechanisms of Disseminated Tumor Cell Suppression.* Annu Rev Pathol, 2021. **16**: p. 409-432.
111. Huang, J.-F., et al., *Incidence of patients with bone metastases at diagnosis of solid tumors in adults: a large population-based study.* Annals of translational medicine, 2020. **8**(7): p. 482-482.
112. Hernandez, R.K., et al., *Incidence of bone metastases in patients with solid tumors: analysis of oncology electronic medical records in the United States.* BMC cancer, 2018. **18**(1): p. 44-44.
113. Hartkopf, A.D., et al., *Prognostic relevance of disseminated tumour cells from the bone marrow of early stage breast cancer patients - results from a large single-centre analysis.* Eur J Cancer, 2014. **50**(15): p. 2550-9.
114. Tjensvoll, K., et al., *Persistent tumor cells in bone marrow of non-metastatic breast cancer patients after primary surgery are associated with inferior outcome.* BMC Cancer, 2012. **12**: p. 190.
115. Janni, W., et al., *Persistence of Disseminated Tumor Cells in the Bone Marrow of Breast Cancer Patients Predicts Increased Risk for Relapse—A European Pooled Analysis.* Clinical Cancer Research, 2011. **17**(9): p. 2967.
116. Morgan, T.M., et al., *Disseminated tumor cells in prostate cancer patients after radical prostatectomy and without evidence of disease predicts biochemical recurrence.* Clin Cancer Res, 2009. **15**(2): p. 677-83.
117. Mastro, A.M., C.V. Gay, and D.R. Welch, *The skeleton as a unique environment for breast cancer cells.* Clinical & Experimental Metastasis, 2003. **20**(3): p. 275-284.
118. Wang, N., et al., *Prostate cancer cells preferentially home to osteoblast-rich areas in the early stages of bone metastasis: evidence from in vivo models.* J Bone Miner Res, 2014. **29**(12): p. 2688-96.

119. Kucia, M., et al., *Trafficking of normal stem cells and metastasis of cancer stem cells involve similar mechanisms: pivotal role of the SDF-1-CXCR4 axis.* Stem Cells, 2005. **23**(7): p. 879-94.
120. Schindlbeck, C., et al., *Comparison of circulating tumor cells (CTC) in peripheral blood and disseminated tumor cells in the bone marrow (DTC-BM) of breast cancer patients.* Journal of Cancer Research and Clinical Oncology, 2013. **139**(6): p. 1055-1062.
121. Hartkopf, A.D., et al., *Disseminated tumor cells from the bone marrow of patients with nonmetastatic primary breast cancer are predictive of locoregional relapse.* Annals of Oncology, 2015. **26**(6): p. 1155-1160.
122. Lawson, M.A., et al., *Osteoclasts control reactivation of dormant myeloma cells by remodelling the endosteal niche.* Nat Commun, 2015. **6**: p. 8983.
123. Yamaguchi, K., P.I. Croucher, and J.E. Compston, *Comparison between the lengths of individual osteoid seams and resorption cavities in human iliac crest cancellous bone.* Bone Miner, 1993. **23**(1): p. 27-33.
124. Andersen, T.L., et al., *A physical mechanism for coupling bone resorption and formation in adult human bone.* Am J Pathol, 2009. **174**(1): p. 239-47.
125. Méndez-Ferrer, S., et al., *Mesenchymal and haematopoietic stem cells form a unique bone marrow niche.* Nature, 2010. **466**(7308): p. 829-34.
126. Yamazaki, S., et al., *Nonmyelinating Schwann Cells Maintain Hematopoietic Stem Cell Hibernation in the Bone Marrow Niche.* Cell, 2011. **147**(5): p. 1146-1158.
127. Bruns, I., et al., *Megakaryocytes regulate hematopoietic stem cell quiescence through CXCL4 secretion.* Nat Med, 2014. **20**(11): p. 1315-20.
128. Zhao, M., et al., *Megakaryocytes maintain homeostatic quiescence and promote post-injury regeneration of hematopoietic stem cells.* Nat Med, 2014. **20**(11): p. 1321-6.
129. Chang, M.K., et al., *Osteal tissue macrophages are intercalated throughout human and mouse bone lining tissues and regulate osteoblast function in vitro and in vivo.* J Immunol, 2008. **181**(2): p. 1232-44.
130. Sugiyama, T., et al., *Maintenance of the hematopoietic stem cell pool by CXCL12-CXCR4 chemokine signaling in bone marrow stromal cell niches.* Immunity, 2006. **25**(6): p. 977-88.
131. Omatsu, Y., et al., *The essential functions of adipo-osteogenic progenitors as the hematopoietic stem and progenitor cell niche.* Immunity, 2010. **33**(3): p. 387-99.
132. Asada, N., S. Takeishi, and P.S. Frenette, *Complexity of bone marrow hematopoietic stem cell niche.* International Journal of Hematology, 2017. **106**(1): p. 45-54.
133. Zhang, J., et al., *Identification of the haematopoietic stem cell niche and control of the niche size.* Nature, 2003. **425**(6960): p. 836-41.
134. Calvi, L.M., et al., *Osteoblastic cells regulate the haematopoietic stem cell niche.* Nature, 2003. **425**(6960): p. 841-6.
135. Nilsson, S.K., H.M. Johnston, and J.A. Coverdale, *Spatial localization of transplanted hemopoietic stem cells: inferences for the localization of stem cell niches.* Blood, 2001. **97**(8): p. 2293-9.
136. Croucher, P.I., M.M. McDonald, and T.J. Martin, *Bone metastasis: the importance of the neighbourhood.* Nature Reviews Cancer, 2016. **16**(6): p. 373-386.
137. Kiel, M.J., et al., *SLAM family receptors distinguish hematopoietic stem and progenitor cells and reveal endothelial niches for stem cells.* Cell, 2005. **121**(7): p. 1109-21.

138. Kunisaki, Y., et al., *Arteriolar niches maintain haematopoietic stem cell quiescence.* Nature, 2013. **502**(7473): p. 637-43.
139. Acar, M., et al., *Deep imaging of bone marrow shows non-dividing stem cells are mainly perisinusoidal.* Nature, 2015. **526**(7571): p. 126-30.
140. Butler, J.M., et al., *Endothelial cells are essential for the self-renewal and repopulation of Notch-dependent hematopoietic stem cells.* Cell Stem Cell, 2010. **6**(3): p. 251-64.
141. Cackowski, F.C. and R.S. Taichman, *Parallels between hematopoietic stem cell and prostate cancer disseminated tumor cell regulation.* Bone, 2019. **119**: p. 82-86.
142. Sipkins, D.A., et al., *In vivo imaging of specialized bone marrow endothelial microdomains for tumour engraftment.* Nature, 2005. **435**(7044): p. 969-73.
143. Price, T.T., et al., *Dormant breast cancer micrometastases reside in specific bone marrow niches that regulate their transit to and from bone.* Science Translational Medicine, 2016. **8**(340): p. 340ra73.
144. Lo Celso, C., et al., *Live-animal tracking of individual haematopoietic stem/progenitor cells in their niche.* Nature, 2009. **457**(7225): p. 92-6.
145. Bowers, M., et al., *Osteoblast ablation reduces normal long-term hematopoietic stem cell self-renewal but accelerates leukemia development.* Blood, 2015. **125**(17): p. 2678-2688.
146. Boyerinas, B., et al., *Adhesion to osteopontin in the bone marrow niche regulates lymphoblastic leukemia cell dormancy.* Blood, 2013. **121**(24): p. 4821-31.
147. Taichman, R.S., et al., *GAS6 receptor status is associated with dormancy and bone metastatic tumor formation.* PLoS One, 2013. **8**(4): p. e61873.
148. Yumoto, K., et al., *Axl is required for TGF-β2-induced dormancy of prostate cancer cells in the bone marrow.* Sci Rep, 2016. **6**: p. 36520.
149. Mishra, A., et al., *Hypoxia stabilizes GAS6/Axl signaling in metastatic prostate cancer.* Mol Cancer Res, 2012. **10**(6): p. 703-12.
150. Axelrod, H.D., et al., *AXL Is a Putative Tumor Suppressor and Dormancy Regulator in Prostate Cancer.* Mol Cancer Res, 2019. **17**(2): p. 356-369.
151. Datto, M.B., et al., *Transforming growth factor beta induces the cyclin-dependent kinase inhibitor p21 through a p53-independent mechanism.* Proc Natl Acad Sci USA, 1995. **92**(12): p. 5545.
152. Hannon, G.J. and D. Beach, *p15INK4B is a potential effector of TGF-beta-induced cell cycle arrest.* Nature, 1994. **371**(6494): p. 257-61.
153. Polyak, K., et al., *p27Kip1, a cyclin-Cdk inhibitor, links transforming growth factor-beta and contact inhibition to cell cycle arrest.* Genes Dev, 1994. **8**(1): p. 9-22.
154. Prunier, C., et al., *TGF-β Family Signaling Pathways in Cellular Dormancy.* Trends Cancer, 2019. **5**(1): p. 66-78.
155. Yin, J.J., et al., *TGF-beta signaling blockade inhibits PTHrP secretion by breast cancer cells and bone metastases development.* J Clin Invest, 1999. **103**(2): p. 197-206.
156. Yu-Lee, L.-Y., et al., *Osteoblast-Secreted Factors Mediate Dormancy of Metastatic Prostate Cancer in the Bone via Activation of the TGFβRIII–p38MAPK–pS249/T252RB Pathway.* Cancer Research, 2018. **78**(11): p. 2911-2924.
157. Bragado, P., et al., *TGF-β2 dictates disseminated tumour cell fate in target organs through TGF-β-RIII and p38α/β signalling.* Nat Cell Biol, 2013. **15**(11): p. 1351-61.
158. Nobre, A.R., et al., *Bone marrow NG2+/Nestin+ mesenchymal stem cells drive DTC dormancy via TGF-β2.* Nature Cancer, 2021.

159. Buijs, J.T., et al., *BMP7, a putative regulator of epithelial homeostasis in the human prostate, is a potent inhibitor of prostate cancer bone metastasis in vivo.* Am J Pathol, 2007. **171**(3): p. 1047-57.
160. Kobayashi, A., et al., *Bone morphogenetic protein 7 in dormancy and metastasis of prostate cancer stem-like cells in bone.* J Exp Med, 2011. **208**(13): p. 2641-2655.
161. Sharma, S., et al., *Secreted Protein Acidic and Rich in Cysteine (SPARC) Mediates Metastatic Dormancy of Prostate Cancer in Bone.* J Biol Chem, 2016. **291**(37): p. 19351-63.
162. Agarwal, P., et al., *Mesenchymal Niche-Specific Expression of Cxcl12 Controls Quiescence of Treatment-Resistant Leukemia Stem Cells.* Cell Stem Cell, 2019. **24**(5): p. 769-784.e6.
163. Ding, L. and S.J. Morrison, *Haematopoietic stem cells and early lymphoid progenitors occupy distinct bone marrow niches.* Nature, 2013. **495**(7440): p. 231-235.
164. Ono, M., et al., *Exosomes from bone marrow mesenchymal stem cells contain a microRNA that promotes dormancy in metastatic breast cancer cells.* Science Signaling, 2014. **7**(332): p. ra63.
165. Bliss, S.A., et al., *Mesenchymal Stem Cell-Derived Exosomes Stimulate Cycling Quiescence and Early Breast Cancer Dormancy in Bone Marrow.* Cancer Res, 2016. **76**(19): p. 5832-5844.
166. Kolb, A.D., et al., *Osteoblasts are "educated" by crosstalk with metastatic breast cancer cells in the bone tumor microenvironment.* Breast Cancer Res, 2019. **21**(1): p. 31.
167. Barkan, D., et al., *Metastatic growth from dormant cells induced by a col-I-enriched fibrotic environment.* Cancer Res, 2010. **70**(14): p. 5706-16.
168. Gao, H., et al., *Multi-organ Site Metastatic Reactivation Mediated by Non-canonical Discoidin Domain Receptor 1 Signaling.* Cell, 2016. **166**(1): p. 47-62.
169. Johnson, R.W., et al., *Induction of LIFR confers a dormancy phenotype in breast cancer cells disseminated to the bone marrow.* Nat Cell Biol, 2016. **18**(10): p. 1078-1089.
170. Parmar, K., et al., *Distribution of hematopoietic stem cells in the bone marrow according to regional hypoxia.* Proc Natl Acad Sci USA, 2007. **104**(13): p. 5431-6.
171. Chow, D.C., et al., *Modeling pO(2) distributions in the bone marrow hematopoietic compartment. II. Modified Kroghian models.* Biophys J, 2001. **81**(2): p. 685-96.
172. Yue, X., L. Wu, and W. Hu, *The regulation of leukemia inhibitory factor.* Cancer Cell Microenviron, 2015. **2**(3).
173. Kusumbe, A.P., *Vascular niches for disseminated tumour cells in bone.* Journal of Bone Oncology, 2016. **5**(3): p. 112-116.
174. Xie, Y., et al., *Detection of functional haematopoietic stem cell niche using real-time imaging.* Nature, 2009. **457**(7225): p. 97-101.
175. Itkin, T., et al., *Distinct bone marrow blood vessels differentially regulate haematopoiesis.* Nature, 2016. **532**(7599): p. 323-328.
176. Mirochnik, Y., A. Kwiatek, and O.V. Volpert, *Thrombospondin and apoptosis: molecular mechanisms and use for design of complementation treatments.* Curr Drug Targets, 2008. **9**(10): p. 851-62.
177. Katayama, Y., et al., *Signals from the sympathetic nervous system regulate hematopoietic stem cell egress from bone marrow.* Cell, 2006. **124**(2): p. 407-21.

178. Decker, A.M., et al., *Sympathetic Signaling Reactivates Quiescent Disseminated Prostate Cancer Cells in the Bone Marrow.* Molecular cancer research : MCR, 2017. **15**(12): p. 1644-1655.
179. Campbell, J.P., et al., *Stimulation of host bone marrow stromal cells by sympathetic nerves promotes breast cancer bone metastasis in mice.* PLoS Biol, 2012. **10**(7): p. e1001363.
180. Naveiras, O., et al., *Bone-marrow adipocytes as negative regulators of the haematopoietic microenvironment.* Nature, 2009. **460**(7252): p. 259-63.
181. DiMascio, L., et al., *Identification of adiponectin as a novel hemopoietic stem cell growth factor.* J Immunol, 2007. **178**(6): p. 3511-20.
182. Cahu, X., et al., *Bone marrow sites differently imprint dormancy and chemoresistance to T-cell acute lymphoblastic leukemia.* Blood Advances, 2017. **1**(20): p. 1760-1772.
183. Liu, Z., et al., *Mature adipocytes in bone marrow protect myeloma cells against chemotherapy through autophagy activation.* Oncotarget, 2015. **6**(33): p. 34329-41.
184. Ghiaur, G., et al., *Regulation of human hematopoietic stem cell self-renewal by the microenvironment's control of retinoic acid signaling.* Proc Natl Acad Sci USA, 2013. **110**(40): p. 16121-16126.
185. Zhao, E., et al., *Bone marrow and the control of immunity.* Cell Mol Immunol, 2012. **9**(1): p. 11-9.
186. Feuerer, M., et al., *Enrichment of memory T cells and other profound immunological changes in the bone marrow from untreated breast cancer patients.* Int J Cancer, 2001. **92**(1): p. 96-105.
187. Pantel, K., et al., *Frequent down-regulation of major histocompatibility class I antigen expression on individual micrometastatic carcinoma cells.* Cancer Res, 1991. **51**(17): p. 4712-5.
188. Bromberg, J.F., et al., *Transcriptionally active Stat1 is required for the antiproliferative effects of both interferon alpha and interferon gamma.* Proc Natl Acad Sci USA, 1996. **93**(15): p. 7673.
189. Kortylewski, M., et al., *Interferon-gamma-mediated growth regulation of melanoma cells: involvement of STAT1-dependent and STAT1-independent signals.* J Invest Dermatol, 2004. **122**(2): p. 414-22.
190. Farrar, J.D., et al., *Cancer Dormancy. VII. A Regulatory Role for CD8+ T Cells and IFN-γ in Establishing and Maintaining the Tumor-Dormant State.* J Immunol, 1999. **162**(5): p. 2842.
191. Owen, K.L., et al., *Prostate cancer cell-intrinsic interferon signaling regulates dormancy and metastatic outgrowth in bone.* EMBO Rep, 2020. **21**(6): p. e50162.
192. Ramasamy, R., et al., *The immunosuppressive effects of human bone marrow-derived mesenchymal stem cells target T cell proliferation but not its effector function.* Cell Immunol, 2008. **251**(2): p. 131-6.
193. Patel, S.A., et al., *Mesenchymal Stem Cells Protect Breast Cancer Cells through Regulatory T Cells: Role of Mesenchymal Stem Cell-Derived TGF-β.* The Journal of Immunology, 2010. **184**(10): p. 5885.
194. Kristensen, H.B., et al., *Increased presence of capillaries next to remodeling sites in adult human cancellous bone.* J Bone Miner Res, 2013. **28**(3): p. 574-85.
195. Kollet, O., et al., *Osteoclasts degrade endosteal components and promote mobilization of hematopoietic progenitor cells.* Nat Med, 2006. **12**(6): p. 657-64.

196. Arnett, T.R., et al., *Hypoxia is a major stimulator of osteoclast formation and bone resorption.* J Cell Physiol, 2003. **196**(1): p. 2-8.
197. Lu, X., et al., *VCAM-1 promotes osteolytic expansion of indolent bone micrometastasis of breast cancer by engaging α4β1-positive osteoclast progenitors.* Cancer Cell, 2011. **20**(6): p. 701-14.
198. Han, H.H., et al., *Angiopoietin-2 promotes ER+ breast cancer cell survival in bone marrow niche.* Endocrine-Related Cancer, 2016. **23**(8): p. 609-623.
199. Ashford, R., et al., *The modern surgical and non-surgical management of appendicular skeletal metastases.* Orthopaedics and Trauma, 2012. **26**(3): p. 184-199.
200. Shiozawa, Y., et al., *Human prostate cancer metastases target the hematopoietic stem cell niche to establish footholds in mouse bone marrow.* J Clin Invest, 2011. **121**(4): p. 1298-312.
201. McDonald, M.M., et al., *Inhibiting the osteocyte-specific protein sclerostin increases bone mass and fracture resistance in multiple myeloma.* Blood, 2017. **129**(26): p. 3452-3464.
202. Corey, E., et al., *Zoledronic acid exhibits inhibitory effects on osteoblastic and osteolytic metastases of prostate cancer.* Clin Cancer Res, 2003. **9**(1): p. 295-306.
203. Jones, D.H., et al., *Regulation of cancer cell migration and bone metastasis by RANKL.* Nature, 2006. **440**(7084): p. 692-6.
204. Scagliotti, G.V., et al., *Overall survival improvement in patients with lung cancer and bone metastases treated with denosumab versus zoledronic acid: subgroup analysis from a randomized phase 3 study.* J Thorac Oncol, 2012. **7**(12): p. 1823-1829.
205. Gnant, M., et al., *Adjuvant denosumab in breast cancer (ABCSG-18): a multicentre, randomised, double-blind, placebo-controlled trial.* The Lancet, 2015. **386**(9992): p. 433-443.
206. Xiao, W., et al., *Risk factors and survival outcomes in patients with breast cancer and lung metastasis: a population-based study.* Cancer medicine, 2018. **7**(3): p. 922-930.
207. Li, J., et al., *Expert consensus on multidisciplinary therapy of colorectal cancer with lung metastases (2019 edition).* Journal of Hematology & Oncology, 2019. **12**(1): p. 16.
208. Lee, Y.T., *Breast carcinoma: pattern of metastasis at autopsy.* J Surg Oncol, 1983. **23**(3): p. 175-80.
209. Fabozzi, S.J., P.F. Schellhammer, and A.M. el-Mahdi, *Pulmonary metastases from prostate cancer.* Cancer, 1995. **75**(11): p. 2706-9.
210. Dang, Q., et al., *Anti-androgen enzalutamide enhances prostate cancer neuroendocrine (NE) differentiation via altering the infiltrated mast cells → androgen receptor (AR) → miRNA32 signals.* Molecular Oncology, 2015. **9**(7): p. 1241-1251.
211. Dong, B., et al., *Influence of abiraterone acetate on neuroendocrine differentiation in chemotherapy-naive metastatic castration-resistant prostate cancer.* The Prostate, 2017. **77**(13): p. 1373-1380.
212. Conteduca, V., et al., *Clinical features of neuroendocrine prostate cancer.* Eur J Cancer, 2019. **121**: p. 7-18.
213. Aggarwal, R., et al., *Clinical and Genomic Characterization of Treatment-Emergent Small-Cell Neuroendocrine Prostate Cancer: A Multi-institutional Prospective Study.* J Clin Oncol, 2018. **36**(24): p. 2492-2503.
214. Saitoh, H., et al., *Metastatic patterns of prostatic cancer. Correlation between sites and number of organs involved.* Cancer, 1984. **54**(12): p. 3078-84.

215. Diaz-Canton, E.A., et al., *Clinical course of breast cancer patients with metastases confined to the lungs treated with chemotherapy. The University of Texas M.D. Anderson Cancer Center experience and review of the literature.* Ann Oncol, 1998. **9**(4): p. 413-8.
216. Barron, L., S.A. Gharib, and J.S. Duffield, *Lung Pericytes and Resident Fibroblasts: Busy Multitaskers.* The American Journal of Pathology, 2016. **186**(10): p. 2519-2531.
217. Suki, B., D. Stamenović, and R. Hubmayr, *Lung parenchymal mechanics.* Compr Physiol, 2011. **1**(3): p. 1317-51.
218. Parker, A.L. and T.R. Cox, *The Role of the ECM in Lung Cancer Dormancy and Outgrowth.* Frontiers in Oncology, 2020. **10**(1766).
219. Stella, G.M., et al., *Lung-Seeking Metastases.* Cancers, 2019. **11**(7): p. 1010.
220. Minn, A.J., et al., *Genes that mediate breast cancer metastasis to lung.* Nature, 2005. **436**(7050): p. 518-24.
221. Chen, Q., X.H.F. Zhang, and J. Massagué, *Macrophage binding to receptor VCAM-1 transmits survival signals in breast cancer cells that invade the lungs.* Cancer cell, 2011. **20**(4): p. 538-549.
222. Gao, H., et al., *The BMP inhibitor Coco reactivates breast cancer cells at lung metastatic sites.* Cell, 2012. **150**(4): p. 764-79.
223. Bornstein, P., *Thrombospondins function as regulators of angiogenesis.* J Cell Commun Signal, 2009. **3**(3-4): p. 189-200.
224. Lee, J.H., et al., *Lung stem cell differentiation in mice directed by endothelial cells via a BMP4-NFATc1-thrombospondin-1 axis.* Cell, 2014. **156**(3): p. 440-55.
225. Barney, L.E., et al., *Tumor cell–organized fibronectin maintenance of a dormant breast cancer population.* Science Advances, 2020. **6**(11): p. eaaz4157.
226. Eyles, J., et al., *Tumor cells disseminate early, but immunosurveillance limits metastatic outgrowth, in a mouse model of melanoma.* Journal of Clinical Investigation, 2010. **120**(6): p. 2030-2039.
227. Malladi, S., et al., *Metastatic Latency and Immune Evasion through Autocrine Inhibition of WNT.* Cell, 2016. **165**(1): p. 45-60.
228. Romero, I., et al., *T lymphocytes restrain spontaneous metastases in permanent dormancy.* Cancer Res, 2014. **74**(7): p. 1958-68.
229. Aqbi, H.F., et al., *Local and distant tumor dormancy during early stage breast cancer are associated with the predominance of infiltrating T effector subsets.* Breast Cancer Res, 2020. **22**(1): p. 116-116.
230. Piranlioglu, R., et al., *Primary tumor-induced immunity eradicates disseminated tumor cells in syngeneic mouse model.* Nature Communications, 2019. **10**(1): p. 1430-1430.
231. Krall, J.A., et al., *The systemic response to surgery triggers the outgrowth of distant immune-controlled tumors in mouse models of dormancy.* Science Translational Medicine, 2018. **10**(436): p. eaan3464.
232. Barkan, D., et al., *Inhibition of metastatic outgrowth from single dormant tumor cells by targeting the cytoskeleton.* Cancer research, 2008. **68**(15): p. 6241-6250.
233. Urosevic, J., et al., *Colon cancer cells colonize the lung from established liver metastases through p38 MAPK signalling and PTHLH.* Nat Cell Biol, 2014. **16**(7): p. 685-94.
234. El Rayes, T., et al., *Lung inflammation promotes metastasis through neutrophil protease-mediated degradation of Tsp-1.* Proc Natl Acad Sci USA, 2015. **112**(52): p. 16000-16005.

235. Rachman-Tzemah, C., et al., *Blocking Surgically Induced Lysyl Oxidase Activity Reduces the Risk of Lung Metastases.* Cell Reports, 2017. **19**(4): p. 774-784.
236. Demicheli, R., et al., *The effects of surgery on tumor growth: a century of investigations.* Ann Oncol, 2008. **19**(11): p. 1821-8.
237. De Cock, J.M., et al., *Inflammation triggers Zeb1-dependent escape from tumor latency.* Cancer Research, 2016: p. canres.0608.2016.
238. Weidenfeld, K., et al., *Dormant tumor cells expressing LOXL2 acquire a stem-like phenotype mediating their transition to proliferative growth.* Oncotarget, 2016. **7**(44): p. 71362-71377.
239. Wu, L. and Y. Zhu, *The function and mechanisms of action of LOXL2 in cancer (Review).* Int J Mol Med, 2015. **36**(5): p. 1200-1204.
240. Calvo, A., et al., *Identification of VEGF-regulated genes associated with increased lung metastatic potential: functional involvement of tenascin-C in tumor growth and lung metastasis.* Oncogene, 2008. **27**(40): p. 5373-84.
241. Oskarsson, T., et al., *Breast cancer cells produce tenascin C as a metastatic niche component to colonize the lungs.* Nature Medicine, 2011. **17**(7): p. 867-874.
242. Malanchi, I., et al., *Interactions between cancer stem cells and their niche govern metastatic colonization.* Nature, 2012. **481**(7379): p. 85-89.
243. Schouten, L.J., et al., *Incidence of brain metastases in a cohort of patients with carcinoma of the breast, colon, kidney, and lung and melanoma.* Cancer, 2002. **94**(10): p. 2698-705.
244. Barnholtz-Sloan, J.S., et al., *Incidence proportions of brain metastases in patients diagnosed (1973 to 2001) in the Metropolitan Detroit Cancer Surveillance System.* J Clin Oncol, 2004. **22**(14): p. 2865-72.
245. Smedby, K.E., et al., *Brain metastases admissions in Sweden between 1987 and 2006.* Br J Cancer, 2009. **101**(11): p. 1919-24.
246. Gavrilovic, I.T. and J.B. Posner, *Brain metastases: epidemiology and pathophysiology.* Journal of Neuro-Oncology, 2005. **75**(1): p. 5-14.
247. Stemmler, H.J. and V. Heinemann, *Central nervous system metastases in HER-2-overexpressing metastatic breast cancer: a treatment challenge.* Oncologist, 2008. **13**(7): p. 739-50.
248. Kolomainen, D.F., et al., *Epithelial ovarian cancer metastasizing to the brain: a late manifestation of the disease with an increasing incidence.* J Clin Oncol, 2002. **20**(4): p. 982-6.
249. Clayton, A.J., et al., *Incidence of cerebral metastases in patients treated with trastuzumab for metastatic breast cancer.* Br J Cancer, 2004. **91**(4): p. 639-43.
250. Delattre, J.Y., et al., *Distribution of brain metastases.* Arch Neurol, 1988. **45**(7): p. 741-4.
251. Schroeder, T., et al., *Mapping distribution of brain metastases: does the primary tumor matter?* J Neurooncol, 2020. **147**(1): p. 229-235.
252. Fitzgerald, D.P., et al., *Reactive glia are recruited by highly proliferative brain metastases of breast cancer and promote tumor cell colonization.* Clin Exp Metastasis, 2008. **25**(7): p. 799-810.
253. Poli, A., et al., *NK Cells in Central Nervous System Disorders.* J Immunol, 2013. **190**(11): p. 5355.
254. Smolders, J., et al., *Tissue-resident memory T cells populate the human brain.* Nature Communications, 2018. **9**(1): p. 4593.

255. Steinbach, K., et al., *Brain-resident memory T cells generated early in life predispose to autoimmune disease in mice.* Science Translational Medicine, 2019. **11**(498): p. eaav5519.
256. Sampson, J.H., et al., *Brain immunology and immunotherapy in brain tumours.* Nature Reviews Cancer, 2020. **20**(1): p. 12-25.
257. Domingues, P.H., et al., *Immunophenotypic Identification and Characterization of Tumor Cells and Infiltrating Cell Populations in Meningiomas.* The American Journal of Pathology, 2012. **181**(5): p. 1749-1761.
258. Alsharifi, M., et al., *NK cell-mediated immunopathology during an acute viral infection of the CNS.* European Journal of Immunology, 2006. **36**(4): p. 887-896.
259. Wakim, L.M., et al., *The Molecular Signature of Tissue Resident Memory CD8 T Cells Isolated from the Brain.* J Immunol, 2012. **189**(7): p. 3462.
260. Smolders, J., et al., *Characteristics of differentiated CD8+ and CD4+ T cells present in the human brain.* Acta Neuropathologica, 2013. **126**(4): p. 525-535.
261. Celio, M.R., et al., *Perineuronal nets: past and present.* Trends Neurosci, 1998. **21**(12): p. 510-5.
262. Dityatev, A. and M. Schachner, *Extracellular matrix molecules and synaptic plasticity.* Nat Rev Neurosci, 2003. **4**(6): p. 456-68.
263. Matthews, R.T., et al., *Aggrecan glycoforms contribute to the molecular heterogeneity of perineuronal nets.* J Neurosci, 2002. **22**(17): p. 7536-47.
264. Wu, C., et al., *Endothelial basement membrane laminin alpha5 selectively inhibits T lymphocyte extravasation into the brain.* Nat Med, 2009. **15**(5): p. 519-27.
265. Daneman, R. and A. Prat, *The blood-brain barrier.* Cold Spring Harb Perspect Biol, 2015. **7**(1): p. a020412.
266. Engelhardt, B. and L. Sorokin, *The blood–brain and the blood–cerebrospinal fluid barriers: function and dysfunction.* Seminars in Immunopathology, 2009. **31**(4): p. 497-511.
267. Louveau, A., et al., *Structural and functional features of central nervous system lymphatic vessels.* Nature, 2015. **523**(7560): p. 337-341.
268. Aspelund, A., et al., *A dural lymphatic vascular system that drains brain interstitial fluid and macromolecules.* J Exp Med, 2015. **212**(7): p. 991-999.
269. Izraely, S., et al., *The metastatic microenvironment: Brain-residing melanoma metastasis and dormant micrometastasis.* International Journal of Cancer, 2012. **131**(5): p. 1071-1082.
270. Hirata, E., et al., *The Brain Microenvironment Induces DNMT1 Suppression and Indolence of Metastatic Cancer Cells.* iScience, 2020. **23**(9): p. 101480-101480.
271. Sarkar, S., et al., *Therapeutic activation of macrophages and microglia to suppress brain tumor-initiating cells.* Nat Neurosci, 2014. **17**(1): p. 46-55.
272. Sarkar, S., et al., *Microglia induces Gas1 expression in human brain tumor-initiating cells to reduce tumorigenecity.* Sci Rep, 2018. **8**(1): p. 15286.
273. Sarkar, S., et al., *ADAM-9 is a novel mediator of tenascin-C-stimulated invasiveness of brain tumor-initiating cells.* Neuro Oncol, 2015. **17**(8): p. 1095-105.
274. Lorger, M. and B. Felding-Habermann, *Capturing changes in the brain microenvironment during initial steps of breast cancer brain metastasis.* Am J Pathol, 2010. **176**(6): p. 2958-71.

275. Heyn, C., et al., *In vivo MRI of cancer cell fate at the single-cell level in a mouse model of breast cancer metastasis to the brain.* Magn Reson Med, 2006. **56**(5): p. 1001-10.
276. Bos, P.D., et al., *Genes that mediate breast cancer metastasis to the brain.* Nature, 2009. **459**(7249): p. 1005-9.
277. Sevenich, L., et al., *Analysis of tumour- and stroma-supplied proteolytic networks reveals a brain-metastasis-promoting role for cathepsin S.* Nat Cell Biol, 2014. **16**(9): p. 876-88.
278. Klein, A., et al., *The metastatic microenvironment: Brain-derived soluble factors alter the malignant phenotype of cutaneous and brain-metastasizing melanoma cells.* International Journal of Cancer, 2012. **131**(11): p. 2509-2518.
279. Rodrigues, G., et al., *Tumour exosomal CEMIP protein promotes cancer cell colonization in brain metastasis.* Nature Cell Biology, 2019. **21**(11): p. 1403-1412.
280. Paku, S., et al., *Organ-specificity of the extravasation process: an ultrastructural study.* Clin Exp Metastasis, 2000. **18**(6): p. 481-92.
281. Valiente, M., et al., *Serpins promote cancer cell survival and vascular co-option in brain metastasis.* Cell, 2014. **156**(5): p. 1002-16.
282. Er, E.E., et al., *Pericyte-like spreading by disseminated cancer cells activates YAP and MRTF for metastatic colonization.* Nature Cell Biology, 2018. **20**(8): p. 966-978.
283. Kim, S.W., et al., *Role of the endothelin axis in astrocyte- and endothelial cell-mediated chemoprotection of cancer cells.* Neuro Oncol, 2014. **16**(12): p. 1585-98.
284. Wang, X., et al., *Astrocytic Fas ligand expression is required to induce T-cell apoptosis and recovery from experimental autoimmune encephalomyelitis.* Eur J Immunol, 2013. **43**(1): p. 115-24.
285. Wasilewski, D., et al., *Reactive Astrocytes in Brain Metastasis.* Front Oncol, 2017. **7**: p. 298.
286. Schwartz, H., et al., *Incipient Melanoma Brain Metastases Instigate Astrogliosis and Neuroinflammation.* Cancer Research, 2016. **76**(15): p. 4359.
287. Yu, T., et al., *Delivery of MGMT mRNA to glioma cells by reactive astrocyte-derived exosomes confers a temozolomide resistance phenotype.* Cancer Lett, 2018. **433**: p. 210-220.
288. Chen, Q., et al., *Carcinoma-astrocyte gap junctions promote brain metastasis by cGAMP transfer.* Nature, 2016. **533**(7604): p. 493-498.
289. Kim, S.J., et al., *Astrocytes upregulate survival genes in tumor cells and induce protection from chemotherapy.* Neoplasia, 2011. **13**(3): p. 286-98.
290. Lin, Q., et al., *Reactive astrocytes protect melanoma cells from chemotherapy by sequestering intracellular calcium through gap junction communication channels.* Neoplasia, 2010. **12**(9): p. 748-54.
291. Seike, T., et al., *Interaction between lung cancer cells and astrocytes via specific inflammatory cytokines in the microenvironment of brain metastasis.* Clin Exp Metastasis, 2011. **28**(1): p. 13-25.
292. Sartorius, C.A., et al., *Estrogen promotes the brain metastatic colonization of triple negative breast cancer cells via an astrocyte-mediated paracrine mechanism.* Oncogene, 2016. **35**(22): p. 2881-92.
293. Neman, J., et al., *Co-evolution of breast-to-brain metastasis and neural progenitor cells.* Clin Exp Metastasis, 2013. **30**(6): p. 753-68.
294. Piomelli, D., G. Astarita, and R. Rapaka, *A neuroscientist's guide to lipidomics.* Nat Rev Neurosci, 2007. **8**(10): p. 743-54.

295. Jin, X., et al., *A metastasis map of human cancer cell lines.* Nature, 2020. **588**(7837): p. 331-336.
296. He, B.P., et al., *Differential reactions of microglia to brain metastasis of lung cancer.* Mol Med, 2006. **12**(7-8): p. 161-70.
297. Berghoff, A.S., et al., *Characterization of the inflammatory response to solid cancer metastases in the human brain.* Clin Exp Metastasis, 2013. **30**(1): p. 69-81.
298. Brantley, E.C., et al., *Nitric oxide-mediated tumoricidal activity of murine microglial cells.* Transl Oncol, 2010. **3**(6): p. 380-8.
299. Pukrop, T., et al., *Microglia promote colonization of brain tissue by breast cancer cells in a Wnt-dependent way.* Glia, 2010. **58**(12): p. 1477-89.
300. Qiao, S., et al., *Long-term characterization of activated microglia/macrophages facilitating the development of experimental brain metastasis through intravital microscopic imaging.* J Neuroinflammation, 2019. **16**(1): p. 4.
301. Flüh, C., et al., *Dormancy and NKG2D system in brain metastases: Analysis of immunogenicity.* Int J Mol Med, 2020. **45**(2): p. 298-314.
302. Gemechu, J.M. and M. Bentivoglio, *T Cell Recruitment in the Brain during Normal Aging.* Front Cell Neurosci, 2012. **6**: p. 38.
303. Budczies, J., et al., *The landscape of metastatic progression patterns across major human cancers.* Oncotarget, 2015. **6**(1): p. 570-583.
304. diSibio, G. and S.W. French, *Metastatic Patterns of Cancers: Results From a Large Autopsy Study.* Archives of Pathology & Laboratory Medicine, 2008. **132**(6): p. 931-939.
305. Hess, K.R., et al., *Metastatic patterns in adenocarcinoma.* Cancer, 2006. **106**(7): p. 1624-33.
306. Chow, F.C.-L. and K.S.-H. Chok, *Colorectal liver metastases: An update on multidisciplinary approach.* World journal of hepatology, 2019. **11**(2): p. 150-172.
307. Abbott, D.E., et al., *Resection of liver metastases from breast cancer: Estrogen receptor status and response to chemotherapy before metastasectomy define outcome.* Surgery, 2012. **151**(5): p. 710-716.
308. Sabanathan, D., G.D. Eslick, and J. Shannon, *Use of Neoadjuvant Chemotherapy Plus Molecular Targeted Therapy in Colorectal Liver Metastases: A Systematic Review and Meta-analysis.* Clin Colorectal Cancer, 2016. **15**(4): p. e141-e147.
309. Paschos, K.A. and N.C. Bird, *Liver Regeneration and its Impact on Post-hepatectomy Metastatic Tumour Recurrence.* Anticancer Research, 2010. **30**(6): p. 2161-2170.
310. Jones, R.P., et al., *Systematic review and meta-analysis of follow-up after hepatectomy for colorectal liver metastases.* Br J Surg, 2012. **99**(4): p. 477-86.
311. Selzner, M., et al., *Liver metastases from breast cancer: Long-term survival after curative resection.* Surgery, 2000. **127**(4): p. 383-389.
312. Adam, R., et al., *Hepatic Resection for Noncolorectal Nonendocrine Liver Metastases: Analysis of 1452 Patients and Development of a Prognostic Model.* Annals of Surgery, 2006. **244**(4): p. 524-535.
313. Ikawa, K., et al., *Genetic detection of liver micrometastases that are undetectable histologically.* J Surg Res, 2002. **106**(1): p. 124-30.
314. Pommier, A., et al., *Unresolved endoplasmic reticulum stress engenders immune-resistant, latent pancreatic cancer metastases.* Science, 2018. **360**(6394).

315. Aqbi, H.F., et al., *Local and distant tumor dormancy during early stage breast cancer are associated with the predominance of infiltrating T effector subsets.* Breast Cancer Research, 2020. **22**(1): p. 116.
316. Clark, A.M., et al., *A liver microphysiological system of tumor cell dormancy and inflammatory responsiveness is affected by scaffold properties.* Lab on a chip, 2016. **17**(1): p. 156-168.
317. Panis, Y., et al., *Dormant liver metastases: an experimental study.* BJS (British Journal of Surgery), 1992. **79**(3): p. 221-223.
318. Kan, Z. and D.C. Madoff, *Liver anatomy: microcirculation of the liver.* Semin Intervent Radiol, 2008. **25**(2): p. 77-85.
319. Martin, M.D., et al., *Rapid extravasation and establishment of breast cancer micrometastases in the liver microenvironment.* Mol Cancer Res, 2010. **8**(10): p. 1319-27.
320. Brodt, P., *Role of the Microenvironment in Liver Metastasis: From Pre- to Prometastatic Niches.* Clin Cancer Res, 2016. **22**(24): p. 5971-5982.
321. Aizarani, N., et al., *A human liver cell atlas reveals heterogeneity and epithelial progenitors.* Nature, 2019. **572**(7768): p. 199-204.
322. Vekemans, K. and F. Braet, *Structural and functional aspects of the liver and liver sinusoidal cells in relation to colon carcinoma metastasis.* World Journal of Gastroenterology, 2005. **11**(33): p. 5095-5102.
323. Wisse, E., *An electron microscopic study of the fenestrated endothelial lining of rat liver sinusoids.* Journal of Ultrastructure Research, 1970. **31**(1): p. 125-150.
324. Mathew, R.P. and S.K. Venkatesh, *Liver vascular anatomy: a refresher.* Abdominal Radiology, 2018. **43**(8): p. 1886-1895.
325. Friedman, S.L., et al., *Hepatic lipocytes: the principal collagen-producing cells of normal rat liver.* Proc Natl Acad Sci USA, 1985. **82**(24): p. 8681-8685.
326. Rockey, D.C., *The Molecular Basis of Portal Hypertension.* Trans Am Clin Climatol Assoc, 2017. **128**: p. 330-345.
327. Kietzmann, T., *Metabolic zonation of the liver: The oxygen gradient revisited.* Redox Biology, 2017. **11**: p. 622-630.
328. Jungermann, K. and T. Kietzmann, *Role of oxygen in the zonation of carbohydrate metabolism and gene expression in liver.* Kidney International, 1997. **51**(2): p. 402-412.
329. Martinez-Hernandez, A. and P.S. Amenta, *The extracellular matrix in hepatic regeneration.* Faseb J, 1995. **9**(14): p. 1401-10.
330. Su T, et al., *Single-cell transcriptomics reveals zone-specific alterations of liver sinusoidal endothelial cells in cirrhosis.* Cellular and Molecular Gastroenterology and Hepatology, 2021.
331. Shachaf, C.M., et al., *MYC inactivation uncovers pluripotent differentiation and tumour dormancy in hepatocellular cancer.* Nature, 2004. **431**(7012): p. 1112-7.
332. Duarte, S., et al., *Matrix metalloproteinases in liver injury, repair and fibrosis.* Matrix Biology, 2015. **44-46**: p. 147-156.
333. Rescan, P.Y., et al., *Distribution and origin of the basement membrane component perlecan in rat liver and primary hepatocyte culture.* The American Journal of Pathology, 1993. **142**(1): p. 199-208.
334. Burnier, J.V., et al., *Type IV collagen-initiated signals provide survival and growth cues required for liver metastasis.* Oncogene, 2011. **30**(35): p. 3766-83.

335. Vaniotis, G., et al., *Collagen IV-conveyed signals can regulate chemokine production and promote liver metastasis.* Oncogene, 2018. **37**(28): p. 3790-3805.
336. Albrengues, J., et al., *Neutrophil extracellular traps produced during inflammation awaken dormant cancer cells in mice.* Science, 2018. **361**(6409): p. eaao4227.
337. Franses, J.W., et al., *Stromal Endothelial Cells Directly Influence Cancer Progression.* Science Translational Medicine, 2011. **3**(66): p. 66ra5.
338. Ma, B. and A. Wells, *The mitogen-activated protein (MAP) kinases p38 and extracellular signal-regulated kinase (ERK) are involved in hepatocyte-mediated phenotypic switching in prostate cancer cells.* J Biol Chem, 2014. **289**(16): p. 11153-61.
339. Chao, Y., et al., *Hepatocyte induced re-expression of E-cadherin in breast and prostate cancer cells increases chemoresistance.* Clin Exp Metastasis, 2012. **29**(1): p. 39-50.
340. Yates, C.C., et al., *Co-culturing human prostate carcinoma cells with hepatocytes leads to increased expression of E-cadherin.* Br J Cancer, 2007. **96**(8): p. 1246-52.
341. Ma, B., et al., *Liver protects metastatic prostate cancer from induced death by activating E-cadherin signaling.* Hepatology, 2016. **64**(5): p. 1725-1742.
342. Stessels, F., et al., *Breast adenocarcinoma liver metastases, in contrast to colorectal cancer liver metastases, display a non-angiogenic growth pattern that preserves the stroma and lacks hypoxia.* Br J Cancer, 2004. **90**(7): p. 1429-36.
343. Taylor, D.P., et al., *Hepatic nonparenchymal cells drive metastatic breast cancer outgrowth and partial epithelial to mesenchymal transition.* Breast Cancer Research and Treatment, 2014. **144**(3): p. 551-560.
344. De Minicis, S., et al., *Gene Expression Profiles During Hepatic Stellate Cell Activation in Culture and In Vivo.* Gastroenterology, 2007. **132**(5): p. 1937-1946.
345. Wendel, C., et al., *CXCR4/CXCL12 participate in extravasation of metastasizing breast cancer cells within the liver in a rat model.* PLoS One, 2012. **7**(1): p. e30046.
346. Cools-Lartigue, J., et al., *Neutrophil extracellular traps sequester circulating tumor cells and promote metastasis.* J Clin Invest, 2013. **123**(8): p. 3446-3458.
347. Deleve, L.D., X. Wang, and Y. Guo, *Sinusoidal endothelial cells prevent rat stellate cell activation and promote reversion to quiescence.* Hepatology (Baltimore, Md.), 2008. **48**(3): p. 920-930.
348. DeLeve, L.D., et al., *Rat liver sinusoidal endothelial cell phenotype is maintained by paracrine and autocrine regulation.* American Journal of Physiology-Gastrointestinal and Liver Physiology, 2004. **287**(4): p. G757-G763.
349. Lenk, L., et al., *The hepatic microenvironment essentially determines tumor cell dormancy and metastatic outgrowth of pancreatic ductal adenocarcinoma.* Oncoimmunology, 2017. **7**(1): p. e1368603-e1368603.
350. Khazali, A.S., A.M. Clark, and A. Wells, *Inflammatory cytokine IL-8/CXCL8 promotes tumour escape from hepatocyte-induced dormancy.* British Journal of Cancer, 2018. **118**(4): p. 566-576.
351. Kondo, T., et al., *The impact of hepatic fibrosis on the incidence of liver metastasis from colorectal cancer.* Br J Cancer, 2016. **115**(1): p. 34-9.
352. Miarka, L., et al., *The Hepatic Microenvironment and TRAIL-R2 Impact Outgrowth of Liver Metastases in Pancreatic Cancer after Surgical Resection.* Cancers (Basel), 2019. **11**(6).
353. Hu, X., et al., *Prediction of hepatic metastasis and relapse in colorectal cancers based on concordance analyses with liver fibrosis scores.* Clin Transl Med, 2020. **9**(1): p. 13.

354. Harun, N., et al., *Liver Regeneration Stimulates Tumor Metastases.* Journal of Surgical Research, 2007. **138**(2): p. 284-290.
355. Bertolotti, M., et al., *Nonalcoholic fatty liver disease and aging: epidemiology to management.* World J Gastroenterol, 2014. **20**(39): p. 14185-204.
356. Tsuchida, T. and S.L. Friedman, *Mechanisms of hepatic stellate cell activation.* Nature Reviews Gastroenterology & Hepatology, 2017. **14**(7): p. 397-411.
357. Gressner, A.M., et al., *Roles of TGF-beta in hepatic fibrosis.* Front Biosci, 2002. **7**: p. d793-807.
358. Bissell, D.M., et al., *Cell-specific expression of transforming growth factor-beta in rat liver. Evidence for autocrine regulation of hepatocyte proliferation.* J Clin Invest, 1995. **96**(1): p. 447-55.
359. Pinzani, M., et al., *Effects of platelet-derived growth factor and other polypeptide mitogens on DNA synthesis and growth of cultured rat liver fat-storing cells.* J Clin Invest, 1989. **84**(6): p. 1786-1793.
360. Schumacher, J.D. and G.L. Guo, *Regulation of Hepatic Stellate Cells and Fibrogenesis by Fibroblast Growth Factors.* BioMed Research International, 2016. **2016**: p. 8323747-8323747.
361. Olsen, A.L., et al., *Hepatic stellate cells require a stiff environment for myofibroblastic differentiation.* American Journal of Physiology-Gastrointestinal and Liver Physiology, 2011. **301**(1): p. G110-G118.
362. Rojkind, M., M.-A. Giambrone, and L. Biempica, *Collagen Types in Normal and Cirrhotic Liver.* Gastroenterology, 1979. **76**(4): p. 710-719.
363. Murphy, F.R., et al., *Inhibition of Apoptosis of Activated Hepatic Stellate Cells by Tissue Inhibitor of Metalloproteinase-1 Is Mediated via Effects on Matrix Metalloproteinase Inhibition: IMPLICATIONS FOR REVERSIBILITY OF LIVER FIBROSIS.* Journal of Biological Chemistry, 2002. **277**(13): p. 11069-11076.
364. Herbst, H., et al., *Tissue inhibitor of metalloproteinase-1 and -2 RNA expression in rat and human liver fibrosis.* Am J Pathol, 1997. **150**(5): p. 1647-59.
365. DeLeve, L.D., *Liver sinusoidal endothelial cells in hepatic fibrosis.* Hepatology (Baltimore, Md.), 2015. **61**(5): p. 1740-1746.
366. Friedman, S.L., *The Cellular Basis of Hepatic Fibrosis -- Mechanisms and Treatment Strategies.* New England Journal of Medicine, 1993. **328**(25): p. 1828-1835.
367. Kuriyama, N., et al., *Tenascin-C: A novel mediator of hepatic ischemia and reperfusion injury.* Hepatology, 2011. **54**(6): p. 2125-2136.
368. Murakami, T., et al., *Tenascin C in colorectal cancer stroma is a predictive marker for liver metastasis and is a potent target of miR-198 as identified by microRNA analysis.* British Journal of Cancer, 2017. **117**(9): p. 1360-1370.
369. Cox, T.R., et al., *LOX-mediated collagen crosslinking is responsible for fibrosis-enhanced metastasis.* Cancer research, 2013. **73**(6): p. 1721-1732.
370. Schwabe, R.F., R. Bataller, and D.A. Brenner, *Human hepatic stellate cells express CCR5 and RANTES to induce proliferation and migration.* Am J Physiol Gastrointest Liver Physiol, 2003. **285**(5): p. G949-58.
371. Chen, C.H., et al., *In vivo immune modulatory activity of hepatic stellate cells in mice.* Hepatology, 2006. **44**(5): p. 1171-81.
372. Yu, M.C., et al., *Inhibition of T-cell responses by hepatic stellate cells via B7-H1-mediated T-cell apoptosis in mice.* Hepatology, 2004. **40**(6): p. 1312-21.

373. Hammel, P., et al., *Regression of liver fibrosis after biliary drainage in patients with chronic pancreatitis and stenosis of the common bile duct.* N Engl J Med, 2001. **344**(6): p. 418-23.
374. Poynard, T., et al., *Impact of pegylated interferon alfa-2b and ribavirin on liver fibrosis in patients with chronic hepatitis C.* Gastroenterology, 2002. **122**(5): p. 1303-1313.
375. Nathwani, R., et al., *A Review of Liver Fibrosis and Emerging Therapies.* European Medical Journal, 2019. **4**(4): p. 105-116.
376. Grzelak, C.A. and C.M. Ghajar, *Metastasis 'systems' biology: how are macro-environmental signals transmitted into microenvironmental cues for disseminated tumor cells?* Curr Opin Cell Biol, 2017. **48**: p. 79-86.
377. Ding, N., et al., *A vitamin D receptor/SMAD genomic circuit gates hepatic fibrotic response.* Cell, 2013. **153**(3): p. 601-613.
378. Perego, M., et al., *Reactivation of dormant tumor cells by modified lipids derived from stress-activated neutrophils.* Science Translational Medicine, 2020. **12**(572): p. eabb5817.
379. Chen, Z., et al., *Surgical stress and cancer progression: the twisted tango.* Molecular Cancer, 2019. **18**(1): p. 132.
380. Böhm, F., et al., *Regulation of liver regeneration by growth factors and cytokines.* EMBO Mol Med, 2010. **2**(8): p. 294-305.
381. Ding, B.S., et al., *HDL activation of endothelial sphingosine-1-phosphate receptor-1 (S1P(1)) promotes regeneration and suppresses fibrosis in the liver.* JCI Insight, 2016. **1**(21): p. e87058.
382. Ding, B.S., et al., *Divergent angiocrine signals from vascular niche balance liver regeneration and fibrosis.* Nature, 2014. **505**(7481): p. 97-102.
383. Yang, L., et al., *NF-κB activation in Kupffer cells after partial hepatectomy.* American Journal of Physiology-Gastrointestinal and Liver Physiology, 2005. **289**(3): p. G530-G538.
384. Selzner, N., et al., *ICAM-1 triggers liver regeneration through leukocyte recruitment and Kupffer cell–dependent release of TNF-α/IL-6 in mice.* Gastroenterology, 2003. **124**(3): p. 692-700.
385. Steiling, H., et al., *Fibroblast growth factor receptor signalling is crucial for liver homeostasis and regeneration.* Oncogene, 2003. **22**(28): p. 4380-8.
386. Stolz, D.B., et al., *Growth factor signal transduction immediately after two-thirds partial hepatectomy in the rat.* Cancer Res, 1999. **59**(16): p. 3954-60.
387. Oe, S., et al., *Intact signaling by transforming growth factor beta is not required for termination of liver regeneration in mice.* Hepatology, 2004. **40**(5): p. 1098-105.
388. Riddiough, G.E., et al., *Liver regeneration and liver metastasis.* Seminars in Cancer Biology, 2020.
389. Fisher, B., et al., *Ten year follow-up results of patients with carcinoma of the breast in a co-operative clinical trial evaluating surgical adjuvant chemotherapy.* Surg Gynecol Obstet, 1975. **140**(4): p. 528-34.
390. Rosen, P.P., et al., *Pathological prognostic factors in stage I (T1N0M0) and stage II (T1N1M0) breast carcinoma: a study of 644 patients with median follow-up of 18 years.* J Clin Oncol, 1989. **7**(9): p. 1239-51.
391. Krag, D.N., et al., *Technical outcomes of sentinel-lymph-node resection and conventional axillary-lymph-node dissection in patients with clinically node-negative breast cancer:*

results from the NSABP B-32 randomised phase III trial. Lancet Oncol, 2007. **8**(10): p. 881-8.
392. Kim, J.P., et al., *Clinicopathologic characteristics and prognostic factors in 10 783 patients with gastric cancer.* Gastric Cancer, 1998. **1**(2): p. 125-133.
393. Datta, K., et al., *Mechanism of lymph node metastasis in prostate cancer.* Future Oncology, 2010. **6**(5): p. 823-836.
394. Cho, J.K., et al., *Significance of lymph node metastasis in cancer dissemination of head and neck cancer.* Transl Oncol, 2015. **8**(2): p. 119-25.
395. Giuliano, A.E., et al., *Association of occult metastases in sentinel lymph nodes and bone marrow with survival among women with early-stage invasive breast cancer.* JAMA, 2011. **306**(4): p. 385-393.
396. Fisher, B. and E.R. Fisher, *Transmigration of Lymph Nodes by Tumor Cells.* Science, 1966. **152**(3727): p. 1397.
397. Brown, M., et al., *Lymph node blood vessels provide exit routes for metastatic tumor cell dissemination in mice.* Science, 2018. **359**(6382): p. 1408-1411.
398. Pereira, E.R., et al., *Lymph node metastases can invade local blood vessels, exit the node, and colonize distant organs in mice.* Science, 2018. **359**(6382): p. 1403-1407.
399. Kodama, T., S. Mori, and M. Nose, *Tumor cell invasion from the marginal sinus into extranodal veins during early-stage lymph node metastasis can be a starting point for hematogenous metastasis.* J Canc Met Treat, 2018. **4**(56).
400. Fisher, B. and E.R. Fisher, *Significance of the interrelationship of the lymph and blood vascular systems in tumor cell dissemination.* Prog Clin Cancer, 1970. **4**: p. 84-96.
401. Coste, A., et al., *Hematogenous Dissemination of Breast Cancer Cells From Lymph Nodes Is Mediated by Tumor MicroEnvironment of Metastasis Doorways.* Front Oncol, 2020. **10**: p. 571100.
402. de Boer, M., et al., *Micrometastases or Isolated Tumor Cells and the Outcome of Breast Cancer.* New England Journal of Medicine, 2009. **361**(7): p. 653-663.
403. Liikanen, J.S., et al., *Prognostic value of isolated tumour cells in sentinel lymph nodes in early-stage breast cancer: a prospective study.* British Journal of Cancer, 2018. **118**(11): p. 1529-1535.
404. Weaver, D.L., et al., *Effect of Occult Metastases on Survival in Node-Negative Breast Cancer.* New England Journal of Medicine, 2011. **364**(5): p. 412-421.
405. Leidenius, M.H., et al., *Influence of isolated tumor cells in sentinel nodes on outcome in small, node-negative (pT1N0M0) breast cancer.* Ann Surg Oncol, 2010. **17**(1): p. 254-62.
406. Querzoli, P., et al., *Axillary Lymph Node Nanometastases Are Prognostic Factors for Disease-Free Survival and Metastatic Relapse in Breast Cancer Patients.* Clinical Cancer Research, 2006. **12**(22): p. 6696-6701.
407. Andersson, Y., et al., *Long-term breast cancer survival in relation to the metastatic tumor burden in axillary lymph nodes.* Breast Cancer Research and Treatment, 2018. **171**(2): p. 359-369.
408. Saphir, O. and G.D. Amromin, *Obscure axillary lymph-node metastasis in carcinoma of the breast.* Cancer, 1948. **1**(2): p. 238-241.
409. Cummings, M.C., et al., *Occult axillary lymph node metastases in breast cancer do matter: results of 10-year survival analysis.* Am J Surg Pathol, 2002. **26**(10): p. 1286-95.
410. Demicheli, R., et al., *Microscopic tumor foci in axillary lymph nodes may reveal the recurrence dynamics of breast cancer.* Cancer Communications, 2019. **39**(1): p. 35.

411. Demicheli, R., et al., *Microscopic tumor foci in axillary lymph nodes may reveal the recurrence dynamics of breast cancer.* Canc Commun, 2019. **39**(35).
412. Osella-Abate, S., et al., *Risk factors related to late metastases in 1,372 melanoma patients disease free more than 10 years.* Int J Cancer, 2015. **136**(10): p. 2453-7.
413. Scheri, R.P., et al., *Isolated Tumor Cells in the Sentinel Node Affect Long-Term Prognosis of Patients with Melanoma.* Annals of Surgical Oncology, 2007. **14**(10): p. 2861-2866.
414. Yasuda, T., et al., *Recurrence of Cutaneous and Lymph Node Metastases 12 Years after Radical Total Gastrectomy for Stage IIA Gastric Cancer.* Intern Med, 2020. **59**(11): p. 1387-1393.
415. Quinn, J.J., et al., *Single-cell lineages reveal the rates, routes, and drivers of metastasis in cancer xenografts.* Science, 2021. **371**(6532): p. eabc1944.
416. Willard-Mack, C.L., *Normal structure, function, and histology of lymph nodes.* Toxicol Pathol, 2006. **34**(5): p. 409-24.
417. Malhotra, D., et al., *Transcriptional profiling of stroma from inflamed and resting lymph nodes defines immunological hallmarks.* Nature Immunology, 2012. **13**(5): p. 499-510.
418. Sixt, M., et al., *The conduit system transports soluble antigens from the afferent lymph to resident dendritic cells in the T cell area of the lymph node.* Immunity, 2005. **22**(1): p. 19-29.
419. Kaldjian, E.P., et al., *Spatial and molecular organization of lymph node T cell cortex: a labyrinthine cavity bounded by an epithelium-like monolayer of fibroblastic reticular cells anchored to basement membrane-like extracellular matrix.* International Immunology, 2001. **13**(10): p. 1243-1253.
420. Bajénoff, M., et al., *Stromal Cell Networks Regulate Lymphocyte Entry, Migration, and Territoriality in Lymph Nodes.* Immunity, 2006. **25**(6): p. 989-1001.
421. Herzog, B.H., et al., *Podoplanin maintains high endothelial venule integrity by interacting with platelet CLEC-2.* Nature, 2013. **502**(7469): p. 105-109.
422. Astarita, J.L., et al., *The CLEC-2–podoplanin axis controls the contractility of fibroblastic reticular cells and lymph node microarchitecture.* Nature Immunology, 2015. **16**(1): p. 75-84.
423. Roozendaal, R., R.E. Mebius, and G. Kraal, *The conduit system of the lymph node.* Int Immunol, 2008. **20**(12): p. 1483-7.
424. Gretz, J.E., et al., *Lymph-borne chemokines and other low molecular weight molecules reach high endothelial venules via specialized conduits while a functional barrier limits access to the lymphocyte microenvironments in lymph node cortex.* J Exp Med, 2000. **192**(10): p. 1425-1440.
425. Junt, T., et al., *Subcapsular sinus macrophages in lymph nodes clear lymph-borne viruses and present them to antiviral B cells.* Nature, 2007. **450**(7166): p. 110-114.
426. Gerner, Michael Y., P. Torabi-Parizi, and Ronald N. Germain, *Strategically Localized Dendritic Cells Promote Rapid T Cell Responses to Lymph-Borne Particulate Antigens.* Immunity, 2015. **42**(1): p. 172-185.
427. Ager, A., *High Endothelial Venules and Other Blood Vessels: Critical Regulators of Lymphoid Organ Development and Function.* Frontiers in Immunology, 2017. **8**(45).
428. Skobe, M., et al., *Induction of tumor lymphangiogenesis by VEGF-C promotes breast cancer metastasis.* Nat Med, 2001. **7**(2): p. 192-8.

429. Qu, C., et al., *Role of CCR8 and other chemokine pathways in the migration of monocyte-derived dendritic cells to lymph nodes.* J Exp Med, 2004. **200**(10): p. 1231-1241.
430. Das, S., et al., *Tumor cell entry into the lymph node is controlled by CCL1 chemokine expressed by lymph node lymphatic sinuses.* J Exp Med, 2013. **210**(8): p. 1509-28.
431. Gunn, M.D., et al., *Mice lacking expression of secondary lymphoid organ chemokine have defects in lymphocyte homing and dendritic cell localization.* J Exp Med, 1999. **189**(3): p. 451-60.
432. Luther, S.A., et al., *Differing activities of homeostatic chemokines CCL19, CCL21, and CXCL12 in lymphocyte and dendritic cell recruitment and lymphoid neogenesis.* J Immunol, 2002. **169**(1): p. 424-33.
433. Cyster, J.G., *Chemokines, sphingosine-1-phosphate, and cell migration in secondary lymphoid organs.* Annual Review of Immunology, 2004. **23**(1): p. 127-159.
434. Müller, A., et al., *Involvement of chemokine receptors in breast cancer metastasis.* Nature, 2001. **410**(6824): p. 50-56.
435. Maolake, A., et al., *Tumor necrosis factor-α induces prostate cancer cell migration in lymphatic metastasis through CCR7 upregulation.* Cancer Science, 2018. **109**(5): p. 1524-1531.
436. Shields, J.D., et al., *Chemokine-mediated migration of melanoma cells towards lymphatics – a mechanism contributing to metastasis.* Oncogene, 2007. **26**(21): p. 2997-3005.
437. Fisher, B., E. Saffer, and E. Fisher, *Tumor inhibition by regional lymph node cells.* Cancer, 1974. **33**(3): p. 631-636.
438. Chen, S., et al., *Suppression of tumor formation in lymph nodes by L-selectin-mediated natural killer cell recruitment.* J Exp Med, 2005. **202**(12): p. 1679-1689.
439. Müller, M., et al., *EblacZ tumor dormancy in bone marrow and lymph nodes: active control of proliferating tumor cells by CD8+ immune T cells.* Canc Res, 1998. **58**(23): p. 5439-5446.
440. Lee, C.-k., et al., *Tumor metastasis to lymph nodes requires YAP-dependent metabolic adaptation.* Science, 2019. **363**(6427): p. 644-649.
441. Oliver, G. and R.S. Srinivasan, *Endothelial cell plasticity: how to become and remain a lymphatic endothelial cell.* Development, 2010. **137**(3): p. 363.
442. Lee, E., N.B. Pandey, and A.S. Popel, *Lymphatic endothelial cells support tumor growth in breast cancer.* Scientific Reports, 2014. **4**(1): p. 5853.
443. Aslakson, C.J. and F.R. Miller, *Selective Events in the Metastatic Process Defined by Analysis of the Sequential Dissemination of Subpopulations of a Mouse Mammary Tumor.* Cancer Research, 1992. **52**(6): p. 1399.
444. Jalkanen, S. and M. Salmi, *Lymphatic endothelial cells of the lymph node.* Nat Rev Immunol, 2020.
445. Jeong, H., et al., *Investigation of the Lack of Angiogenesis in the Formation of Lymph Node Metastases.* J Natl Cancer Inst, 2015. **107**(9): p. djv155.
446. Das, S., et al., *Tumor cell entry into the lymph node is controlled by CCL1 chemokine expressed by lymph node lymphatic sinuses.* J Exp Med, 2013. **210**(8): p. 1509-1528.
447. Hayashi, K., et al., *Real-time imaging of tumor-cell shedding and trafficking in lymphatic channels.* Cancer Res, 2007. **67**: p. 8223-8228.
448. Dadiani, M., et al., *Real-time Imaging of Lymphogenic Metastasis in Orthotopic Human Breast Cancer.* Cancer Research, 2006. **66**(16): p. 8037-8041.

449. Nombela-Arrieta C, et al., *Quantitative Imaging of Hematopoietic Stem and Progenitor Cell localization and hypoxic status in the Bone Marrow microenvironment.* Nat Cell Biol, 2014. **15**(5): p. 533-543.
450. Gomariz, A., et al., *Imaging and spatial analysis of hematopoietic stem cell niches.* Annals of the New York Academy of Sciences, 2020. **1466**(1): p. 5-16.
451. Morris, V., et al., *Tumor progression and metastasis in murine D2 hyperplastic alveolar nodule mammary tumor cell lines.* Clin Exp Met, 1993. **11**: p. 103-112.
452. Lawler, P.R. and J. Lawler, *Molecular basis for the regulation of angiogenesis by thrombospondin-1 and -2.* Cold Spring Harb Perspect Med, 2012. **2**(5): p. a006627.
453. Berendam, S.J., et al., *Comparative Transcriptomic Analysis Identifies a Range of Immunologically Related Functional Elaborations of Lymph Node Associated Lymphatic and Blood Endothelial Cells.* Frontiers in immunology, 2019. **10**: p. 816-816.
454. Lee, E., et al., *Breast cancer cells condition lymphatic endothelial cells within pre-metastatic niches to promote metastasis.* Nat Commun, 2014. **5**: p. 4715.
455. Meijer, E.F.J., et al., *Murine chronic lymph node window for longitudinal intravital lymph node imaging.* Nat Protoc, 2017. **12**(8): p. 1513-1520.
456. Ghajar, C.M., et al., *The perivascular niche regulates breast tumour dormancy.* Nat Cell Biol, 2013. **15**(7): p. 807-17.
457. Evensen, L., et al., *Mural cell associated VEGF is required for organotypic vessel formation.* PLoS One, 2009. **4**(6): p. e5798.
458. Rao, R.R., et al., *Matrix composition regulates three-dimensional network formation by endothelial cells and mesenchymal stem cells in collagen/fibrin materials.* Angiogenesis, 2012. **15**(2): p. 253-264.
459. Fletcher, A.L., S.E. Acton, and K. Knoblich, *Lymph node fibroblastic reticular cells in health and disease.* Nat Rev Immunol, 2015. **15**(6): p. 350-61.
460. Katakai, T., et al., *Lymph node fibroblastic reticular cells construct the stromal reticulum via contact with lymphocytes.* The Journal of experimental medicine, 2004. **200**(6): p. 783-795.
461. Helm, C.-L.E., A. Zisch, and M.A. Swartz, *Engineered blood and lymphatic capillaries in 3-D VEGF-fibrin-collagen matrices with interstitial flow.* Biotechnology and Bioengineering, 2007. **96**(1): p. 167-176.
462. Knezevic, L., et al., *Engineering Blood and Lymphatic Microvascular Networks in Fibrin Matrices.* Frontiers in bioengineering and biotechnology, 2017. **5**: p. 25-25.
463. Gibot, L., et al., *Cell-based approach for 3D reconstruction of lymphatic capillaries in vitro reveals distinct functions of HGF and VEGF-C in lymphangiogenesis.* Biomaterials, 2016. **78**: p. 129-139.
464. Seandel, M., et al., *Generation of a functional and durable vascular niche by the adenoviral E4ORF1 gene.* Proceedings of the National Academy of Sciences, 2008. **105**(49): p. 19288.
465. Podgrabinska, S., et al., *Molecular characterization of lymphatic endothelial cells.* Proceedings of the National Academy of Sciences of the United States of America, 2003. **99**: p. 16069-74.
466. Briand, P., et al., *Trisomy 7p and malignant transformation of human breast epithelial cells following epidermal growth factor withdrawal.* Cancer Res, 1996. **56**(9): p. 2039-44.

467. Provenzano, P.P., et al., *Collagen density promotes mammary tumor initiation and progression.* BMC medicine, 2008. **6**: p. 11-11.
468. Rizwan, A., et al., *Metastatic breast cancer cells in lymph nodes increase nodal collagen density.* Sci Rep, 2015. **5**: p. 10002.
469. Hill, R.C., et al., *Quantification of extracellular matrix proteins from a rat lung scaffold to provide a molecular readout for tissue engineering.* Mol Cell Proteomics, 2015. **14**(4): p. 961-73.
470. Korpal, M., et al., *Direct targeting of Sec23a by miR-200s influences cancer cell secretome and promotes metastatic colonization.* Nat Med, 2011. **17**(9): p. 1101-8.
471. Shen, M., et al., *Tinagl1 Suppresses Triple-Negative Breast Cancer Progression and Metastasis by Simultaneously Inhibiting Integrin/FAK and EGFR Signaling.* Cancer Cell, 2019. **35**(1): p. 64-80.e7.
472. Yang, X., et al., *A public genome-scale lentiviral expression library of human ORFs.* Nat Methods, 2011. **8**(8): p. 659-61.
473. Subramanian, A., et al., *Gene set enrichment analysis: a knowledge-based approach for interpreting genome-wide expression profiles.* Proc Natl Acad Sci U S A, 2005. **102**(43): p. 15545-50.
474. Liberzon, A., et al., *The Molecular Signatures Database (MSigDB) hallmark gene set collection.* Cell Syst, 2015. **1**(6): p. 417-425.
475. Yeh, H.-W., et al., *A New Switch for TGFβ in Cancer.* Cancer Research, 2019. **79**(15): p. 3797.
476. Batlle, E. and J. Massagué, *Transforming Growth Factor-β Signaling in Immunity and Cancer.* Immunity, 2019. **50**(4): p. 924-940.
477. Derynck, R., R.J. Akhurst, and A. Balmain, *TGF-beta signaling in tumor suppression and cancer progression.* Nat Genet, 2001. **29**(2): p. 117-29.
478. Bierie, B. and H.L. Moses, *TGFβ: the molecular Jekyll and Hyde of cancer.* Nature Reviews Cancer, 2006. **6**(7): p. 506-520.
479. Kang, Y., et al., *Breast cancer bone metastasis mediated by the Smad tumor suppressor pathway.* Proceedings of the National Academy of Sciences of the United States of America, 2005. **102**(39): p. 13909-13914.
480. Guasch, G., et al., *Loss of TGFbeta signaling destabilizes homeostasis and promotes squamous cell carcinomas in stratified epithelia.* Cancer Cell, 2007. **12**(4): p. 313-27.
481. Schober, M. and E. Fuchs, *Tumor-initiating stem cells of squamous cell carcinomas and their control by TGF-β and integrin/focal adhesion kinase (FAK) signaling.* Proc Natl Acad Sci U S A, 2011. **108**(26): p. 10544-9.
482. Yang, Y., et al., *The Outcome of TGFβ Antagonism in Metastatic Breast Cancer Models In Vivo Reflects a Complex Balance between Tumor-Suppressive and Proprogression Activities of TGFβ.* Clinical Cancer Research, 2020. **26**(3): p. 643.
483. Seoane, J., et al., *TGFbeta influences Myc, Miz-1 and Smad to control the CDK inhibitor p15INK4b.* Nat Cell Biol, 2001. **3**(4): p. 400-8.
484. Murphy-Ullrich, J.E. and M.J. Suto, *Thrombospondin-1 regulation of latent TGF-β activation: A therapeutic target for fibrotic disease.* Matrix Biol, 2018. **68-69**: p. 28-43.
485. Sideek, M.A., et al., *A Central Bioactive Region of LTBP-2 Stimulates the Expression of TGF-β1 in Fibroblasts via Akt and p38 Signalling Pathways.* Int J Mol Sci, 2017. **18**(10).
486. Kenny, P.A., et al., *The morphologies of breast cancer cell lines in three-dimensional assays correlate with their profiles of gene expression.* Mol Oncol, 2007. **1**(1): p. 84-96.

487. Siegel, P.M., et al., *Transforming growth factor beta signaling impairs Neu-induced mammary tumorigenesis while promoting pulmonary metastasis.* Proc Natl Acad Sci U S A, 2003. **100**(14): p. 8430-5.
488. Dasoveanu, D.C., et al., *Regulation of Lymph Node Vascular-Stromal Compartment by Dendritic Cells.* Trends in Immunology, 2016. **37**(11): p. 764-777.
489. Benahmed, F., et al., *Multiple CD11c+ Cells Collaboratively Express IL-1β To Modulate Stromal Vascular Endothelial Growth Factor and Lymph Node Vascular–Stromal Growth.* J Immunol, 2014. **192**(9): p. 4153.
490. Chyou S, et al., *Coordinated regulation of lymph node vascular-stromal growth first by CD11c+ cells and then by T and/or B cells.* J Immunol, 2011. **187**(11): p. 5558-5567.
491. Angeli V, et al., *B Cell-Driven Lymphangiogenesis in Inflamed Lymph Nodes Enhances Dendritic Cell Mobilization.* Immunity, 2006. **24**(2): p. P203-215.
492. Kumar, V., et al., *Global lymphoid tissue remodeling during a viral infection is orchestrated by a B cell-lymphotoxin-dependent pathway.* Blood, 2010. **115**(23): p. 4725-33.
493. Halin, C., et al., *VEGF-A produced by chronically inflamed tissue induces lymphangiogenesis in draining lymph nodes.* Blood, 2007. **110**(9): p. 3158-3167.
494. Acton, S.E., et al., *Dendritic cells control fibroblastic reticular network tension and lymph node expansion.* Nature, 2014. **514**(7523): p. 498-502.
495. Yang, C.-Y., et al., *Trapping of naive lymphocytes triggers rapid growth and remodeling of the fibroblast network in reactive murine lymph nodes.* Proc Natl Acad Sci USA, 2014. **111**(1): p. E109-E118.
496. Martinez, V.G., et al., *Fibroblastic Reticular Cells Control Conduit Matrix Deposition during Lymph Node Expansion.* Cell Reports, 2019. **29**(9): p. 2810-2822.e5.
497. Chyou, S., et al., *Fibroblast-type reticular stromal cells regulate the lymph node vasculature.* J Immunol, 2008. **181**(6): p. 3887-3896.
498. Webster , B., et al., *Regulation of lymph node vascular growth by dendritic cells.* J Exp Med, 2006. **203**(8): p. 1903-1913.
499. Liao, S. and N.H. Ruddle, *Synchrony of High Endothelial Venules and Lymphatic Vessels Revealed by Immunization.* The Journal of Immunology, 2006. **177**(5): p. 3369.
500. Mondor, I., et al., *Clonal Proliferation and Stochastic Pruning Orchestrate Lymph Node Vasculature Remodeling.* Immunity, 2016. **45**(4): p. 877-888.
501. Gregory, J.L., et al., *Infection Programs Sustained Lymphoid Stromal Cell Responses and Shapes Lymph Node Remodeling upon Secondary Challenge.* Cell Rep, 2017. **18**(2): p. 406-418.
502. Twisk, A.J.T., P.H.P. Groeneveld, and G. Kraal, *The effects of bacterial lipopolysaccharide (LPS) on high endothelial venules and interdigitating cells in mouse lymph nodes.* Immunobiology, 1988. **176**(4): p. 410-422.
503. Harrell, M.I., B.M. Iritani, and A. Ruddell, *Tumor-induced sentinel lymph node lymphangiogenesis and increased lymph flow precede melanoma metastasis.* Am J Pathol, 2007. **170**(2): p. 774-86.
504. Tzeng, T.-C., et al., *CD11c hi Dendritic Cells Regulate the Re-establishment of Vascular Quiescence and Stabilization after Immune Stimulation of Lymph Nodes.* The Journal of Immunology, 2010. **184**(8): p. 4247-4257.
505. Banan, B., et al., *Development of a novel murine model of lymphatic metastasis.* Clin Exp Metastasis, 2020. **37**(2): p. 247-255.

506. Li, L., et al., *Mouse Model of Lymph Node Metastasis via Afferent Lymphatic Vessels for Development of Imaging Modalities.* PLOS ONE, 2013. **8**(2): p. e55797.
507. Clark, A.M., et al., *A Model of Dormant-Emergent Metastatic Breast Cancer Progression Enabling Exploration of Biomarker Signatures.* Molecular & cellular proteomics : MCP, 2018. **17**(4): p. 619-630.
508. Rodda, L.B., et al., *Single-Cell RNA Sequencing of Lymph Node Stromal Cells Reveals Niche-Associated Heterogeneity.* Immunity, 2018. **48**(5): p. 1014-1028.e6.
509. Brulois, K., et al., *A molecular map of murine lymph node blood vascular endothelium at single cell resolution.* Nature Communications, 2020. **11**(1): p. 3798.
510. Fujimoto, N., et al., *Single-cell mapping reveals new markers and functions of lymphatic endothelial cells in lymph nodes.* PLOS Biology, 2020. **18**(4): p. e3000704.
511. Xiang, M., et al., *A Single-Cell Transcriptional Roadmap of the Mouse and Human Lymph Node Lymphatic Vasculature.* Frontiers in Cardiovascular Medicine, 2020. **7**(52).
512. Takeda, A., et al., *Single-Cell Survey of Human Lymphatics Unveils Marked Endothelial Cell Heterogeneity and Mechanisms of Homing for Neutrophils.* Immunity, 2019. **51**(3): p. 561-572.e5.
513. Tamburini, B.A., M.A. Burchill, and R.M. Kedl, *Antigen capture and archiving by lymphatic endothelial cells following vaccination or viral infection.* Nat Commun, 2014. **5**: p. 3989.
514. Tan, K.W., et al., *Expansion of Cortical and Medullary Sinuses Restrains Lymph Node Hypertrophy during Prolonged Inflammation.* The Journal of Immunology, 2012. **188**(8): p. 4065-4080.
515. Li, C. and Y.R. Chan, *Lipocalin 2 regulation and its complex role in inflammation and cancer.* Cytokine, 2011. **56**(2): p. 435-41.
516. Sin, W.X., et al., *IRF-7 Mediates Type I IFN Responses in Endotoxin-Challenged Mice.* Front Immunol, 2020. **11**: p. 640.
517. Buss, C., et al., *Essential role of mitochondrial antiviral signaling, IFN regulatory factor (IRF)3, and IRF7 in Chlamydophila pneumoniae-mediated IFN-beta response and control of bacterial replication in human endothelial cells.* J Immunol, 2010. **184**(6): p. 3072-8.
518. Vigl, B., et al., *Tissue inflammation modulates gene expression of lymphatic endothelial cells and dendritic cell migration in a stimulus-dependent manner.* Blood, 2011. **118**(1): p. 205-15.
519. Luig, M., et al., *Inflammation-Induced IL-6 Functions as a Natural Brake on Macrophages and Limits GN.* J Am Soc Nephrol, 2015. **26**(7): p. 1597-607.
520. West, N.R., *Coordination of Immune-Stroma Crosstalk by IL-6 Family Cytokines.* Front Immunol, 2019. **10**: p. 1093.
521. Krishnamurty, A.T. and S.J. Turley, *Lymph node stromal cells: cartographers of the immune system.* Nat Immunol, 2020. **21**(4): p. 369-380.
522. Jin, S.P., et al., *Prognostic significance of loss of c-fos protein in gastric carcinoma.* Pathol Oncol Res, 2007. **13**(4): p. 284-9.
523. Mahner, S., et al., *C-Fos expression is a molecular predictor of progression and survival in epithelial ovarian carcinoma.* Br J Cancer, 2008. **99**(8): p. 1269-75.
524. Wang, Y., et al., *Systematic identification of the key candidate genes in breast cancer stroma.* Cellular & Molecular Biology Letters, 2018. **23**(1): p. 44.

525. O'Connell, J.T., et al., *VEGF-A and Tenascin-C produced by S100A4+ stromal cells are important for metastatic colonization.* Proc Natl Acad Sci U S A, 2011. **108**(38): p. 16002-7.
526. Imanishi, Y., et al., *Angiopoietin-2 stimulates breast cancer metastasis through the alpha(5)beta(1) integrin-mediated pathway.* Cancer research, 2007. **67**(9): p. 4254-4263.
527. Schulz, P., et al., *Angiopoietin-2 drives lymphatic metastasis of pancreatic cancer.* The FASEB Journal, 2011. **25**(10): p. 3325-3335.
528. Moffat, J., et al., *A lentiviral RNAi library for human and mouse genes applied to an arrayed viral high-content screen.* Cell, 2006. **124**(6): p. 1283-98.
529. Siegel, P.M., et al., *Transforming growth factor β signaling impairs Neu-induced mammary tumorigenesis while promoting pulmonary metastasis.* Proceedings of the National Academy of Sciences, 2003. **100**(14): p. 8430.
530. Munn, D.H. and A.L. Mellor, *The tumor-draining lymph node as an immune-privileged site.* Immunol Rev, 2006. **213**: p. 146-58.
531. Dubrot, J., et al., *Lymph node stromal cells acquire peptide–MHCII complexes from dendritic cells and induce antigen-specific CD4+ T cell tolerance.* J Exp Med, 2014. **211**(6): p. 1153-1166.
532. Fletcher, A.L., et al., *Reproducible isolation of lymph node stromal cells reveals site-dependent differences in fibroblastic reticular cells.* Frontiers in immunology, 2011. **2**: p. 35-35.
533. Nobre, A.R., et al., *NG2+/Nestin+ mesenchymal stem cells dictate DTC dormancy in the bone marrow through TGFβ2.* bioRxiv, 2020: p. 2020.10.22.349514.
534. Silva-Vargas, V. and F. Doetsch, *A New Twist for Neurotrophins: Endothelial-Derived NT-3 Mediates Adult Neural Stem Cell Quiescence.* Neuron, 2014. **83**(3): p. 507-509.
535. Zhang, J., et al., *In situ mapping identifies distinct vascular niches for myelopoiesis.* Nature, 2021. **590**(7846): p. 457-462.
536. Bautch, V.L. and K.M. Caron, *Blood and Lymphatic Vessel Formation.* Cold Spring Harbor Perspectives in Biology, 2015. **7**(3).
537. Belanger, M.C., et al., *Acute lymph node slices are a functional model system to study immunity ex vivo.* bioRxiv, 2019: p. 865543.
538. Christiansen, A.J., et al., *Lymphatic endothelial cells attenuate inflammation via suppression of dendritic cell maturation.* Oncotarget, 2016. **7**(26): p. 39421-39435.
539. Yu, M., et al., *Fibroblastic reticular cells of the lymphoid tissues modulate T cell activation threshold during homeostasis via hyperactive cyclooxygenase-2/prostaglandin E2 axis.* Scientific Reports, 2017. **7**(1): p. 3350.
540. Lukacs-Kornek, V., et al., *Regulated release of nitric oxide by nonhematopoietic stroma controls expansion of the activated T cell pool in lymph nodes.* Nat Immunol, 2011. **12**(11): p. 1096-104.
541. Beliveau, A., et al., *Raf-induced MMP9 disrupts tissue architecture of human breast cells in three-dimensional culture and is necessary for tumor growth in vivo.* Genes Dev, 2010. **24**(24): p. 2800-11.
542. Kim, D., et al., *TopHat2: accurate alignment of transcriptomes in the presence of insertions, deletions and gene fusions.* Genome Biology, 2013. **14**(4): p. R36.
543. Chou, J., et al., *Phenotypic and transcriptional fidelity of patient-derived colon cancer xenografts in immune-deficient mice.* PLoS One, 2013. **8**(11): p. e79874.

544. Lawrence, M., et al., *Software for Computing and Annotating Genomic Ranges.* PLOS Computational Biology, 2013. **9**(8): p. e1003118.
545. Robinson, M.D., D.J. McCarthy, and G.K. Smyth, *edgeR: a Bioconductor package for differential expression analysis of digital gene expression data.* Bioinformatics, 2010. **26**(1): p. 139-40.
546. Ritchie, M.E., et al., *limma powers differential expression analyses for RNA-sequencing and microarray studies.* Nucleic Acids Res, 2015. **43**(7): p. e47.

VITA

Andrea R. Lim attended Pepperdine University where she received a Bachelor of Science degree in Biology with Honors, graduating Magna Cum Laude in 2013. At Pepperdine, she studied how extracellular matrix proteins affect angiogenic behavior under Dr. Donna Nofziger, completing a summer undergraduate research program and an honors thesis on the topic. She entered the Molecular and Cellular Biology doctoral program at the University of Washington & Fred Hutchinson Cancer Research Center in 2014 and joined the lab of Dr. Cyrus Ghajar to study how the microenvironment influences tumor cell behavior. During her graduate work, she was funded though a T32 training grant, F31 NRSA Individual Research Grant, and F99 Pre-doctoral to Post-doctoral Transition Grant through the National Cancer Institute, under the National Institutes of Health. In addition to research pursuits, she enjoyed developing science communication skills, working with the Science and Education Partnership at Fred Hutch, presenting for lay audiences, and illustrating figures for publications. These skills will aid her as she pursues a career in cancer research.